Title
BOSE-EINSTEIN CORRELATIONS OF PIONS IN e+ e-ANNIHILATION AT 29-GeV CENTER-OF-MASS ENERGY

Author
Avery, Robert Ellsworth

Publication Date
1989

Lawrence Berkeley Laboratory
UNIVERSITY OF CALIFORNIA

Physics Division

Bose-Einstein Correlations of Pions in e^+e^- Annihilation at 29 GeV Center-of-Mass Energy

R.E. Avery
(Ph.D. Thesis)

January 1989

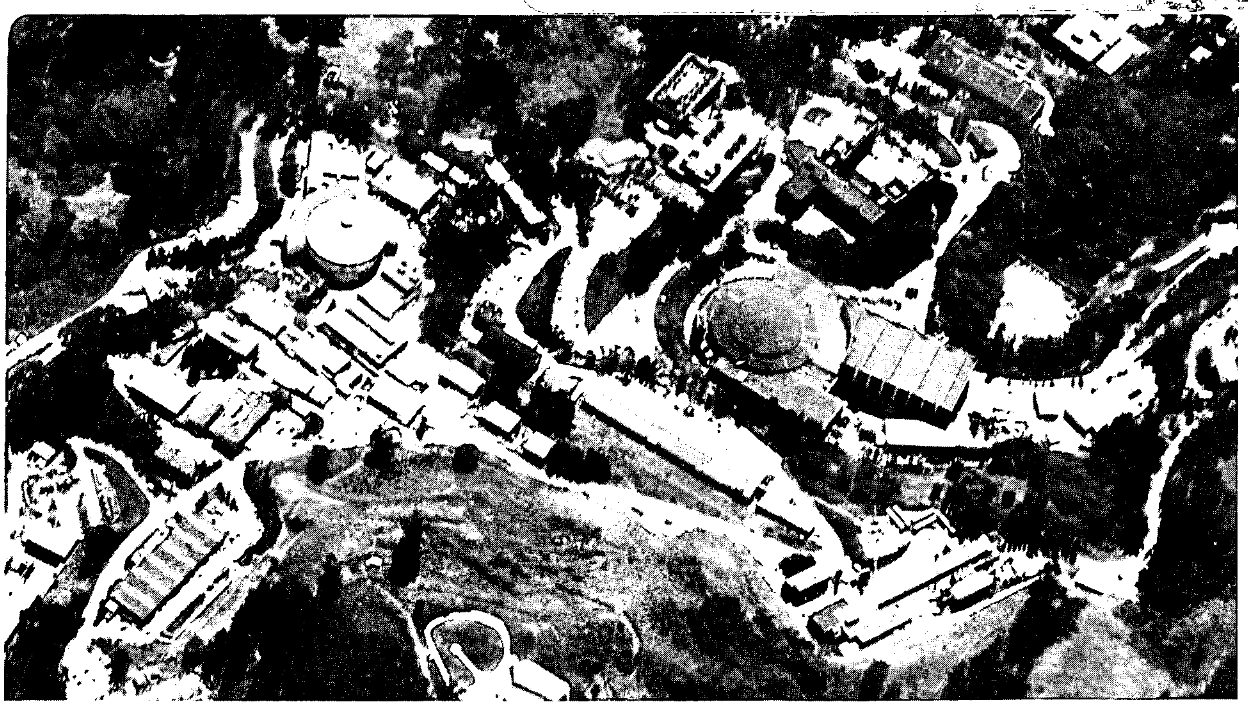

Prepared for the U.S. Department of Energy under Contract Number DE-AC03-76SF00098.

DISCLAIMER

LBL-26593

Bose-Einstein Correlations of Pions in e^+e^- Annihilation at 29 GeV Center-of-Mass Energy [1]

By
Robert Ellsworth Avery
Ph.D. Thesis
January 13, 1989

Lawrence Berkeley Laboratory,
1 Cyclotron Rd.,
Berkeley, CA 94720

Abstract

Measurements of two- and three-particle correlations between like-sign pions produced in e^+e^- annihilation at 29 GeV center-of-mass energy are presented. The analysis is based on data taken during the period 1982-1986 using the TPC/2γ detector at PEP. Two-particle correlations are studied as a function of Q, the momentum difference as measured in the rest frame of the pion pair, and as a function of q_0, the energy difference as measured in the lab frame. The Bose-Einstein enhancement is observed when Q is small even when the energy difference, q_0, is substantial. This observation provides evidence that the Bose-Einstein correlations are best described by a model that correctly accounts for the relativistic motion of the particle sources. Three-pion correlations are measured both by using a standard three-pion correlation function, and also by using a correlation function for which the correlations between the pairs of pions within the triplet have been subtracted. The observation of three-pion correlations after pair correlations have been subtracted supports the interpretation that the observed correlations are due to Bose-Einstein interference.

[1]This work was supported by the Director, Office of Energy Research, Office of High Energy and Nuclear Physics, Division of High Energy Physics, of the U.S. Department of Energy under Contract DE-AC03-76SF00098.

Contents

Acknowledgements

Because of the nature of modern high energy physics, the list of physicists, engineers, programmers, and other support people whose dedicated efforts make an experiment such as this possible is a very long one, and includes many whom I have never met and many whose names I don't know. Nonetheless, without all of their efforts, the work described in this thesis would not have been possible. I give my thanks to all of them.

During the time that I have been a member of the TPC/2γ collaboration, I have met several physicists whose dedication and ability have inspired me. These include Mike Ronan, Al Clark, Dick Kofler, and Pierre Oddone. From them I have learned most of what I know about what it takes to make a high energy physics experiment work. Gerry Lynch's understanding of how to use the data produced by the TPC was invaluable to me and to all who have done physics analysis with the TPC. When I was sensible enough to ask him, my advisor, Werner Hofmann, consistently provided me with good ideas about physics and invaluable advice about my analysis.

I was lucky enough to have Werner, Gerson Goldhaber, and John Rasmussen, on my thesis committee, each of whom have expertise and interest in the subject of Bose-Einstein correlations. I am very appreciative of the comments they have given me and of the time they have spent reading my thesis.

I would like to thank Hiro Yamamoto and Ed Wang, whose lunch time conversations, whether about Bose-Einstein correlations or wormholes and time-travel, kept me thinking about physics. I would like to thank Ed Whipple and Jack Eastman for trying to teach good taste to all of us in the TPC/2γ collaboration, in physics, computers and other things. In addition I would like to thank the other graduate students and post-docs working on the TPC whose friendship I have enjoyed over the last five years: Aurelio Bay, Glen Cowan, Tim Edberg, Bill Gary, Steve Kaye, Lisa Mathis, Bill Moses, Sung Park, Margie Shapiro, Mike Strauss, Tad Takahashi, Shahin Toutounchi, Rem van Tyen, Zack Wolf, and Cary Zeitlin.

Thanks to my friends Jack, Glen, Andy and Linda for dinner and movies. I thank Laura, Lisa, Elliot, and Rick who were my friends when I was deciding whether to become physicist, and who remained my friends, even after I decided. I thank my family for everything else.

Chapter 1

Introduction

The primary goals of high energy particle physics are to learn what the fundamental particles that constitute matter are, and to learn how these particles are produced and how they interact with each other. We classify the particles that are presently known to exist according to the forces that act on them. For example, particles such as protons, neutrons and pions interact the via the strong nuclear interaction, the force that binds together the nuclei of atoms. We call strongly interacting particles hadrons. Particles that do not interact via the strong force, such as electrons and muons, we call leptons. In this thesis we study the production of hadrons resulting from the interaction of high energy electrons and positrons.

The development of a modern understanding of particle interactions had its beginning early this century with the development of quantum theory. A fundamental aspect of quantum theory is that particles have a wave nature that determines their microscopic interactions, just as does light. In the classical description of light, the intensity of light is determined by the absolute square of the sum of electro-magnetic fields. Similarly in quantum mechanics, the probability for particle propagation or production is determined by the absolute square of the sums of wave functions or amplitudes for that process. This means that there can be interference between different contributions to a process, i.e., cross terms in this square of sums may contribute constructively or destructively to the probability for the process to occur. It has become clear that any theory attempting to describe the microscopic interactions of particles must be a quantum theory.

Quantum Chromodynamics (QCD) has so far has been quite successful in describing the strong nuclear interactions of hadrons. QCD describes hadrons as being composed of fundamental particles called quarks and gluons. There is now much evidence for the composite nature of hadrons, but a quark or gluon has never been observed in isolation. The absence of free quarks or gluons, a phenomenon called confinement, is believed to follow from QCD, although it has not yet been shown conclusively that this is true.

QCD predicts that the coupling strength of strong interactions becomes large when the energy scale of the interacting particles is small. Application of perturbation theory, the method that is ordinarily used to calculate probabilities for interactions, requires that couplings be small if the results of calculation are to be meaningful. As a result, QCD calculations of low energy phenomena become difficult or impossible. An example of interest to us is the transformation into low mass hadrons of a quark produced by a high energy reaction. This process is called quark fragmentation, or hadronization. The initial process that produces the quark, for example the reaction $e^+e^- \rightarrow q\overline{q}$, may be described by perturbation theory, as can the early strong interactions of the quark (radiation of gluons). Thus perturbation theory describes the early production of quarks and gluons, which are collectively referred to as partons. But at some point the energy scale of the interactions approaches that of the low mass final hadrons, and the process is no longer well described by perturbation theory.

The study of QCD necessarily requires that some attempt be made to understand hadron production, since we cannot observe the initial quarks and gluons directly. Models have been developed that make use of QCD concepts but make various simplifying assumptions about the final production of primary hadrons. These models generally have parameters that can be varied so as to bring the model predictions of particle distributions into agreement with measured distributions. These models are necessary in order to test that QCD correctly describes the initial parton production stage. It is also hoped that the relative success of different approaches may provide some insight into the physics of the final stages of hadron production.

The models that are presently used are mostly classical (not quantum mechanical), in the treatment of hadron production. Hadron production in these models is typically an iterative process lending itself easily to a Monte Carlo implementation for calculations. Quantum mechanical interference effects are not expected to strongly influence the most obvious features of single particle distributions. This is because the typical wavelength of particles produced ($1\ (\mathrm{GeV/c})^{-1} = 0.2$ fm) is smaller than the distance scale of particle production (~ 30 fm). Distributions that depend on soft particle or parton production, or multiple particle distributions in regions of small relative momenta may reveal interference effects to be important. Interference has been found to be important at both the parton level and at the hadronization level. Destructive interference of soft gluons can explain the deficit of hadrons opposite the gluon jet in three jet events (events with a hard radiative gluon, $e^+e^- \rightarrow q\overline{q}g$) [Bar83,Aih85a].

The subject of this thesis is an interference effect, important at the hadronization stage, that occurs as a result of the quantum statistics of the hadrons. The amplitude for producing two identical bosons is required to be symmetric under interchange of the two particles (or antisymmetric for fermions). It follows that the amplitude can be written $A(p_1, p_2) + A(p_2, p_1)$, so that the probability for producing two particles in the same state (*i.e.* such that $p_1 \sim p_2$ and $A(p_1, p_2) \sim A(p_2, p_1)$) will be enhanced by constructive interference between the direct amplitude ($A(p_1, p_2)$) and the exchanged amplitude ($A(p_2, p_1)$).

As we will see in the theoretical discussion in the next chapter, the ability to observe this interference depends on details of particle production. If the particles are of different momentum, and also produced at separated points in space, the interference may be diminished or destructive, and not observable. Correlations caused by Bose-Einstein symmetry can thus be used to probe the space distribution of the sources of particles. This method was first used by observing photon correlations from stars to measure star diameters by Hanbury-Brown and Twiss in 1956 [Han56]. In 1959 Goldhaber *et al.* observed that like-signed pairs of pions produced in proton–anti-proton annihilation were more likely to be produced with small opening angles compared to unlike-signed pion pairs [Gol59]. Goldhaber, Goldhaber, Lee and Pais showed that this effect could be simply explained by taking into account the Bose-Einstein symmetry of the pion wave function using a simple phase space model of multiparticle production [Gol60]. Since that time the Bose-Einstein effect has been studied in a variety of high energy reactions as a probe of the space structure of the particle emitting region (see [Gol86,Zaj88] and references therein).

More recently, interest has shifted to the influence of of particle production dynamics on Bose-Einstein interference. This shift in interest started in the mid-seventies with the demonstration that if particles are emitted coherently from a source, then Bose-Einstein correlations would be unobservable. The observation of Bose-Einstein correlations depends on the sources emitting particles incoherently, or chaotically, so that one could test whether particle production was completely chaotic or if there was a partial coherent component to particle production[Fow77,Gyu79]. It was further realized that other important dynamic aspects of particle production, such as the relativistic motion of sources, and the correlation of source position with particle momentum, could affect whether interference is seen [Pra84,And86,Bow85]. In short, the study of Bose-Einstein correlations is a much more complex and rich field than may have been suspected from initial observations.

In this thesis we study Bose-Einstein interference in the hadronization process following e^+e^- annihilation. It is hoped that the relatively simple e^+e^- system provides an better environment for the study of Bose-Einstein interference during hadronization than do more complex systems. We will try to answer the question: "Is the observation of correlations consistent with our understanding of how Bose-Einstein interference is exhibited in this process?" We begin in the next chapter with a brief review of the current theoretical understanding of Bose-Einstein interference between particles produced during hadronization. Chapters 3 and 4 discuss the experimental apparatus used and the reconstruction of the events $e^+e^- \rightarrow q\overline{q} \rightarrow hadrons$. Chapter 5 discusses the analysis of correlations between pion pairs, and Chapter 6 discusses the correlations between pion triplets.

Chapter 2

Theory of Bose-Einstein Correlations

In 1959, Goldhaber *et al.* observed that like-signed pairs of pions produced by proton-antiproton annihilation were more likely to be produced with small opening angles than were unlike signed pions [Gol59]. To explain this effect, Goldhaber, Goldhaber, Lee and Pais [Gol60], extended a simple phase space model for multiparticle production that was first proposed by Fermi. In Fermi's original model [Fer50], the probability for proton-antiproton annihilation into an N pion state is proportional to Lorentz-invariant phase space multiplied by the factor, $P_N(\Omega) = (\Omega/V)^N$. Ω is interpreted as the "reaction volume" in which the particles are produced; V is the volume of a large box with periodic boundary conditions, and is used for consistent normalization. $P_N(\Omega)$ is interpreted as the probability to find N free pions in the volume Ω. Goldhaber, Goldhaber, Lee and Pais assumed that $P_N(\Omega)$ must be proportional to the square of the free particle wave function of the pions in the volume Ω. They extended the original Fermi model by requiring that the wave function of the particles obey Bose-Einstein symmetry when two particles are exchanged. For particles of similar momentum, constructive interference occurs. They were then able to compute the expected distribution of particle pairs based on this extended model. This extension brought the theory into good agreement with the data.

2.1 The Bose-Einstein Correlation Function

The method developed by Goldhaber *et al.* consisted of taking a model for particle production, extending that model to account for Bose-Einstein interference, and then comparing data directly with predictions of the extended model. It is difficult to develop a simple, reliable model for the dynamics of particle production for higher energy processes with many final-state particles. The two particle correlation function was developed in order to study particle correlations in data without need for a model of multiparticle production. The inclusive two-particle cross section, $d^8\sigma(\pi\pi)/d^4p_1d^4p_2$, is compared with the product of inclusive single-

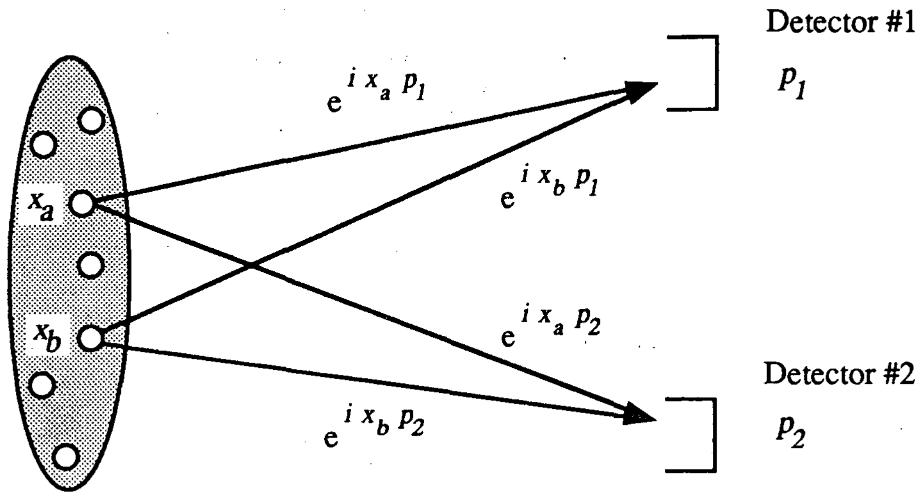

Figure 2.1: Amplitudes for two particles measured with momentum p_1 and p_2 emitted from the points x_a and x_b.

particle cross sections, $d^4\sigma(\pi)/d^4p$, rather than being compared directly with model predictions. The correlation function for pions may be defined as [1],

$$\begin{aligned}
R(p_1,p_2) &= \frac{\langle N_\pi\rangle^2}{\langle N_\pi(N_\pi-1)\rangle}\frac{\sigma_\pi d^8\sigma(\pi\pi)/d^4p_1d^4p_2}{(d^4\sigma(\pi)/d^4p_1)(d^4\sigma(\pi)/d^4p_2)}, \qquad (2.1)\\
\langle N_\pi\rangle &= \text{average pion multiplicity } (N_\pi).\\
\sigma_\pi &= \text{Total } \pi \text{ cross section.}
\end{aligned}$$

In the absence of of correlations between this would just be equal to one. The factors in front ensure that the correlation function is not affected by global correlations, which only affect N_π, the multiplicity of the pions in the event, and not the relative momenta of particles in the event.

We give here a simplified description of a derivation by Kopylov and Podgoretskiĭ [Kop74b,Kop74c] of the two particle correlation function. First consider the production amplitude from two independent particle sources each emitting one particle, as shown schematically in Fig. 2.1. By assuming the particles obey a first quantized Klein-Gordon equation, it is shown that the amplitude for two particles with four-momenta p_1, p_2 to be emitted from sources at point and time

[1]The following conventions will be followed throughout this thesis: four-vectors are written as plain variables, *e.g.* x, three-vectors are written as bold variables, *e.g.* $\mathbf{x}$, and the speed of light, c, and $\hbar$ will be suppressed (taken to be 1).

denoted by four vectors x_a and x_b is proportional to

$$\psi(1,2) \propto e^{i(p_1 x_a + p_2 x_b)} + e^{i(p_1 x_b + p_2 x_a)}. \tag{2.2}$$

The second term is required in order that the amplitude obey Bose-Einstein symmetry. If there are only these two sources, then the probability to emit the pair is simply:

$$P(1,2) \propto 1 + \cos(q\Delta x), \tag{2.3}$$
$$\text{with, } q \equiv (q_0, \mathbf{q}) \equiv \Delta p.$$

If particles are assumed to be emitted from sources that are distributed randomly according to the space-time distribution $\rho(x)$, then the probability to produce a pair is the integral of the above expression over the density of source positions for each particle,

$$P(p_1, p_2) \propto \int |\psi(1,2)|^2 \rho(x_a)\rho(x_b) d^4x_a d^4x_b. \tag{2.4}$$

The correlation function is found to be a function of q,

$$R(q) = 1 + |\tilde{\rho}(q)|^2. \tag{2.5}$$

where $\tilde{\rho}(q)$ is the fourier transform of $\rho(x)$. It is clear from this expression that the measurement of two particle correlations reveals the space-time structure of the particle emitting source.

The correlation function was originally defined for examining data from low energy nuclear collisions; as a result, the typical source distributions that were used to derive the correlation function were chosen to be appropriate for such reactions. In particular, the emission region is chosen to be a distribution of static individual sources, or at least a distribution that does not change in time. It is typically assumed that the sources decay independently, and exponentially in time. (Sometimes a gaussian time dependence is assumed, but the results are qualitatively the same.) If we make these assumptions, the enhancement will always factor into two *decreasing* functions, one depending on $\mathbf{q}$, derived from the spatial distribution of the sources, and one depending on q_0, derived from the time dependence of the sources:

$$R(q) = 1 + |f(\mathbf{q})g(q_0)|^2. \tag{2.6}$$

Thus if either $|\mathbf{q}|$ or q_0 is large, the correlations disappear. A typical example is to assume a spherically symmetric gaussian distribution of radius r, the sources having an exponential lifetime, τ. The result is,

$$R(q) = 1 + \frac{\exp(-r|\mathbf{q}|)}{1 + \tau q_0}. \tag{2.7}$$

This picture is unlikely to be a good description of high energy reactions, in which the final particles, and most likely the particle sources, are highly relativistic and certainly not static. Whether the failure of this simple picture is demonstrated experimentally is an important question that this thesis will address. This question will be returned to in Sect. 2.3.1.

2.1.1 Bose-Einstein Correlations Between Multiplets.

So far, we have just discussed the influence of Bose-Einstein correlations on the pair production of identical bosons. If more than two identical bosons are produced, the total production amplitude must be completely symmetric upon interchange of any of the identical bosons. We symmetrize the amplitude for producing a multiplet of n particles by summing over all of the possible permutations of the n particles:

$$\psi_s(1,2,...,n) \propto \sum_{perm:i=1}^{n!} \psi(\xi_i); \tag{2.8}$$

ξ_i represents the $n!$ possible permutations of $(1, 2, \ldots, n)$. We compute the probability to produce the n particle state, normalizing by the amplitude to produce the particles in absence of interference:

$$R(1,2,...,n) = \frac{\left|\sum_{perm:i=1}^{n!} \psi(\xi_i)\right|^2}{\sum_{perm:i=1}^{n!} |\psi(\xi_i)|^2}. \tag{2.9}$$

If the particles are all produced in approximately the same state, such that $p_1 \sim p_2 \sim \ldots \sim p_n$ and $\psi(\xi_1) \sim \psi(\xi_1) \sim \ldots \sim \psi(\xi_{n!})$, then the enhancement is maximal. For maximal enhancement, the probability to produce an n-tuplet is $n!$ times what it would be in the absence of interference. We already saw that the enhancement for pairs of bosons is a factor of two above what would be seen in absence of interference; we now can predict that the enhancement for triplets is a factor of $3! = 6$ above. From this we might think that Bose-Einstein correlations are much easier to see in distributions of larger multiplets; however, the fraction of n particle phase space which corresponds to maximal correlations becomes smaller for a larger number of particles. It may therefore be difficult to observe maximal Bose-Einstein correlations for large multiplets.

The derivation of the three-pion correlation function is similar to that of the two-pion correlation function [Alt86,Liu85]. The normalized probability to produce identical bosons with momenta p_1, p_2, and p_3 from sources at positions x_a, x_b, and x_c is

$$\begin{aligned} R(p_1,p_2,p_3;x_a,x_b,x_c) &= \frac{\left|\sum_{i,j,k\in all\ perm} e^{i(p_ix_a+p_jx_b+p_kx_c)}\right|^2}{\left\{\sum_{i,j,k\in all\ perm} \left|e^{i(p_ix_a+p_jx_b+p_kx_c)}\right|^2\right\} = 6} \\ &= 1 \\ &\quad +1/3\left[\cos(q_{12}\Delta x_{ab}) + \cos(q_{12}\Delta x_{bc}) + \cos(q_{12}\Delta x_{ca})\right] \\ &\quad +1/3\left[\cos(q_{23}\Delta x_{ab}) + \cos(q_{23}\Delta x_{bc}) + \cos(q_{23}\Delta x_{ca})\right] \\ &\quad +1/3\left[\cos(q_{31}\Delta x_{ab}) + \cos(q_{31}\Delta x_{bc}) + \cos(q_{31}\Delta x_{ca})\right] \\ &\quad +1/6\left\{\sum_{l,m,n\in all\ 6\ perm} \left(e^{i(q_{12}x_l+q_{23}x_m+q_{31}x_n)} + \text{c.c.}\right)\right\}; \end{aligned}$$

$$q_{ij} \equiv p_i - p_j; \quad \Delta x_{ij} \equiv x_i - x_j. \tag{2.10}$$

We now integrate this expression over the density of source positions x_a, x_b and x_c:

$$\begin{aligned} R(p_1,p_2,p_3) &= \int R(p_1,p_2,p_3;x_a,x_b,x_c)\rho(x_a)\rho(x_b)\rho(x_c)d^4x_a d^4x_b d^4x_c \\ &= 1 + |\tilde{\rho}(q_{12})|^2 + |\tilde{\rho}(q_{23})|^2 + |\tilde{\rho}(q_{31})|^2 \\ &\quad +2Re[\tilde{\rho}(q_{12})\tilde{\rho}(q_{23})\tilde{\rho}(q_{31})]. \end{aligned} \tag{2.11}$$

The first three enhancement terms are the result of permutation of pairs of pions in the triplet, and are similar to the pair correlations already discussed. The last term is unique to triplets, becoming small if any one particle in the triplet has a large momentum difference from the others. Its source is interference between permutations involving all three particles, not just a pair within the triplet. This extra enhancement for pion triplets, if observed, provides evidence that maximal correlations for triplets can occur. Chapter 6 of this thesis will describe a measurement of this extra, or "pure triplet", enhancement.

2.1.2 The Effect of Resonances on the Ability to Observe Correlations.

Mesons that are the decay products of resonances must obey Bose statistics just as do primary mesons, so we should expect that constructive interference should also contribute to their production amplitude just as it does for primary particles. In practice, however, the Bose-Einstein correlation between pairs where one particle is the product of a resonance is generally not observable except for short lived resonances (such as the ρ) [Gra77]. One simple way to understand this is that the resonance products effectively have a larger source radius, since the resonance will decay far from the primary meson source. This large effective source size could in principle be seen as a spike in the correlation function at low momentum difference, if one had a perfect detector. For a real detector of finite resolution, this spike (which occurs in a very small region of two particle phase space) will be smeared out and not observable. Another essentially equivalent description is that if a primary particle is exchanged with a decay product of a resonance, then the resonance is off its mass, and so the exchange diagram (hence the Bose-Einstein interference) is suppressed by the shape of the Breit-Wigner resonance. If the resonance is a short-lived, strongly decaying resonance, such as the ρ, this picture may be too simple. As will be discussed later, the mesons in e^+e^- annihilation are produced on the same time scale as the decay of short lived resonances. There is some theoretical uncertainty as to whether the resonance suppression effect is relevant in this case [Art88].

2.1.3 The Importance of Incoherence

While the above derivation of the correlation function is appealing in its simplicity, a more careful derivation introduces important complications. The above derivation assumed that a single particle was emitted from each source, and also ignored the possibility of there being a coherent phase associated with each production point (we will see that these assumptions implicitly amount to an assumption that the relative phase is random). A more correct derivation (due to Bowler [Bow85], although similar results were earlier derived in Refs. [Fow77,Gyu79]), begins by writing the amplitude for single particle production (from two possible sources) as,

$$\psi(1) \propto f_a e^{ip_1 x_a} + f_b e^{ip_1 x_b}. \tag{2.12}$$

f_a and f_b are the phase factors for the sources. The amplitude to produce two particles is just the product,

$$\psi(1,2) = \psi(1)\psi(2) \propto \left[f_a e^{ip_1 x_a} + f_b e^{ip_1 x_b}\right]\left[f_a e^{ip_2 x_a} + f_b e^{ip_2 x_b}\right], \tag{2.13}$$

which is already Bose symmetric.

What it means for source a and b to be mutually coherent is that their relative phase doesn't change, so that the average of this relative phase is non-zero: $\langle f_a f_b^* \rangle = f_a f_b^*$. In this case it is clear that the probability of producing two particles,

$$\begin{aligned} P(1,2) &= \left(|f_a|^2 + |f_b|^2 + \left[f_a f_b^* e^{ip_1(x_a - x_b)} + \text{c.c.}\right]\right) \times \\ &\quad \left(|f_a|^2 + |f_b|^2 + \left[f_a f_b^* e^{ip_2(x_a - x_b)} + \text{c.c.}\right]\right) \end{aligned} \tag{2.14}$$

is just the product of the probabilities of producing each individual particle,

$$P(1) = |f_a|^2 + |f_b|^2 + \left[f_a f_b^* e^{ip_1(x_a - x_b)} + \text{c.c.}\right]. \tag{2.15}$$

Correlation is therefore not observable, since the correlation function is just $\frac{\langle P(1,2)\rangle}{\langle P(1)\rangle\langle P(2)\rangle}$. When particles are produced coherently, interference affects even the single particle distribution, and it is this interference which makes the two particle correlations unobservable.

If the sources are incoherent, this means that the relative phase varies randomly in time so that the average of the relative phase is zero: $\langle f_a f_b^* \rangle = 0$. The probability to produce a pair is then the average of the expression above, with terms proportional to $\langle f_a f_b^* \rangle$ vanishing:

$$\langle P(1,2)\rangle = (|f_a|^2 + |f_b|^2)^2 + 2|f_a|^2|f_b|^2 \cos[(p_2 - p_1)(x_a - x_b)], \tag{2.16}$$

and,

$$\langle P(1)\rangle\langle P(2)\rangle = (f_a^2 + f_b^2)^2. \tag{2.17}$$

Assuming $f_a^2 = f_b^2$, the correlation function is then,

$$\frac{\langle P(1,2)\rangle}{\langle P(1)\rangle\langle P(2)\rangle} = 1 + \frac{1}{2}\cos[(p_2 - p_1)(x_a - x_b)]. \tag{2.18}$$

It is seen that the enhancement for pairs smaller than what we previously derived by a factor of two; however, if there are many sources, it can be shown that the full enhancement is maintained. It is only when each source phase is random with respect to the others that the full interference due to Bose-Einstein correlations is seen.

In Ref. [Gyu79], Gyulassy *et al.* provide a rigorous derivation of the correlation function found in heavy nuclear collisions using a model inspired by intranuclear cascade models. In their model, which uses field theory to compute the correlations, and which takes multiparticle production into account, a random number of current sources are distributed randomly. They show that the random variation in the space time separation of sources introduces chaotic randomness of the phases for each source; if the wavelength of the particles is small compared to the size of the source, this chaotic randomness is enough to produce maximal Bose-Einstein correlation.

The assumptions of Gyulassy's model seem quite reasonable when applied to collisions of heavy nuclei, but are not particularly appropriate when applied to e^+e^- annihilation. It would be preferable to have a model that is more closely based on the dynamics of e^+e^- annihilation. We will therefore take some time to discuss current ideas about hadron production in e^+e^- annihilation and then try to apply these ideas to a more realistic picture of Bose-Einstein correlations. Recent attempts to describe Bose-Einstein correlations using models more appropriate to the production of particles in the reaction $e^+e^- \to q\overline{q} \to hadrons$ will then be discussed.

2.2 Hadron Production in e^+e^- Annihilation

The process of hadron production in e^+e^- collisions occurs in several stages, as illustrated in Fig. 2.2. These stages are determined by the kinds of interactions experienced by the particles and by the typical energy transfer experienced by the particles during these interactions. The process begins with the annihilation of the e^+e^- pair to produce a highly virtual photon. The creation of a pair of fermions is described to first order by simple Quantum Electrodynamics, so that the cross section to produce a pair of fermions of charge e_f is,

$$\sigma_{f\overline{f}} = \frac{4\pi}{3s}\alpha^2 e_f^2 \tag{2.19}$$

If quarks are produced, this process is significantly modified because of the strong interactions of the quarks. Since quarks come in three different colors according to QCD, the cross section is increased by a factor of three. Also, there are QCD corrections to the cross section caused by the coupling of quarks to the color field. The quarks can radiate and perhaps reabsorb gluons. This will change the total cross section, and also affect the distributions of particles that are produced.

If the initial energy of the $q\overline{q}$ pair is large, perturbative QCD can be used to describe the initial distribution of quarks and gluons. The strong coupling constant of QCD, α_s, depends on the momentum transfer at the vertex (Q^2). For large momentum transfer, the coupling constant is small, and therefore perturbation theory is valid. As the initial quarks emit gluons, and as these gluons in

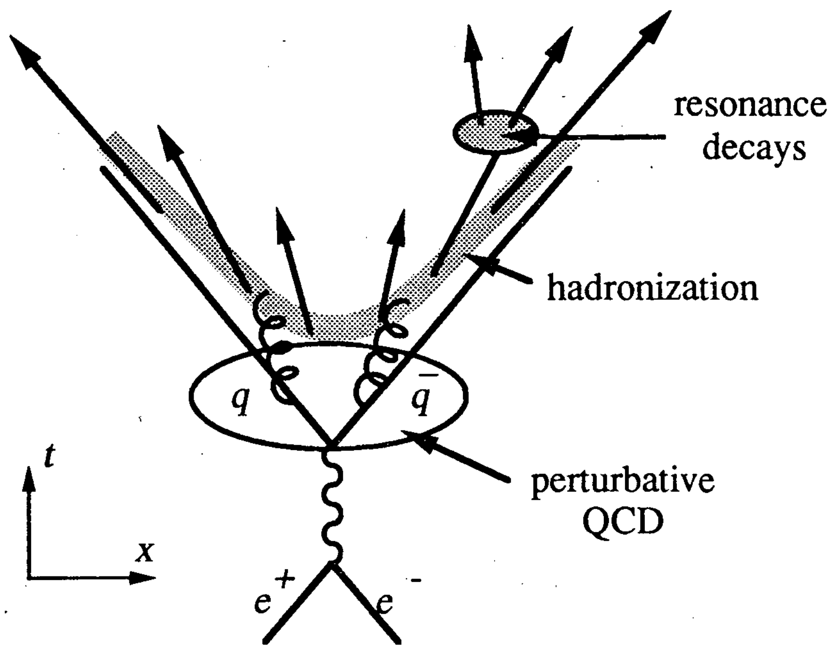

Figure 2.2: Illustration of different stages of hadron production in e^+e^- annihilation.

turn emit more gluons, there is less energy available per parton, and eventually the energy transfers become too small for perturbation theory to be valid.

Hadronization models are necessary to describe the evolution of the event past the point where perturbation theory is no longer useful. The point at which it is no longer appropriate to describe the process in terms of partons is not well defined and depends somewhat on what hadronization model is used. The purpose of fragmentation models is to describe the process by which an initial configuration of high energy partons, as described by perturbative QCD, is transformed into the final primary hadrons. Some of these hadrons may be resonances that decay, a process that is well understood for the most part. Although several hadronization models exist, most of the current attempts at understanding Bose-Einstein correlations have started with the string picture, so we will discuss that model in some detail.

2.2.1 The String Picture of Hadronization

Consider a simple system of a $q\overline{q}$ pair, each particle with relativistic momentum. Since quarks have color charge, the $q\overline{q}$ system will be joined by color field lines. In a theory in which confinement occurs, it is necessary that the force on each quark due to this field does not vanish if the $q\overline{q}$ pair is infinitely separated. This is possible if the field lines are confined to a thin tube of flux of constant diameter, so that the energy per unit length of the tube is independent of the separation of the particles. It is reasonable to expect such a flux tube to arise in QCD because of the ability of the gluon field to self couple and thus shield the flux tube field from the surrounding vacuum.

If a second $q\overline{q}$ pair is produced within the flux tube, the color charge of this pair can be such as to shield the color field in the region between the pair. The energy of the field that would exist in that region is then used to provide the energy in the mass and transverse momenta of the quarks; therefore, the quark pair must not be produced at a point but be produced with some separation. This is possible because of quantum tunneling of the quark wave function into the classically excluded region. Quark pair production allows the flux tube to break down in several places along its length. Eventually the segments of $q\overline{q}$ pairs connected by flux tubes all form mesons that are stable to further decay. Within this simple picture of hadronization, it is possible to understand many of the observed features of hadrons produced by e^+e^- annihilation, such as the limited momentum distribution transverse to the axis of the event, and the suppression of heavier flavored mesons, except for those containing the leading quark [Cas79].

The flux tubes described so far are presumed to have some finite radius; however, physical properties of the final particles do not seem to depend on this radius as long as it is restricted to reasonable limits. A description of hadronization based on a classical string with no transverse dimension is found to be quite successful. A description of hadronization based on strings was first explored by Artru and Mennessier [Art74]. They assume that the $q\overline{q}$ pair is connected by a string with tension κ (κ is typically typically taken to be 0.2 GeV^2), that the string can break by the production of a $q\overline{q}$ pair, and that the probability for such a break to occur in a region of space-time $\Delta x \Delta t$ is $P_0 \Delta x \Delta t$. Such breaks can, of course, only occur where the string still exists, and cannot occur in the forward light-cone of a previous break. The distribution of the $q\overline{q}$ vertices is found to be exponential in the variable $\Gamma = \kappa^2(t^2 - x^2)$, where Γ is a measure of the time for the production of a $q\overline{q}$ pair, as measured in the local rest frame of the string.

$$dP/d\Gamma = b \exp(-b\Gamma),$$

with $b = P_0/2\kappa^2$. This simple model is inadequate in itself, however, since it leads to mesons with a continuous mass spectrum (since the quark production points are independent).

The Lund group has developed a model using an iterative process of string fragmentation that is quite successful in simulating real data [And83]. We first describe how the meson is modeled (production of baryons is described by the model, but will not be discussed here since baryon production is not important to the subject of this thesis). As two quarks separate, their kinetic energy must decrease to provide the energy stored in the field. Eventually the kinetic energy of a quark will approach zero and the quarks will reverse direction. (This will happen simultaneously in the center of mass of the system.) The meson is sometimes referred to as a "yo-yo" in this model, as suggested by the space-time

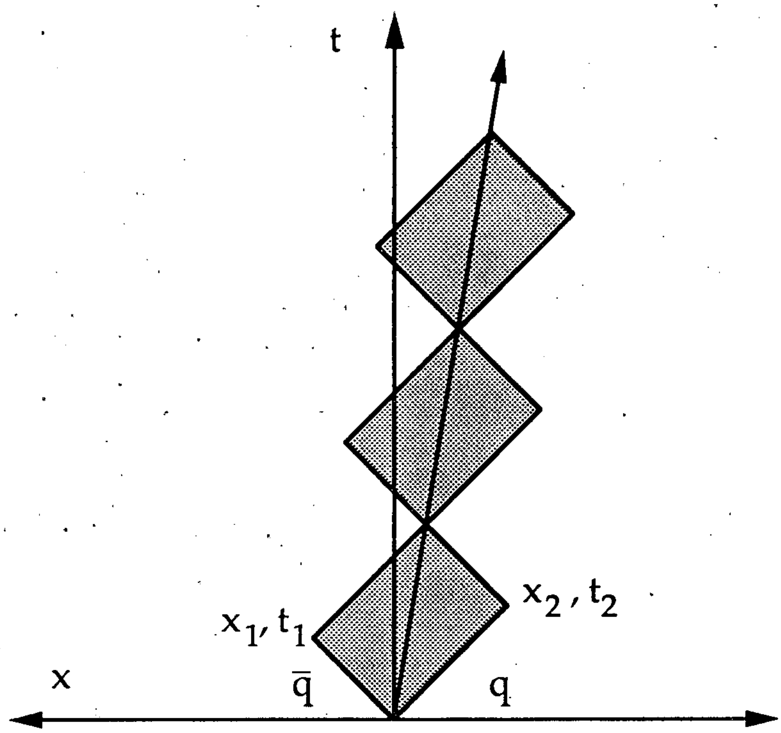

Figure 2.3: Diagram of meson as described in string model. x_i, t_i represent turn around points of quarks.

trajectories of the quarks (Fig. 2.3). If we ignore the mass of the quarks and any possible transverse degrees of freedom, the turn around points of the quarks are simply related to the energy and momentum of the meson,

$$E = \kappa|x_1 - x_2|, \quad p = \kappa(t_2 - t_1), \tag{2.20}$$

so that if m is the mass of the meson,

$$m^2/\kappa^2 = (x_1 - x_2)^2 - (t_1 - t_2)^2. \tag{2.21}$$

Fragmentation of the string occurs when a new pair, $q_1\overline{q}_1$, breaks the string by tunneling, as described earlier. When such a break occurs, there can be no more pairs produced in the forward light-cone of that pair; therefore, all quark pairs that are produced in the fragmentation of the string are space-like separated. Except near the ends of the string, the probability for the string to break depends only on the time since the initial $q\overline{q}$ pair was created, time being measured in the local rest frame of the string. In the lab frame, the string will most likely first break near its center, where the string is at rest, with breaks closer to the leading quark and anti-quark occurring later, because of time dilation. This process is pictured in Fig. 2.4(a). This feature is called inside-out production of hadrons. We can, however, always transform to a reference frame where the first break in time occurs adjacent to the leading quark on one end of the string (Fig. 2.4(b)). The new $\overline{q}_1$ combines with the leading q to form a meson. The Lund model chooses the transverse momentum with the assumption of an exponential distribution of the square of the transverse mass (defined as $m_\perp^2 = m^2 + p_\perp^2$). This distribution, $\exp(-m_\perp^2/\sigma_\perp^2)$, is what one would expect from a WKB quantum tunneling calculation. The flavour content of the $q\overline{q}$ pair as well as the angular momentum of the produced momentum are randomly chosen from a distribution based on parameters of the model.

At this point, the longitudinal momentum of the meson is still not determined. By assuming that the string provides the energy for the transverse mass of the produced meson, the production point of the $q_1\overline{q}_1$ pair is determined (as in Eqn. 2.21) to be on a hyperbola: $x^2 - t^2 = m_\perp^2/\kappa^2$. Because of the relationship between the space-time and momentum representation of the string (as in Eqns. 2.20), determination of the production point along this hyperbola determines the longitudinal momentum of the produced meson. Defining the quantity $p^+ = E + p_l$ for the leading quark, the meson that contains the leading quark will carry some fraction, z, of p^+. With this definition, z is invariant to boosts along the string direction. The distribution function for z, $f(z)$, is related to the the probability for the string to break up, and can have a variety of forms. If, however, we require that the distribution of hadrons does not depend on which side of the string we begin fragmentation, *i.e.* if the fragmentation is symmetric, then it can be shown [And83] that there is only a limited class of possible distribution functions of z. These functions can be expressed as (to be called the Lund symmetric fragmentation function):

$$f(z) = N\frac{z^{a_\alpha}}{z}\left(\frac{1-z}{z}\right)^{a_\beta} \exp -(bm_\perp^2/z). \tag{2.22}$$

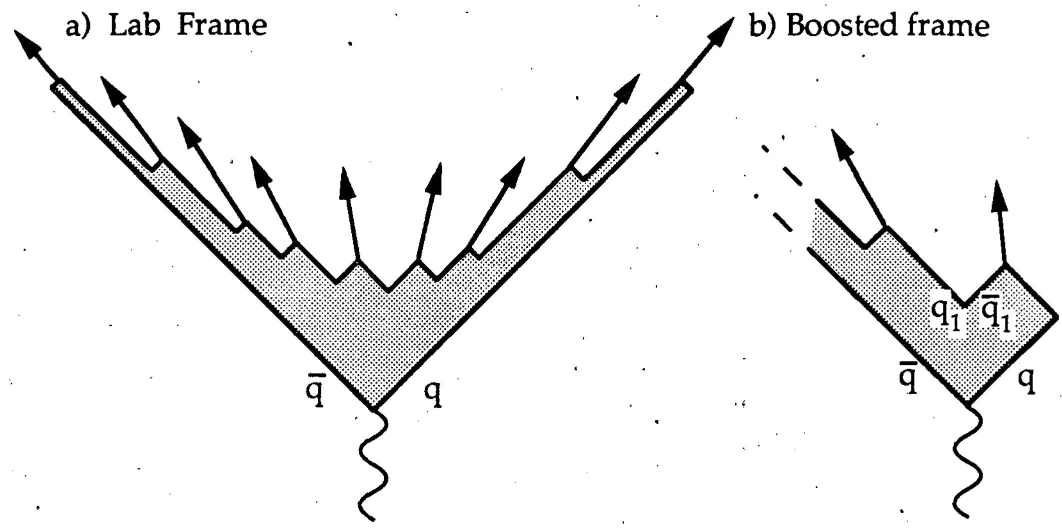

Figure 2.4: Break up of Lund string during hadronization. a) in laboratory frame of reference. b) in boosted frame.

α and β indicate the flavour of the quark and anti-quark. In practice it is generally not necessary to use different values for a_α for each flavour. Like the Artru-Mennessier string model [Art88], the symmetric fragmentation function implies that the probability for the production of some n particle configuration is suppressed by an exponential of the space time area enclosed by the string field (A_n):

$$dP_n = \left(\prod_j N dp_j \delta(p_j^2 - m_j^2)\right) \delta(\sum_j p_j - P) \exp(-bA_n), \qquad (2.23)$$

with P the total four momentum of the state.

2.3 Bose-Einstein Correlations in e^+e^- Annihilation

The picture of hadron production provided by the string model as described above reveals several areas where the traditional description of Bose-Einstein correlations may not be appropriate. Within this picture, where hadronization occurs via breaking up of the string, the concept of a production point is somewhat ambiguous. The quarks that make up a meson are themselves produced at separate points in space and time, and this separation may be comparable to the "size" revealed by the analysis of the Bose-Einstein correlation function. One must ask if one is measuring the distribution of production points of mesons, or the amount of ambiguity in the position of the production point. The interpretation of Bose-Einstein correlations as a measure of the spatial distribution of particle sources should probably not be taken with the same seriousness in the instance of e^+e^- annihilation as it is in the physics of heavy nuclei, or in the measurement of star sizes. In any event, the appropriate description will certainly require a departure from the picture of a static distribution of current sources emitting hadrons.

With the proviso made above, we can arbitrarily define the hadron production position as the point at which the two quark lines of a meson first meet in x–t. With this definition, the time for meson production in the local rest frame of the string, τ, is typically on the order of $1/\sqrt{\kappa}$. In the lab frame of reference, the hadron production points on the average lie on a hyperbola, $t^2 - x^2 = \tau^2$. This also implies that there is a strong correlation between the longitudinal momentum of a hadron and the point where it was produced. This strong correlation of source position with momentum has important consequences for the observation of Bose-Einstein correlations, as observed in Refs. [Pra84,Bow85,And86]. Since mesons that are produced near opposite ends of the string are very unlikely to have similar momentum, they will contribute only slightly to Bose-Einstein enhancement. The observed Bose-Einstein enhancement will only be important for particles coming from regions of the string in which the momentum spectrum overlaps substantially. Measurement of the correlation function does not provide information about the spatial extension of the string in the longitudinal direction. Instead it reveals the distance at which the momentum spectrum no longer overlaps for particles emitted from different portions of the string.

Because of the connection between the quark space-time production points and the momentum of the produced hadron, the departure of perfect correlation between momentum and position is equivalent to the departure of the production points from the hyperbola in x–t, or from the variation in the time for particle production in the rest frame of the string. Therefore, we would expect the variation in momentum of particles from a portion of the string will be about equal to $1/\tau$, so that the longitudinal "distance" measured by the Bose-Einstein correlation function is expected to be about equal to τ. If one imagines the limited transverse momentum of hadrons to be attributed to the transverse size of the flux tube (by the uncertainty principle), then this size is also given by τ. There is therefore no reason to expect the source to appear elongated in the direction of the jet axis even though the separation of production points may be up to 30 fm for a 29 GeV $q\overline{q}$ system. Our experiment has in fact previously observed that, in e^+e^- physics, the source as measured by Bose-Einstein correlations is not significantly extended in the jet direction [Aih85b]. Does this picture then lead us back to the traditional picture of a static spherical source described in Sect. 2.1 ? Not quite, because we still must consider the relativistic motion of the source of the hadrons. The consequences of the relativistic dynamics of hadron production are most easily understood by examining a model for Bose-Einstein correlations in string fragmentation.

2.3.1 String Based Models for Bose-Einstein Correlations

A simple approach to incorporating Bose-Einstein correlations into a string hadronization model is to assume a reasonable definition of the hadron production point, such as that given above, then to use one of the string models to determine the distribution of these points. One can take this distribution to be the source density of hadron emitters and apply the traditional treatment of correlation functions described in Sect. 2.1. The string model describes the relativistic production of hadrons along the the $q\overline{q}$ (or jet) axis; therefore, the correlation function obtained in this way will no longer have the properties of the traditional static source distribution described by Eqn. 2.6. This is essentially the method used by Bowler [Bow85], where he finds a correlation function that depends upon the the longitudinal variable, $Q_L^2 \equiv \mathbf{q}_L^2 - q_0{}^2$, which is invariant to boosts along the jet axis, and also upon $Q_T^2 \equiv \mathbf{q}_T^2$ (the subscripts T and L refer to the jet axis):

$$R(Q_L, Q_T) = 1 + A\left[\frac{1}{1-[\beta_L^2 Q_L^2]}\ln(\beta_L|Q_L|)\right]\exp(-\beta_T^2 Q_T^2). \qquad (2.24)$$

The factorization of the enhancement term into a parts depending on Q_L and Q_T is an artifact of the independence of longitudinal and transverse dimensions in the string treatment of hadronization and is not expected to be valid. The order of magnitude of β_L and β_T are both determined by the hadronization scale; thus, as we had suggested earlier, the range of correlations transverse to the jet is about the same as that along the jet. (β_L is closely related to the string breakup probability, P_0, while β_T is related to the string tension, κ.)

The conceptual problem of whether the space-time production points of hadrons are well defined in string fragmentation models led Andersson and Hofmann to take a different approach [And86], which nonetheless arrives at a result similar to that of Bowler. In order to avoid the difficulties of defining the production points of hadrons, Bose-Einstein interference is described entirely in terms of the momentum representation of the produced hadrons. We have already noted (Eqn. 2.23) that the probability to produce a given configuration of hadrons is determined by the area in space-time that is swept out by the string, A. The model of Andersson and Hofmann is based on the hypothesis that the amplitude for a final particle configuration with area A is to be given by,

$$\mathcal{M}_0 = \exp(i\xi A), \tag{2.25}$$

with ξ being a complex spring tension that can be written,

$$\xi = \kappa - i(b/2), \tag{2.26}$$

and that the area law found for the probability is due to the complex term of the string tension. This amplitude is suggested by assuming a classical string action for a string of area A [Art88], or similarly is suggested by amplitudes derived from Wilson loops of lattice gauge theory [Wil74]. The area swept out by the string, A, can be expressed in terms of the momenta of the hadrons if their order of production along the string is known, making use of the relationship of hadron momentum and quark production points. We can thus describe the amplitude for the process without having to refer to production points of the hadrons themselves.

If this hypothesis for the amplitude is correct, then interference between identical bosons will arise from the requirement that the amplitude be symmetric upon permutation of the identical bosons. Changing the order in which particles are produced results in a configuration with a different area for the string, as is illustrated in Fig. 2.5. The symmetrized amplitude is,

$$\mathcal{M}_s = 1/\sqrt{2}\left(\exp(i\xi A(1,2)) + \exp(i\xi A(2,1))\right), \tag{2.27}$$

where $A(1,2)$ represents the area when the particles are unpermuted and $A(2,1)$ with particles 1 and 2 permuted. The probability to produce a configuration is enhanced by an interference term that is constructive if ΔA, the difference in the space-time area swept out by the string after permuting identical bosons, is not large. This will be the case if the momentum of the bosons is about the same. ΔA depends on the momenta of the pair of exchanged particles and also on the momentum of particles produced between them along the string. It is approximately true that $\Delta A \sim Q_L^2/\kappa$ for the pair.

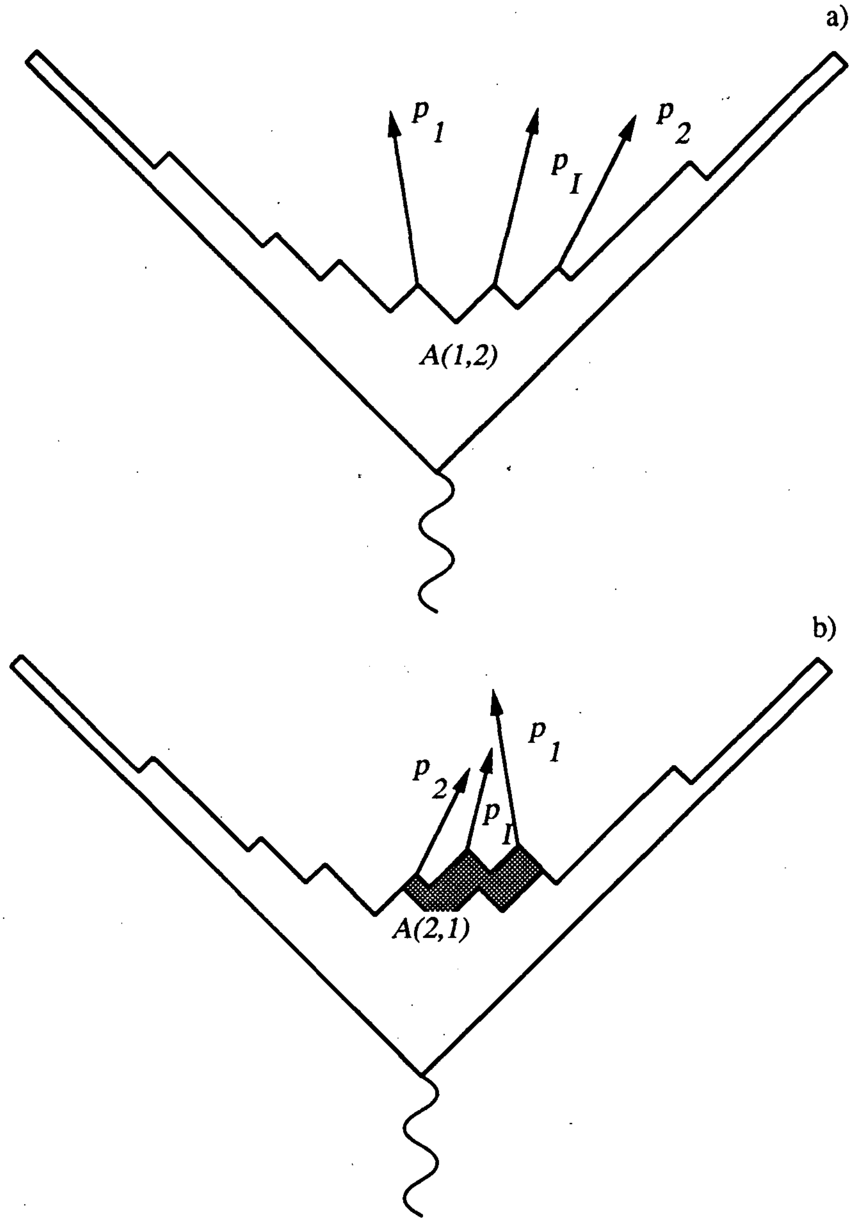

Figure 2.5: Space-time area swept out by string. a) Non-permuted particles. b) Particles 1 and 2 permuted, resulting in an increase in area.

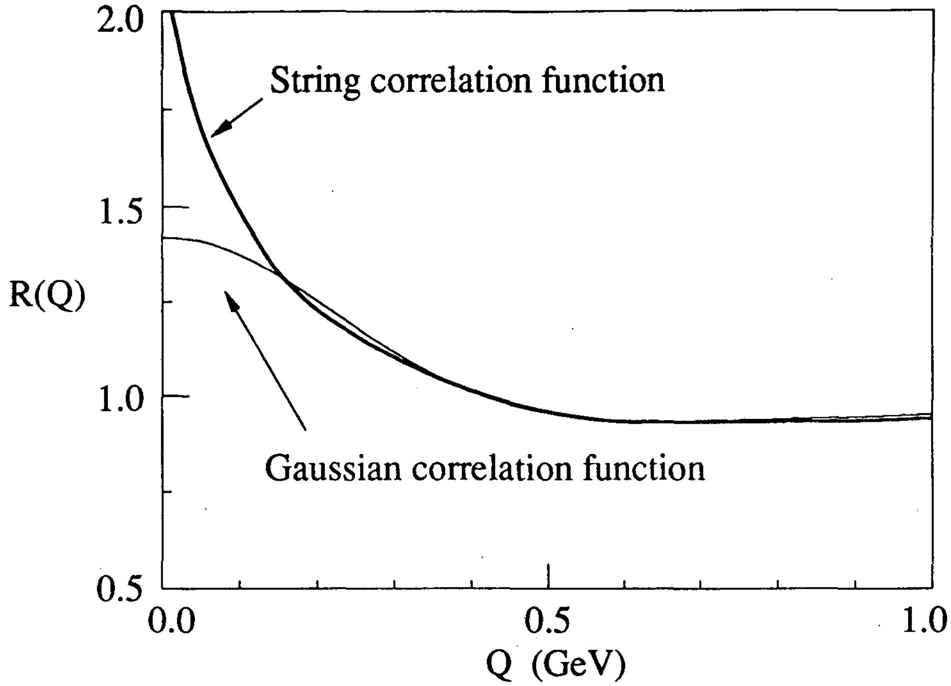

Figure 2.6: Correlation function computed using the string model of Andersson and Hofmann. For comparison, a correlation function of Gaussian shape is also shown.

To compute the expected correlation function, one generates Monte Carlo events using the Lund model, and for each pair one computes the expected enhancement due to Bose-Einstein interference. This enhancement is

$$\frac{|\mathcal{M}_s|^2}{|\mathcal{M}_0|^2} = 1 + \frac{\cos(\kappa \Delta A)}{\cosh(b\Delta A/2)}. \tag{2.28}$$

The enhancement can in this way be computed as a function of a relative momentum variable for the pair, such as Q^2. Such a computation is done in Ref. [And86]. Transverse effects of the string are also included which result in correlations of about the same range as in the longitudinal direction. The resulting correlation function is similar to that obtained by Bowler. The correlation function, computed as a function of Q, is found to be somewhat more peaked at low Q than a gaussian shape (see Fig. 2.6), as is Bowler's expression. Most notable, however, is that because the relativistic motion of the string is implicitly part of this model, the correlation does not decrease for pairs that have large q_0.

The most significant result of both of these models is that the relativistic development of hadronization must be taken into account in describing Bose-Einstein correlations of high energy particles. The correlation scale in both of these models tends to be about equal in both the transverse and longitudinal direction; thus, it would be reasonable to hypothesize that a correlation function that depends only on the invariant $Q^2 \equiv |\mathbf{q}|^2 - q_0{}^2$ would give a good description of the data. A simple expression that has qualitatively similar features to the expected correlation function is,

$$R(Q) = 1 + \exp\left(-r^2 Q^2\right), \tag{2.29}$$

which has in fact been traditionally used (though with little theoretical justification) to describe e^+e^- data. The notable difference between this and the correlation function for a static distribution of sources, Eqn. 2.6, is that the enhancement can no longer be factored into decreasing functions of q_0 and $|\mathbf{q}|$ because of the inherent relativistic nature of the hadronization process.

In order to qualitatively compare this prediction with what is expected based on a static distribution, let us consider a correlation function similar to Eqn. 2.7, but with the q_0 dependence in its general form, as a (possibly slowly) decreasing function of q_0. The correlation function is then:

$$R(q) = 1 + \exp(-r^2 |\mathbf{q}|^2) |g(q_0)|^2, \tag{2.30}$$

which can be rewritten as,

$$R(Q, q_0) = 1 + \exp(-r^2 Q^2) \exp(-r^2 q_0{}^2) |g(q_0)|^2. \tag{2.31}$$

If q_0 is large compared to $1/r$, the correlations would be suppressed even for $Q^2 \to 0$; this is true independent of the form of $g(q_0)$ as long as it is a decreasing function. A realistic model that takes the relativistic motion of the sources into account would predict that the correlations should only depend on the relativistic invariant Q^2. It is therefore interesting to measure the correlation function as a function of Q in bands of q_0 in order to determine if the correlation drops off strongly with q_0 as the simpler static models would predict, or if the correlations are visible even when q_0 is large. Pairs of particles having small momentum difference in their own rest frame will nevertheless have large q_0 if they are boosted. This measurement is the main result of this thesis.

Chapter 3

The TPC/2γ facility at PEP

The results of this thesis were based on data collected using the TPC/2γ experiment at the PEP storage ring, which is located at SLAC. This chapter provides a brief description of PEP and the detectors that make up the TPC/2γ experiment.

3.1 Description of PEP

The PEP storage ring provides positron and electron collisions at 29 Gev Center of Mass Energy at six different interaction regions. The electrons and positrons are accelerated to an energy of 14.5 GeV by the two mile long Stanford Linear Accelerator and are each injected into the storage ring in three separate bunches, the three electron bunches rotating counter to the direction of the three positron bunches. Bunches collide at each interaction region with a spacing of 2.45μs between beam crossings. A typical luminosity of $(1.–2.)\times 10^{31}$ cm^{-2}s^{-1} was achieved during our running.

3.2 An Overview of the TPC/2γ Facility

TPC/2γ was designed with the goal of being a general purpose detector providing complete identification and measurement of as many of the particles produced in e^+e^- collisions as possible. Many specialized subsystems are required in order to accomplish this goal. Figure 3.1 shows the components that make up TPC/2γ (excluding forward detectors). The following detectors are a part of TPC/2γ:

IDC: The Inner Drift Chamber [Aih83b] is a four layer drift chamber originally intended to aid in measuring track position and to provide a fast trigger for TPC/2γ. Unfortunately, because of degraded resolution, it has not been useful in providing tracking information, but has been an important part of the trigger. The IDC, TPC and PTC all reside in the same high pressure gas volume (8.5 ATM of 80% Argon and 20% Methane).

TPC: The Time Projection Chamber [Mad84] is the central tracking chamber. The TPC measures particle trajectories and provides particle identification

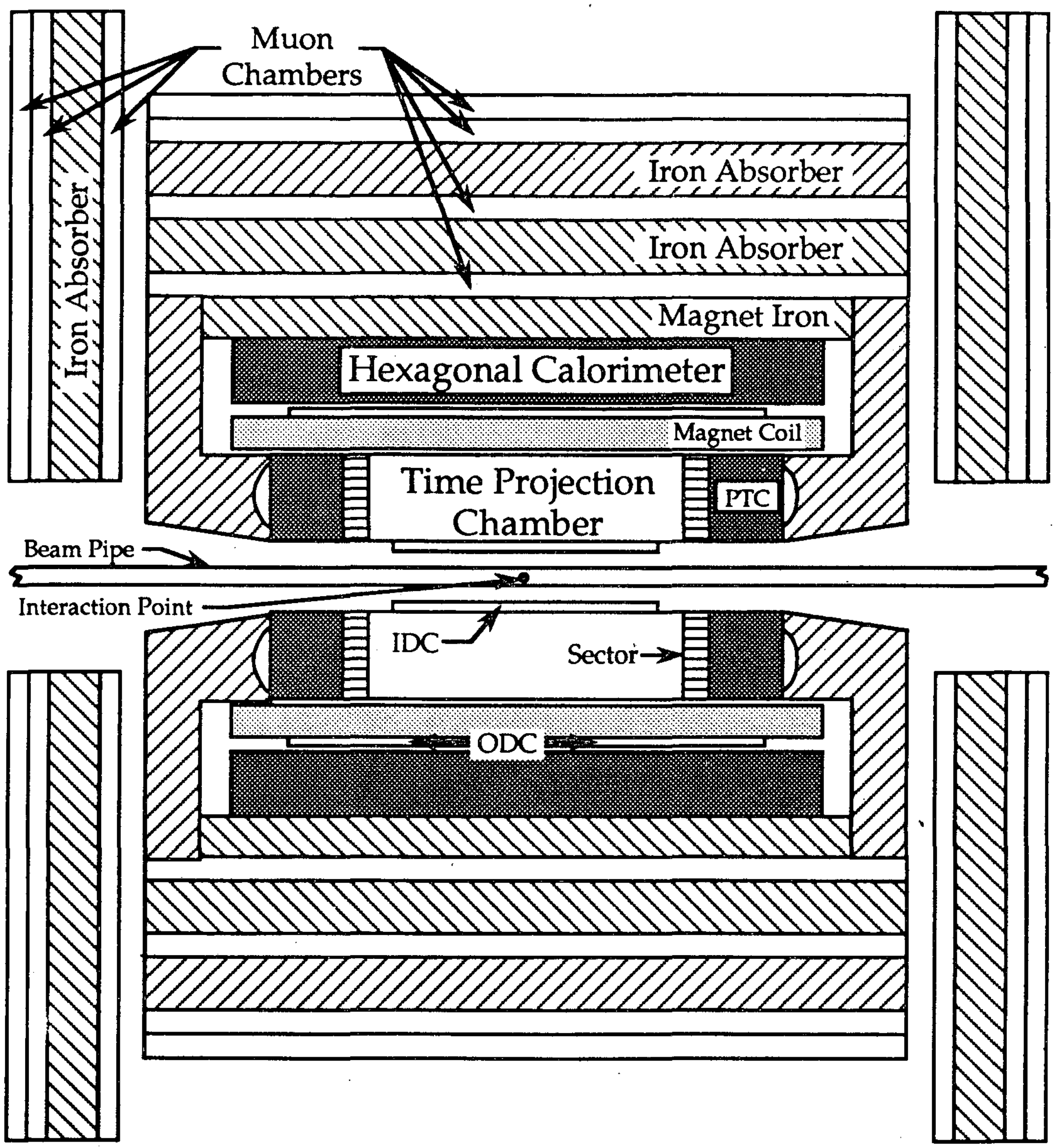

Figure 3.1: TPC/2γ facility excluding the forward detectors.

by measuring the energy loss of particles. The TPC is surrounded by a superconducting magnet that provides a 13.25 kG field, allowing the momentum of the detected particles to be measured. Before our 1984 upgrade a 4 kG conventional coil was used. The TPC will be discussed in detail in the next section.

ODC: The Outer Drift Chamber [Aih83b] is a three layer drift chamber similar to the IDC, operating in 1 ATM of 80% Argon and 20% Methane. Like the IDC, it is not used for tracking, but is used for triggering. It is also used to tag photons that convert in the coil.

PTC & HEX: The Pole Tip Calorimeter and the Hexagonal electromagnetic calorimeter measure the energies of electromagnetic showers originating from photons and electrons.

The PTC [Buc82] resides in the TPC high pressure gas volume and consists of alternating layers of lead absorber and gas proportional wire chambers. Typical resolution is $\sigma_E/E = 11\%/\sqrt{E}$ below 10 GeV and 6% at 14.5 GeV.

The HEX [Aih83a] electromagnetic calorimeter surrounds the coil and ODC. It consists of layers of lead absorber and gas sampling wire chambers operating in geiger mode. Three projective views are provided by the wire plane and the two surrounding cathode planes, which are segmented into strips. A resolution of $\sigma_E/E = 17\%/\sqrt[4]{E}$ is achieved.

Muon Chambers: The Muon chambers [Aih83c] make use of 90 cm of steel for the barrel detector and 50 cm of steel for the endcap detector to act as a hadronic absorber. This steel also serves as flux return for the magnet. The muon chambers are triangular shaped wire drift chambers, achieving spatial resolution of 700 μm.

2γ detectors: In addition to the above, a full set of detectors exists in the forward and backward directions. These are not shown in Fig. 3.1 and are described elsewhere (see Ref. [Cai84]). The purpose of these detectors is to tag two photon events, in which there is typically a low angle electron produced, and to provide low angle coverage for particles produced in these events.

Since the results of this thesis primarily involve the TPC detector, it will now be described in more detail.

3.3 The Time Projection Chamber

The TPC is the central tracking chamber of the TPC/2γ experiment. The TPC was designed to serve two important purposes. First, it provides accurate tracking of the charged particle trajectories in three dimensions. A good measurement of particle momentum is then obtained by measuring the track curvature in the

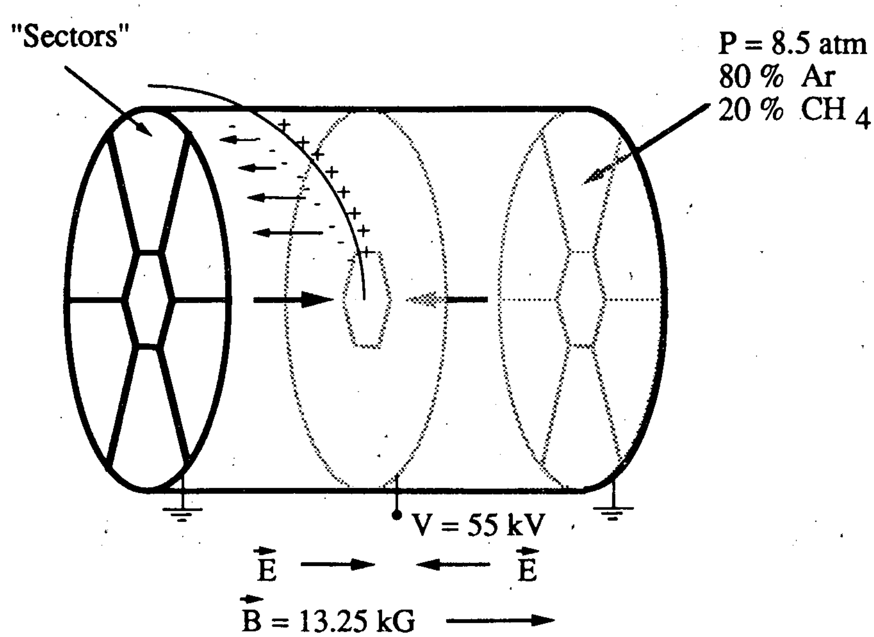

Figure 3.2: Schematic view of the TPC. Electrons drift from track towards sectors at each end cap.

13.25 kG magnetic field in the TPC volume. Secondly, the TPC provides a measurement of a particle's energy loss due to ionization (dE/dx). This measurement, when combined with the momentum measurement, provides particle identification over a large range of momenta.

3.3.1 Principles of Operation

Figure 3.2 schematically illustrates the principles by which the TPC measures charged tracks. The volume of the TPC is filled with a high pressure (8.5 ATM) mixture of 80% Argon and 20% Methane gas. A charged particle that traverses the gas volume leaves in its path a trail of ionization (typically 200 electron-ion pairs per cm are produced for a minimum ionizing particle). A highly uniform axial electric field produced by a central membrane at high voltage causes the electrons to drift towards the endcaps. The magnetic field, parallel to the electric field, limits the amount of transverse diffusion of the electrons; thus, good position resolution is possible even after long drift distances (up to 1 m). At the endcaps, the ionization is collected and measured by multiwire proportional chambers. These endcap chambers are divided azimuthally into six sectors.

The 183 proportional wire cells on each kite shaped sector (shown in Fig. 3.3) measure the amount and the radial position of ionization from a track. Underneath 15 of these sense wires, the cathode plane is segmented into a row of pads. As they drift to the region of high field near the sense wire, the ionization electrons create an avalanche of electron-ion pairs. The avalanche also induces a signal on several of the cathode pads underneath the wire. The pad signals directly measure the position of the initial ionization in the plane perpendicular to the beam direction (the x–y plane). The drift time of the ionization then measures the position of points along the track in the z-direction. The TPC thus measures up to 15 points on track, in all three dimensions, allowing full reconstruction of the track's trajectory.

Most of the sense wires are not in the vicinity of a pad row. The signals from these wires each measure the number of ionization electrons, hence the energy loss, along approximately 4mm of the track's path. Having many independent measurements of the track's energy loss allows measurement of the dE/dx distribution for the track. This measurement is used in conjunction with the momentum measurement to identify the track.

3.3.2 Field Uniformity and Field Cage Modification

A high degree of field uniformity is required if the position as measured at the endcap is to reflect true position of charge deposition along the original track. The electric field within the TPC is defined by the central membrane at the midplane, held at high voltage, an inner and an outer radius field cage, over which the potential is linearly graded, and the endcaps, essentially at ground. The outer field cage is the cylindrical outer boundary of the TPC volume, and the inner field cage is hexagonal, forming the inner boundary of the TPC volume. The inner and outer radius field cage each consists of a fine field cage, on the surface facing the TPC volume, and a course field cage layer underneath the fine field cage. The course field cage shields the inner field cage (and the TPC volume) from the strong field in the surrounding insulator, where the transition from the field in the TPC to the surrounding ground is made. Each field cage consists of Nema G10 on which a series of copper rings has been etched. Each successive ring is held at its proper (linearly graded) potential by being connected to the high voltage system through a resister chain.

During the first running cycle (before the upgrade in 1984), the measured trajectories of tracks were highly distorted. These distortions were found to be primarily due to non-uniformity in the electric field. One source of this non-uniformity was that positive ions, produced during the avalanche process at the sense wire, would drift back into the TPC volume, resulting in the accumulation of space charge in the TPC. This problem was solved by installation of a gated grid system described in Sect. 3.3.4. The other important source of non-uniformity was the fine field cage. Regions of anomalous conductivity within the G10 result in local distortion of the field. During the upgrade, a uniform resistive coating was applied to the field cage [Mar82]. This results in a uniform current

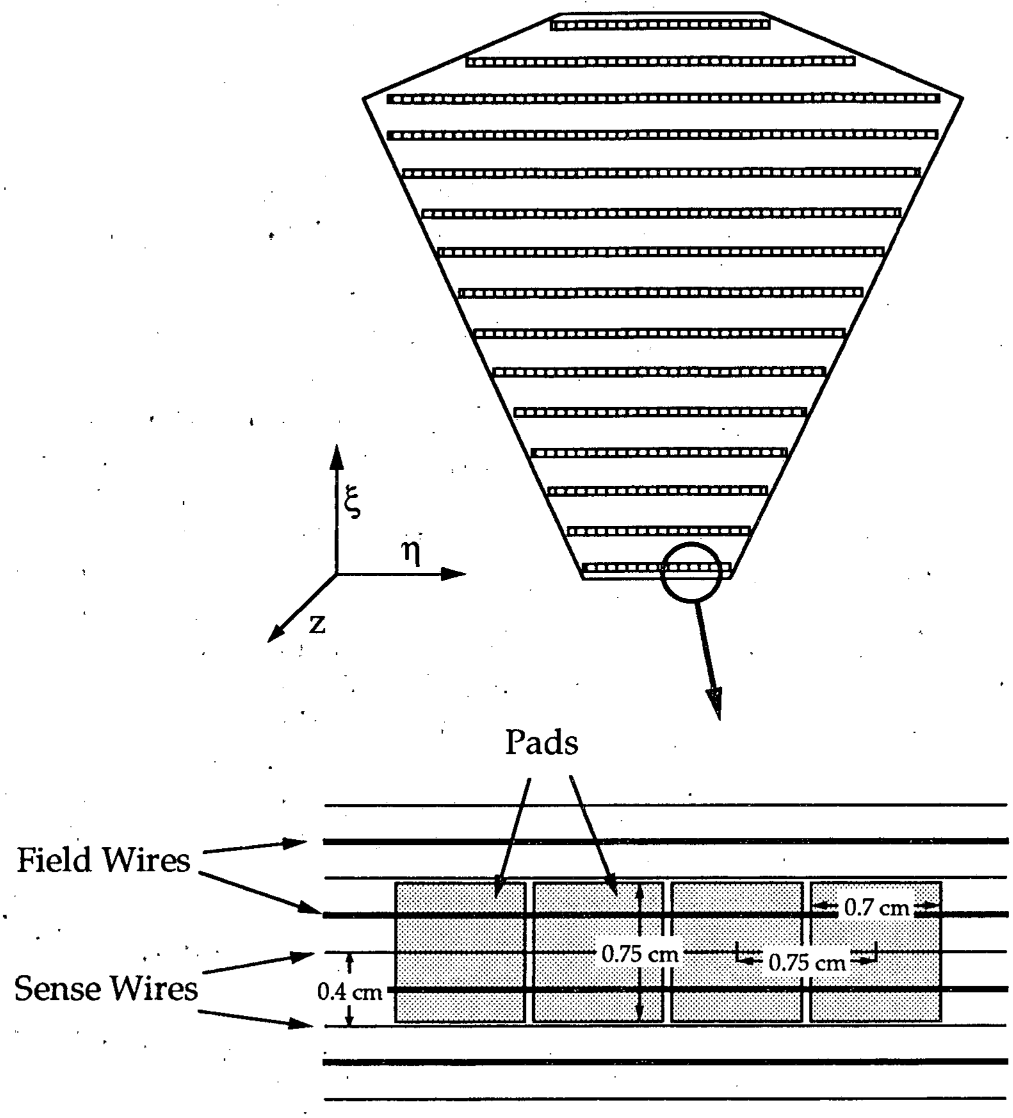

Figure 3.3: A TPC sector. Configuration of pad row

flowing between the rings, maintaining the surface at the correctly graded potential. The resistor chain still sets the potentials of the rings themselves, since the resistive coating provides an inter-ring resistance much higher than that of the resistors.

3.3.3 TPC Sectors

A prime consideration in the design of the TPC sectors [Fuz84] and of the accompanying electronics [Aih83d] was to insure that systematic variations in the measurement of dE/dx were kept below the level of 1%. This is necessary in order to obtain dE/dx resolution sufficiently low to statistically separate π,K, and P by dE/dx measurement at high momentum. Wire planes are positioned with high accuracy (to within 20 μm). The wire geometry for a few cells of a sector is illustrated in Fig. 3.4. The sense and field wire plane is separated from the main TPC volume by a grounded shielding grid and by the gated grid, which is discussed in the next section. Sense wire and field wire voltages were chosen so as to provide a suitable gain, such that the signals are proportional to the number of ionization electrons, and so as to maintain wire stability. Wire gain is typically 10^3, resulting in a signal of 10^5 electrons at the sense wire. Sense wires are capacitively coupled to low noise preamplifiers mounted on the back of the sectors. Field wires are capacitively coupled to ground, in order to prevent cross talk between sense wires. Wire gain is strongly sensitive to pressure and temperature variations; however, the preamplifiers, which are mounted asymmetrically on the back of the sector, would cause large temperature variations across the sector if the heat of the preamplifiers were not removed. A water cooled system of aluminum bars between the preamplifiers and the ground plane of the sector cools the preamplifiers and shields the wire plane from heat produced by the preamplifiers. The temperature of the wire plane is kept constant to within 1°C. Calibration must remove remaining gain variations.

3.3.4 The Gated Grid

Even with the modest gain of the TPC sense wires (10^3), a significant number of positive ions are produced and escape into the TPC volume. Before the Gated Grid was installed (during the 1984 upgrade) typically 40% of the positive ions would enter the TPC volume, the rest being caught by the shielding grid, by the field wires or by the cathode plane. The space charge of these ions would cause track distortions as large as 1 cm. The gated grid acts as an electric shutter to capture these ions before they can escape into the TPC volume [Nem83]. The gated grid wires are spaced 1 mm apart, and are 8 mm above the shielding grid, as shown in Fig. 3.4. The wires of the grid are alternately ganged to two independently controlled potentials. While the TPC is waiting for an interesting event, the grid is in the "closed" state. The potential of the wires is set to $V_{ref} \pm \Delta V$, the sign alternating for each wire. The field lines, from both sides of the grid, all terminate on a grid wire (as seen in Fig. 3.4(b). When interesting

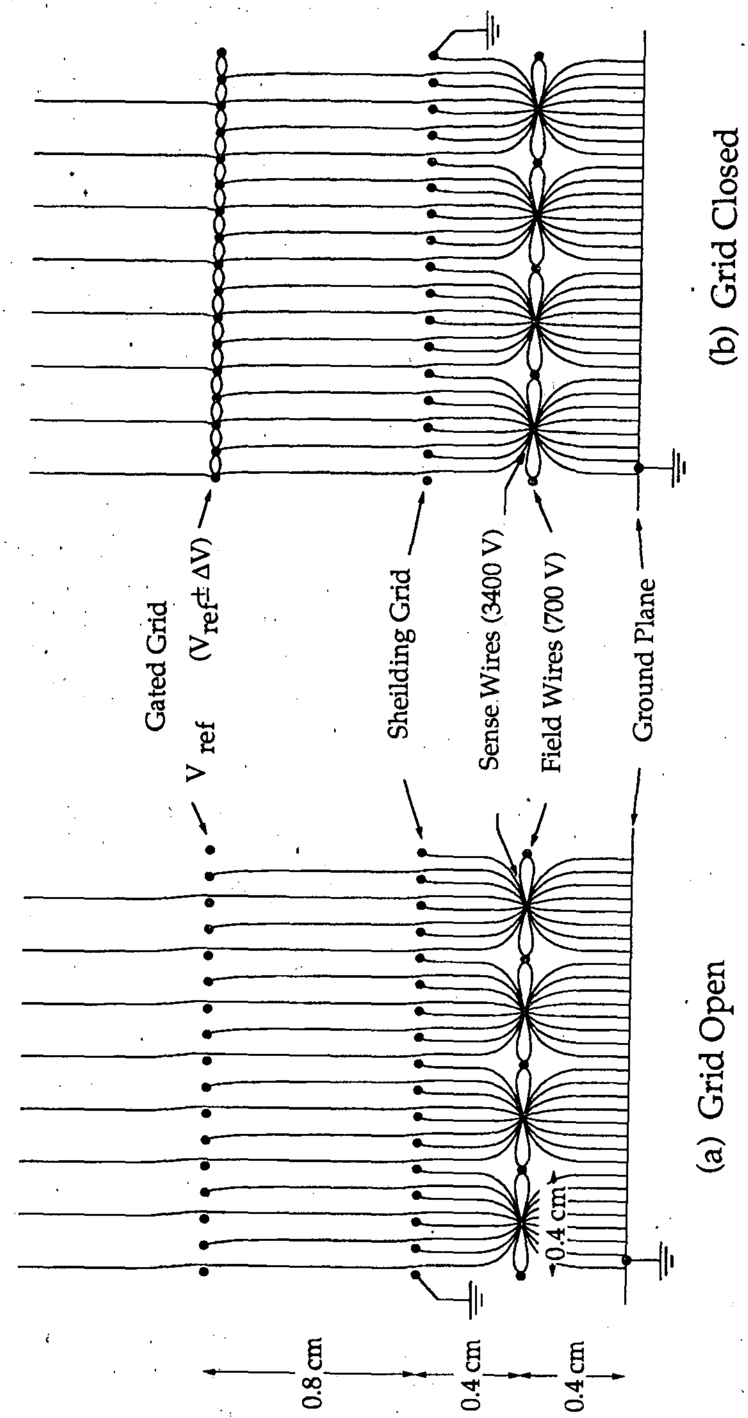

Figure 3.4: Sector wire geometry. Field lines are shown for the gated grid in its open (a) and in its closed (b) state.

data exists in the TPC, the grid switches to an "open" state; the potentials of all of the grid wires switch to V_{ref}. We choose the potential V_{ref} so that the grid is transparent to electrons drifting from the TPC volume (the condition for this to be true is that the field inside the grid is twice the field in the TPC volume). The grid closes again after all drift electrons have had time to be collected. Ions move very slowly, taking about 1 ms to reach the grid. They follow the field lines of the closed grid, and are trapped by the grid wires.

The rapid switching of the gated grid potentials from the closed to the open state inevitably affects the output of the sense wire. We must control the amount of pickup resulting from this switching so that the pickup does not cause biases in the measurement of particle dE/dx. We will see a signal on the sense wire if either the initial voltage on the two grids is unbalanced, or the capacitance between each grid to the sense wire is unbalanced. The pulser that switches the voltages provides well balanced pulses, and allows each pulser to be tuned by a tunable output filtering stage to compensate for capacitance mismatch of the gated grids. We have evidence that this capacitance mismatch is largely caused by unequal electrostatic displacement of the two grids in the drift field. The force on each grid in the closed state is not equal, since they are at different potentials [Hut84]. We minimize the pickup on the sense wire caused by this mismatch by keeping V_{ref} and ΔV as small as possible. This was part of the motivation for operating the TPC at lower field in the upgraded detector (50 kV as opposed to 75 kV). Typically 1 μs after the grid has been pulsed, the amount of pickup on the sense wire has been reduced to an acceptable level.

The data used for this thesis was taken with the following operating voltages for the gating grid and TPC high voltage membrane:

Running period	High Voltage	V_{ref}	ΔV
1982–84	-75 kV	no gated grid	
1985	-50 kV	-830 kV	90 V
1986	-55 kV	-910 kV	90 V

With these parameters the grid in its closed state was found to transmit approximately 10–15% of the electrons produced in the TPC volume. The grid is not completely opaque because the electrons do not simply follow the electric field lines, but are deflected by the magnetic field, allowing some electrons to pass. The magnetic field has much less effect on the more slowly moving ions, and the grid is essentially opaque to the positive ions produced at the sense wires. The effectiveness of the grid is thus determined by the percentage of time that the grid is in the open state. This is about 3%, resulting in reduction of ions in the TPC volume of about 10^{-3}.

3.3.5 Signal Processing

The signal processing chain for the TPC [Jar82b] is shown schematically in Fig. 3.5. The signal on the sense wire, primarily induced by the movement of

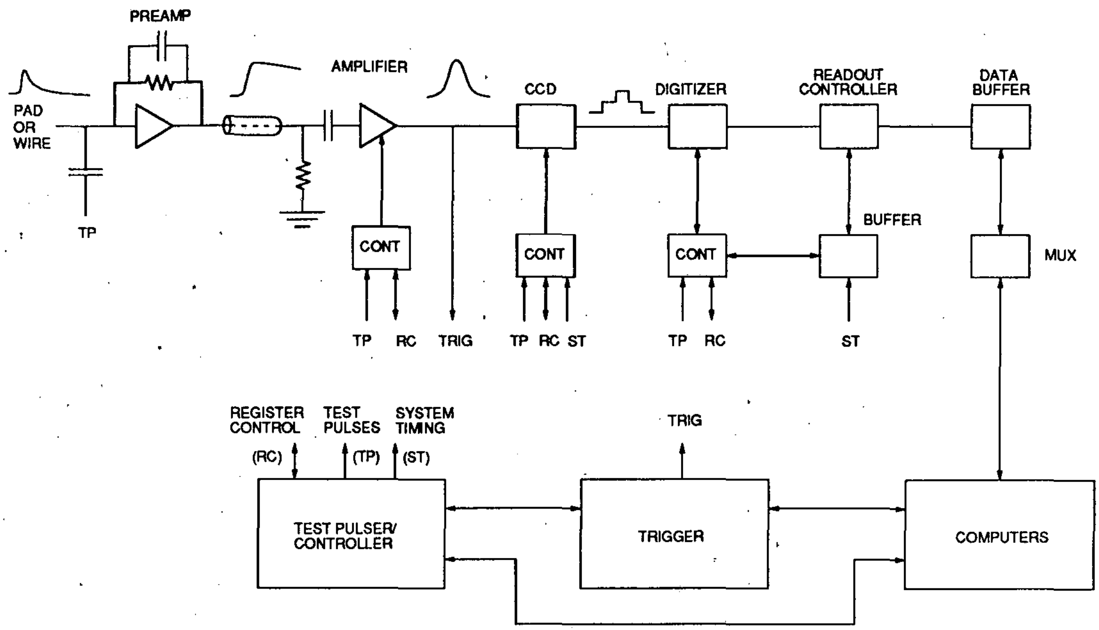

Figure 3.5: Schematic view of the TPC signal processing chain.

positive ions produced in the avalanche, is mostly collected within about 100 ns; however, a long tail persists while the positive ions move further from the high field region at the sense wire. The preamplifier produces a signal proportional to the accumulated charge but which decays with a 5 μs time constant [Lan82]. The signal is sent via coaxial cable to the shaper amplifiers, which remove the the 5 μs decay, and remove the tail caused by positive ion drift. The output of the shaper amplifier is an approximately gaussian signal with a rise time of 250 ns and with an area proportional to the charge as measured by the preamplifier.

In order to extract the time and amplitude from the measured signal, at least three or four samplings must be taken. The signal is sampled every 100 ns. Since the signal cannot be digitized this quickly, a CCD is used as an analog shift register to store the signal [Jar82a]. The CCD holds up to 455 samples, or "buckets" of data. This is more than enough to store signals from the entire 30 μs drift time of the TPC. If a trigger is received, the output of the CCD is read into an ADC at 20 kHz. During the first 40 μs of each clock cycle, the ADC converts the signal to a 9 bit number. During the last 10 μs, all ADC channels that exceed a locally stored threshold are read into a large data buffer, which can subsequently be read by any of our online computers.

3.3.6 TPC Calibration

In order to achieve less than 1% systematic variation in the measurement of dE/dx, great care must be taken to calibrate the measurements of pulse size that lead to a measurement of dE/dx [Aih83d]. The output of the CCD in the absence of a signal consists of a non-zero base value (or pedestal) that increases with time of readout (and therefore with bucket number). This slope is caused by an increase in charge in each CCD bucket from dark current. The pedestal and slope are measured by setting the readout threshold to zero and reading out about 300 buckets for each channel. The gain curve of the electronics is calibrated channel by channel; a series of pulses of known amplitude and rise time is coupled to the shielding grid above the sense wire plane (the shielding gris is, of course, not grounded during this procedure as it would usually be). The response of the electronics to these pulses is stored and the resulting gain curve parameterized. This data is used to correct for non-linear response of the electronics, particularly that of the CCD's.

The normalization of the gain curve is determined by the response to a source of known energy. Before the TPC was assembled, a gain map for each sector was made. Each wire was scanned with an ^{55}Fe source (emitting a 5.9 keV γ-ray), in order to account for variations in gain due to non-uniform wire diameter and due to temperature variation across the sector. Such corrections are on the order of 3–4%. During our running, adjustments were made to this map using calibrating sources painted on rods that are embedded in the TPC sectors. Each sector has three rods extending radially at angles -16°, 0° and 30° from the center of the sector. The sources are exposed to the wires only during a calibration run. These corrections are of order 1–2%, and stable to within 0.3% over several months, except for overall variations in the gain of the entire detector. In addition to these corrections, several corrections based on the data itself are made. these will be described in the next chapter.

3.4 The Trigger

At the rate of 2.45 μs per beam crossing, it is obviously not possible (or desirable) to record data at every beam crossing. The TPC drift time is 30 μs and the time required for the online computers to read the data buffer is on the order of 100 ms. Several levels of triggers are required to determine which events are of enough interest to continue processing. During the running cycle during 1985–1986, a three level trigger was used, which will be described briefly [Ron87,Ron82]. We will not describe the somewhat simpler trigger used before the upgrade or describe triggers used for tagged two gamma events.

In the first 2 μs after the beams cross, a decision is made whether or not to open the gated grid so that the TPC can collect data. This decision level is called the pre-pretrigger. A pre-pretrigger is generated if there is a minimum amount of energy in the calorimeters, or if there is evidence of at least two charged tracks.

For the purposes of the pre-pretrigger, evidence of a track consists of a hit in the IDC in conjunction with a hit in either the ODC or the TPC endcap. The latter is possible because a track passing through the TPC sector will generate a wire hit even though the gated grid is closed. The pre-pretrigger rate is typically 1–4 kHz.

The next trigger level, called the pretrigger, uses information in the first 20 cm of the TPC. The pretrigger allows for rejection of an event based on more complete information from the TPC. The gated grid can then be closed and the TPC reset for the next event. This allows for a smaller amount of dead time. The pretrigger decision is made within 7.5 μs of the beam crossing.

The final trigger uses TPC wire signals from the full 35 μs drift length of the TPC. Wire hits are combined so as to find continuous tracks that are consistent with originating from the beam vertex. The primary trigger used for multihadron annihilation physics requires at least two such TPC tracks in separate sectors. Additional triggers are formed that make use of calorimeter information. These are largely redundant for multihadronic events, and the trigger efficiency for multihadronic events is larger than 99%. In the event of a final trigger, all detectors are read out, requiring about 100 ms. The final trigger rate was typically 1–2 Hz, resulting in a total electronics dead time of about 20%.

Chapter 4

Reduction of Data and Event Selection

The results of this thesis depend primarily upon the properties, as measured by the TPC, of charged tracks produced in multihadron events. For each event, the raw pulse height data is collected by the electronics, and read by the computer, as described in the last chapter. From this raw data event, we must produce a list of particles and for each particle a list of physical properties, as best as they can be determined by the data and our understanding of the detector. This chapter will discuss discuss aspects of track reconstruction for charged particles (a more complete discussion is given in Ref. [Gar85]). We then discuss the selection process that leads to a sample of multihadron events resulting from e^+e^- annihilation.

4.1 Cluster Finding and Track Reconstruction

The first step in reconstructing track information from the TPC is to organize the time ordered pulse height data into clusters of hits that represent space points. The coordinates of these points are defined by a coordinate system that is local to each sector: the distance of the point from the center of the sector along a pad row is called η; the distance of a point from the beam in the direction perpendicular to both the pad row and the beam line is called ξ; and finally, the distance of a point from the midplane along in the direction of the beam line is called z (see Figs. 3.3 and 4.1). For each pad and wire channel, clusters in z are found by looking for at least three consecutive CCD buckets containing hits, with the middle bucket being a local maximum. The z position of a cluster is determined by the maximum of a parabolic fit to the three hits of maximum pulse height. Corrections to this measurement are necessary due to time dependence of drift velocity, as well as a vertical temperature gradient in the TPC.

Because of diffusion and the characteristic pad response to an avalanche, a single track will typically cause pickup on two pads (55% of the time) or three pads (40% of the time) in each pad row. Therefore, pad z clusters must be

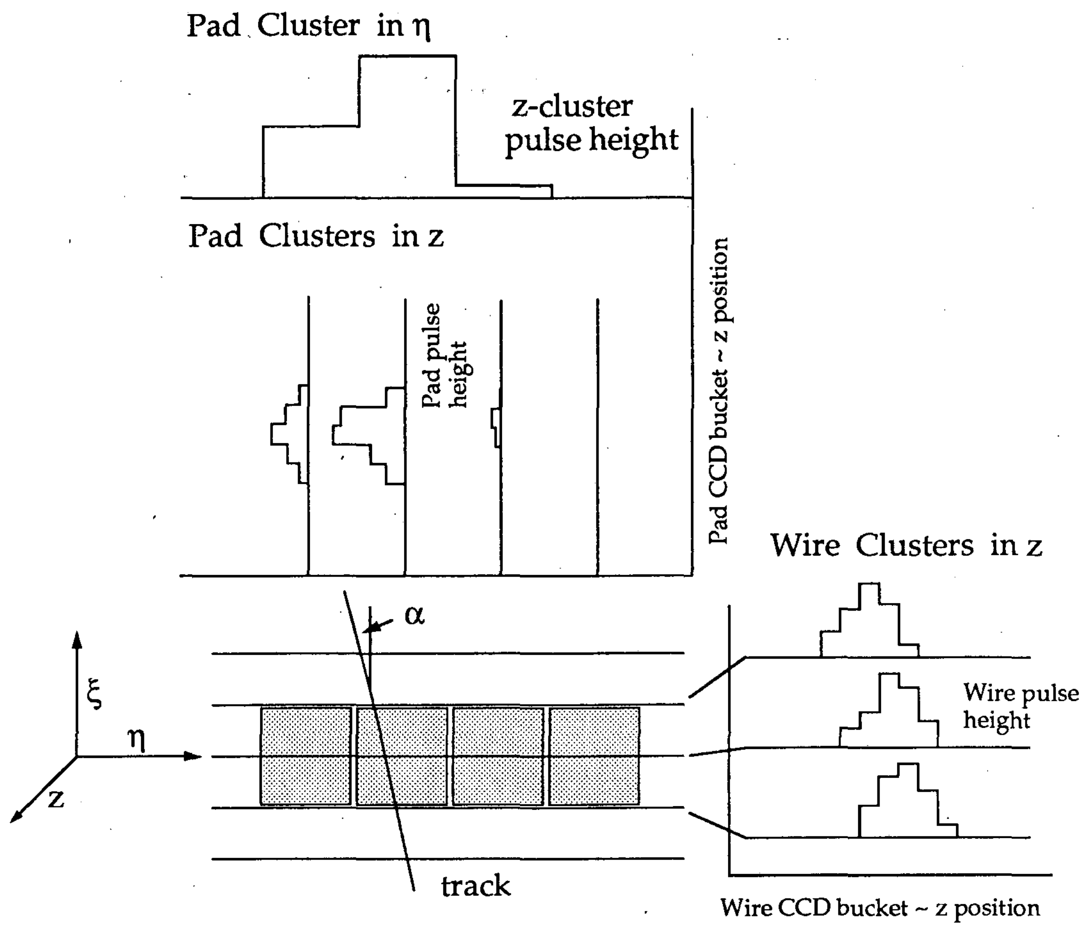

Figure 4.1: Illustration of track clusters seen on several wire and three pad channels. Each z cluster consists of 5–7 CCD buckets. A pad cluster consists of typically 2–3 z clusters.

combined to form a pad η cluster from which a measurement of the η position may be obtained (as illustrated by Fig. 4.1). The η of a pad cluster is determined by a gaussian fit to the pad hits in the cluster. If there are 3 or more pads in the cluster, the σ of the gaussian is a parameter of the fit. Otherwise, the σ must be estimated based on the intrinsic width of a pad signal, monitored run by run, and on the understood variation of this width with drift distance and the crossing angle of the track with the wire. The ξ position is to first order taken to be the position of the associated wire or pad row. The ξ for pad clusters is corrected, weighted by relative pulse heights of the five wires that couple most strongly to that pad row.

We next search the space points for sets of points consistent with the trajectories of charged tracks. Within the axial magnetic field of the TPC, the trajectory of a charged track is expected to be a helix. A combination of pattern recognition algorithms, which are described elsewhere [Had83], is used to assign clusters to tracks. We estimate the efficiency of pattern recognition to be 97%

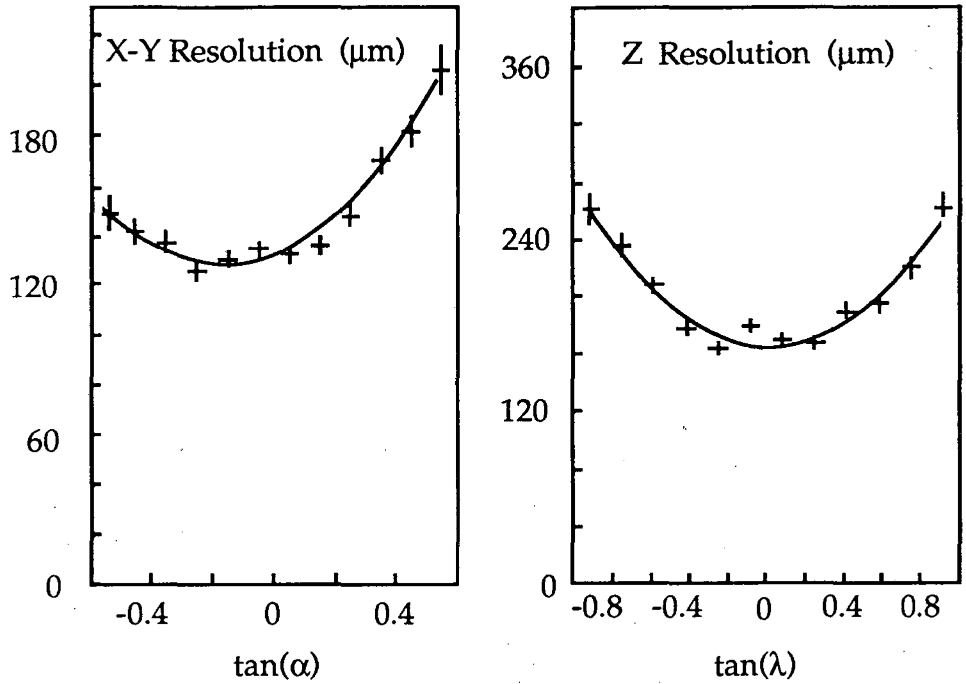

Figure 4.2: Position resolution, a) σ_{xy} as a function the tangent of the crossing angle, α, b) σ_z as a function of the tangent of the dip angle, λ.

for all but very low angle tracks.

We must correct the positions of the measured space points for the effect of electrostatic distortions in the TPC. The details of these corrections are described in the next section. The errors in the position measurement are due to distortions, electronic noise, transverse and longitudinal diffusion, and fluctuations in the amount of ionization collected by each wire. We must estimate the error of each measured point in order to perform a fit to the momentum of each track. The size of the errors can be determined from residuals to fitted trajectories of tracks, and is dependent on the drift length (L), the angle of the track with respect to the pad rows (α), and the angle of dip with respect to the midplane (λ). Figure 4.2 shows the errors in η as a function of $\tan(\alpha)$ and in z as a function of $\tan(\lambda)$ determined from the residuals of cosmic ray tracks. The innermost and outermost pad rows have additional errors resulting from distortions, which we must add to our error estimates.

With the space points and their errors determined, it is now possible to perform a χ^2 fit to a helix and determine the momentum of the original track [Edb87]. A χ^2 is defined having two terms for each measured point, the distance between the point and the track in the x–y plane, and the distance in the z direction:

$$\chi^2 = \sum_{i=1}^{N_p}[d_{xy_i}/\sigma_{xy_i} + d_{z_i}/\sigma_{z_i}].$$

The track parameters that provide a minimum of this χ^2 provide a measurement of the track's properties. Five parameters are used to describe the helix of each track, corresponding to the momentum vector of the track at some point, and the position of the intersection of the helix with some reference plane. An initial guess of the particle mass (based on the dE/dx particle identification described in Sect. 4.3) allows us to correct the momentum for energy loss in the TPC and also to provide a measurement of the momentum at the closest approach to the beam, taking into account the energy loss before the TPC. Multiple scattering is taken into account when computing momentum errors.

A global vertex fit, making use of all of the tracks in an event, further improves the momentum measurement. The five measured parameters and the error matrix for each track are used in this fit. The fit is done in iterations, initially assuming that all tracks originate from a single common vertex. Tracks with a large χ^2 for coming from the vertex are removed from the fit, and the fit is recomputed until a set of tracks consistent with one vertex is found. The determination of the event vertex is useful for finding tracks that are decay products of long lived particles.

4.2 Distortion Corrections

The measurements of the space points along a track in the TPC are known to suffer from systematic biases and fluctuations due to distortions in the uniformity of the electric field and to a lesser degree of the magnetic field in the TPC. In order to obtain an accurate measurement of particle momentum, we must reduce these biases as much as possible. Distortions in position measurement were as large as 1 cm in the data taken between 1983–1984. Reference [Gar85] describes the attempts to correct these distortions. Improvements made in the TPC detector during the upgrade between 1983 and 1985 greatly reduced the magnitude of the distortions in the data taken from 1985 to 1986, but distortions were still large enough (typically 1 mm) that they needed to be corrected.

4.2.1 Evidence of Distortions in the TPC

Figure 4.3 illustrates the effect that displacements of space point have on a measured track in the TPC. We find evidence of distortions in the TPC in several ways. We observe systematic deviations from the expected properties of well understood tracks, such as those in Bhabha events ($e^+e^- \to e^+e^-$). In particular we look for systematic deviation of tracks from their expected energy, deviation of track pairs from being back-to-back, and deviation of tracks from originating at the vertex. Another measure of distortions is the systematic bias in residuals of measured positions after tracks are fit. Since the mis-measurement of space points will vary along a track, the track will no longer be well fit by a helix. These studies indicate several sources of distortions in the TPC.

Distortions in the magnetic field were mapped with NMR probes before the

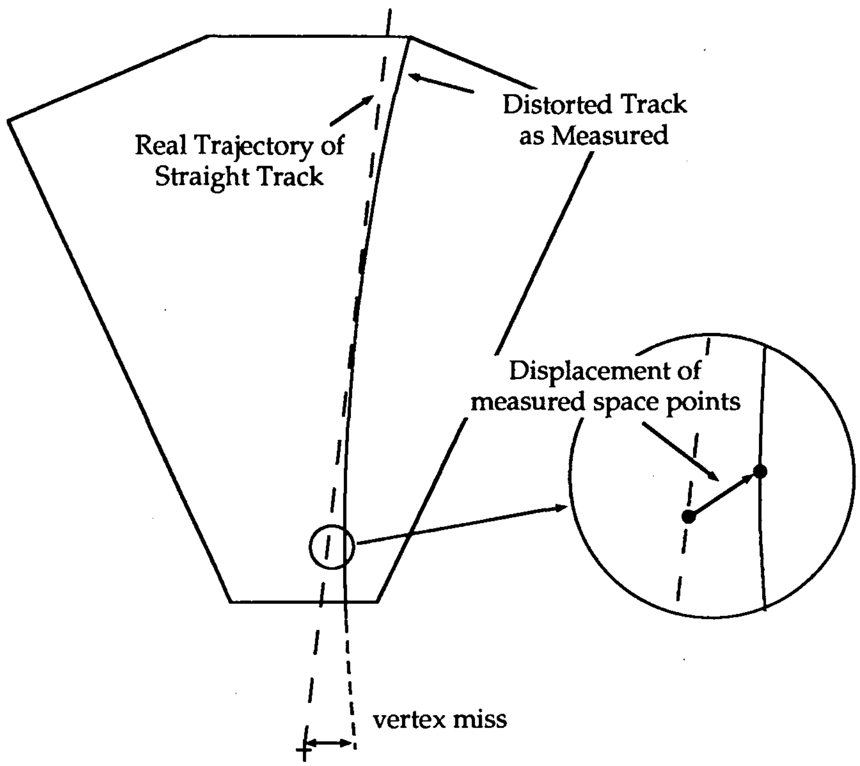

Figure 4.3: Illustration of the effect of space point displacements on a measured track.

TPC was installed in the coil. For this reason, these are probably the best understood distortions in TPC at present. Unfortunately, less well understood track distortions overwhelm these, so that the corrections based on the magnetic field map are of limited value.

Distortions in the electric field caused by the shielding grid of the TPC not being a solid ground plane are known to exist. The field in the TPC is distorted in a way that is well approximated by assuming that the grid is a plane at the wrong potential. The variation of the distortions over a sector in the upgraded TPC is similar to what is expected based on this model. These distortions have one property that cannot be easily explained by the grid model; they have a time dependence over a long time scale, changing in magnitude substantially over the entire running period. The track distortions seen are what would be expected if the grid were to change by 50V over the four months of running. It would also be explained by a change in the position of the plane of the sectors by 1mm. Neither of these explanations seems likely to be correct. The source of this time dependent distortion is not at present understood; the distortions are corrected assuming a model that the grid voltage is changing with the observed time dependence.

After these distortions have been removed there is evidence of distortions that are essentially constant in time but have irregular fluctuations with position (not obviously correlated with the hexagon geometry of the TPC). This is what we would expect if the distortions were due to field cage non-uniformity. It is surprising that distortions from this source should still be noticeable, since they should be greatly reduced by the resistive coating on the field cage (as discussed in Sect. 3.3.2). At present, only the distortions in the plane perpendicular to the B field are corrected. These have the largest effect on the measurement of the curvature of a track, and thus are the most important for improving momentum resolution. Since the nature of the distortions is not known, an empirical correction is made based on the data. The data consists primarily of tracks that extend radially from the vertex, so it is only possible (to first order) to measure displacements that are in the azimuthal direction. Corrections made based on these displacements should be adequate for tracks that are also radial, but possibly not for tracks that do not originate from the vertex. For simplicity, the corrections are performed assuming a displacement in the direction parallel to the pad rows (the η direction).

The displacements that are used to make corrections are obtained from two different sources. The first is to make a map of the residuals in η direction, using well measured tracks with momentum greater than 1 GeV/c from multihadronic events. These residuals, binned by pad row and by azimuth, were found to be particularly large and irregular near the inner and outer pad rows. The residuals to track fits are not sufficient to determine the displacement of each point, however, since biases in track fit parameters probably exist. We attempt to remove these biases by using data from Bhabha events. We histogram the momentum of each track and the amount by which the track misses the vertex (in η direction) in bins of azimuth. The expected momentum distribution of tracks from Bhabha events is computed by Monte Carlo, so that biases in average track curvature can be determined. Biases that are found this way are then removed by adding a curvature term and a term linear in radius to the η displacement of each point, such that the point near the center radius (at 60 cm) is not displaced, and such that the track points to the expected vertex. Our corrections are based on the assumption that the distortions are small near the central radius of the sector (as suggested by our residual measurements). In addition to the momentum bias and bias in the vertex miss distance, we also measure the angle difference of the two tracks in the event. Bias in angle difference as a function of azimuth is strongly correlated with the other two biases. After the corrections are performed, the bias in angle difference disappears, even though it was not explicitly corrected for. This supports our model that the distortions are small except near the inner and outer radius.

The largest source of distortions before the TPC upgrade was space-charge from positive ions produced in the avalanche process. These are expected to be reduced to a negligible level by introducing a gated grid (see Sect. 3.3.4). The lack of any strong dependence of the observed distortions on luminosity supports this expectation.

4.2.2 Momentum Resolution

The effectiveness of distortion corrections is demonstrated by the improvement in momentum resolution after the corrections are performed. There are two main contributions to momentum resolution. Measurement errors on the space points are most important for high momentum tracks, since a small error in curvature for such tracks translates into a large momentum error. For low momentum tracks, the dominant contribution is the effect of coulomb scattering. The momentum resolution of tracks in hadronic events is parameterized as

$$\left(\frac{\sigma_p}{p}\right)^2 = \sigma_{CS}^2 + \sigma_{meas}^2 p^2.$$

The momentum resolution for high energy tracks is measured by using $e^+e^- \rightarrow \mu^+\mu^-$ events. Tracks from $\mu^+\mu^-$ events have a known energy as long as they are selected as being back-to-back (this eliminates radiative $\mu^+\mu^-$ events). Their angular distribution is also similar to that of tracks in hadronic events (unlike bhabha tracks or cosmic rays for example). The measured momentum spectrum of these events thus provides a good measure of momentum resolution for high energy tracks. Figure 4.4 shows the distribution of $1/p$ for tracks from $\mu^+\mu^-$ events (of varying dip angles and track lengths). This is the momentum obtained from a fit that constrains the tracks to a common vertex. A gaussian fit to this spectrum gives the resolution due to measurement error, $\sigma_{meas} = \sigma(1/p) = 0.65$ % $(\mathrm{GeV/c})^{-1}$. A small amount of background due to cosmic rays is assumed to be flat. If the tracks are not constrained to a common vertex, the resolution is found to be $\sigma_{meas} = 0.90$ % $(\mathrm{GeV/c})^{-1}$. If no distortion corrections are applied to the data, the momentum resolution with (without) the vertex constraint is 2.1(1.4) % $(\mathrm{GeV/c})^{-1}$ (the distortions are such that the vertex constraint makes the resolution worse). Even the momentum resolution for uncorrected data is a substantial improvement over the resolution obtained before the TPC upgrade, which was 3.5(6.0) % $(\mathrm{GeV/c})^{-1}$ with (without) a vertex constraint. A factor of 3.4 improvement is from the increase in magnetic field from 3.9 kG to 13.25 kG, the remaining improvement results from controlling the distortions in the TPC.

The contribution of Coulomb scattering to the momentum resolution is computed using a formula obtained from Gluckstern [Glu63], and depends on the tracks length and dip angle. The increased magnetic field also improves the Coulomb scattering contribution to the resolution from 6.0% to 1.5%.

4.3 Particle Identification using dE/dx

When a charged particle traverses matter, the energy loss due to ionization per unit of distance traveled (dE/dx), depends on the velocity of the particle, and not on its mass. The dependence of dE/dx on the momentum of a particle will therefore depend on its mass, and the measurement of dE/dx in conjunction with a momentum measurement allows us to identify particles types. Figure 4.5,

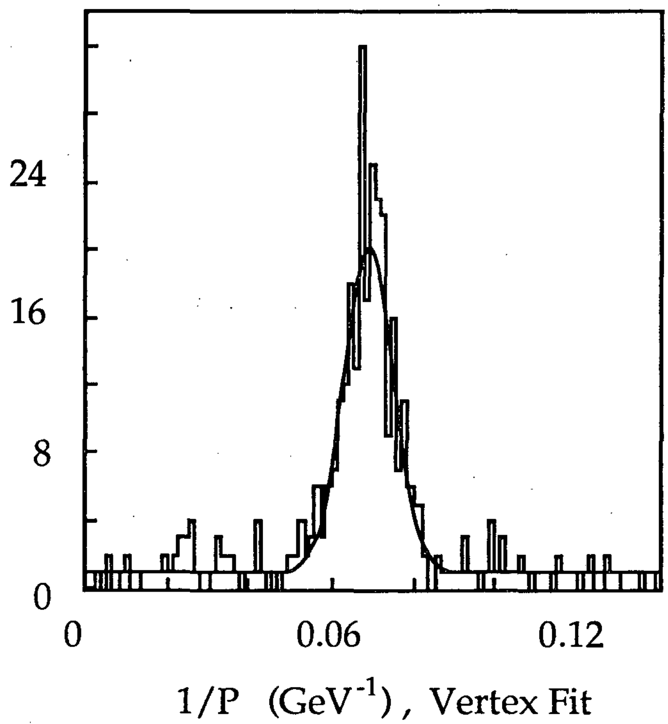

Figure 4.4: $1/p$ for tracks in events $e^+e^- \rightarrow \mu^+\mu^-$. Fit is gaussian giving resolution $\sigma_p/p^2 = 0.65$ % $(\mathrm{GeV/c})^{-1}$, and center at $1/p = 1/(14.5\mathrm{GeV/c})$ as it should be.

shows the measured dE/dx for each track versus its measured momentum with the theoretical prediction superposed. Except in regions where the curves for two particle types cross, it is possible to distinguish electrons, pions, kaons and protons. We can observe the following general characteristics of the dE/dx vs p curve. At low particle velocity, the curve is sharply falling (as $1/\beta^2$). At intermediate velocity it reaches a minimum, which is referred to as the minimum ionizing region. As the particle becomes highly relativistic, the dE/dx rises and eventually reaches a plateau.

4.3.1 dE/dx Measurement

The energy loss of a track is assumed to be proportional to the total number of electrons that are produced as the track traverses the TPC. Some of these electrons are primary electrons, produced directly by interactions of the original particle, whereas some electrons are secondary, being produced by the interactions of primary or other secondary electrons. Through a hard Rutherford scatter, the particle occasionally frees a very energetic electron, which results in a large number of secondary electrons. These relatively rare events cause large fluctuations in the number of measured electrons in each sample, resulting in a wide, non-Poisson distribution with a long tail. Because of the resulting non-Poisson shape of the energy loss distribution, one can obtain the best measurement of the ionizing properties of the track by measuring the energy loss many times in small samples. The distribution of the resulting measurements can then be used to obtain an estimate of the "Most Probable" dE/dx for the track.

As discussed in the previous chapter, the TPC measures the energy loss of a track in up to 183 samples of typically 4mm length. Figure 4.6 shows the distribution of energy loss measurements for each sample (and also the predictions of a theoretical model [Cow88]). Rather than attempt to perform a fit to the distribution of energy loss measurements for each track, it is convenient to use a simple parameter of the distribution as an estimator of the most probable dE/dx for the track. The average of the dE/dx measurements for a track is dominated by fluctuations in the tail at large energy loss. The lower portion of the distribution provides a better indication of the most probable dE/dx of the track, so we use a "truncated mean", which is the average of the lowest 65% of the dE/dx measurements for a track. Monte Carlo studies show that the truncated mean is proportional to the most probable dE/dx measurement, and that the resolution of the truncated mean is insensitive to the amount of truncation as long as the percentage of samples used is between 40–70%. In the following the truncated mean of dE/dx measurements for a track will simply be referred to as the dE/dx measurement of a track.

A wire cluster is assigned to a track if the z coordinate is within 0.7 cm of the track and there is no other track within 2.4 cm (in z). The pulse height of each cluster, determined by a parabolic fit to the three maximum hits in the cluster, is divided by the track length of that sample. This track length can be calculated if the helix that describes the track is known. This provides a raw measurement

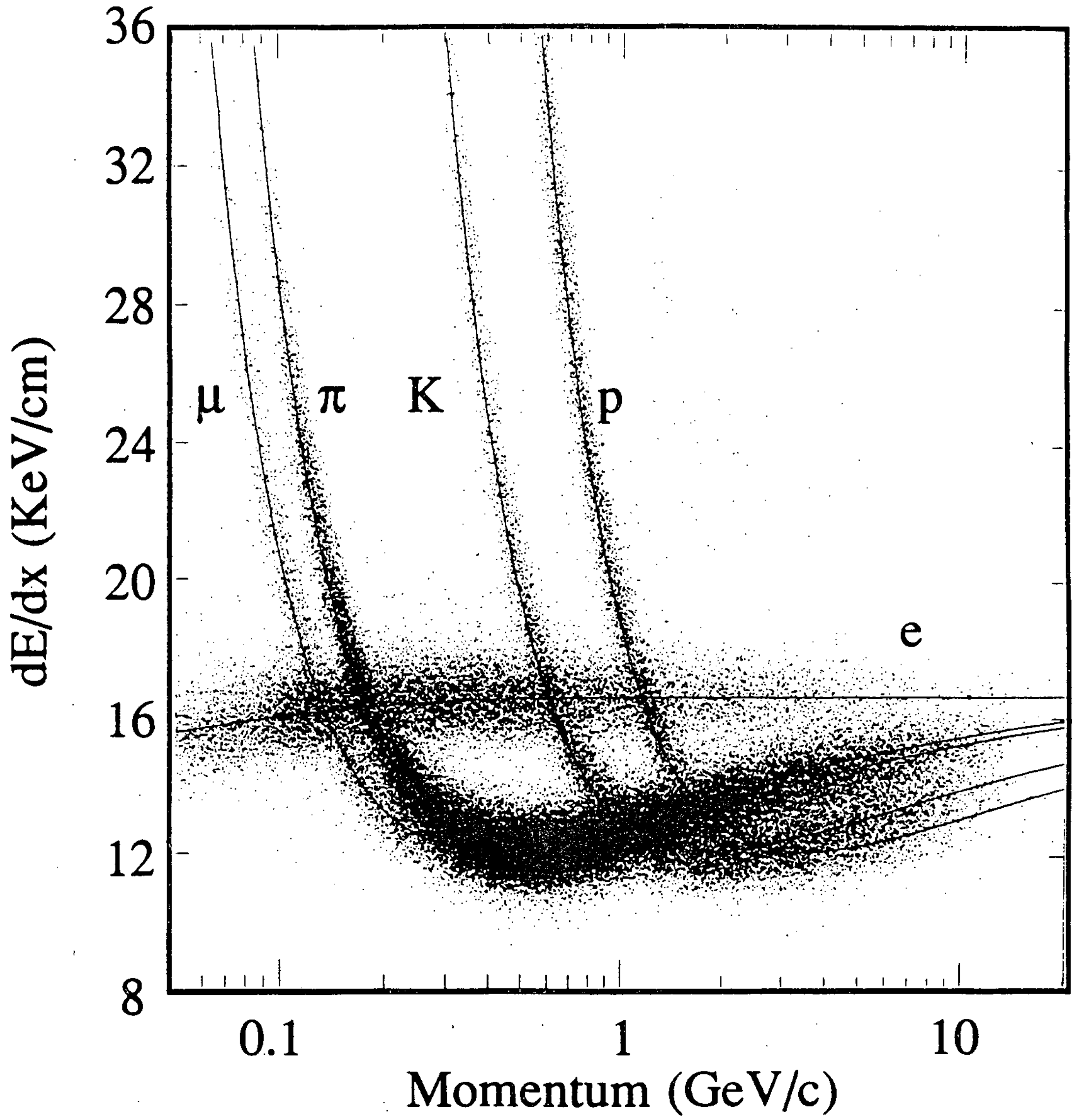

Figure 4.5: Measured dE/dx as a function of momentum of all tracks in multi-hadron events. Solid curves represent the expected dependence of the average dE/dx for e,μ,π,K and p.

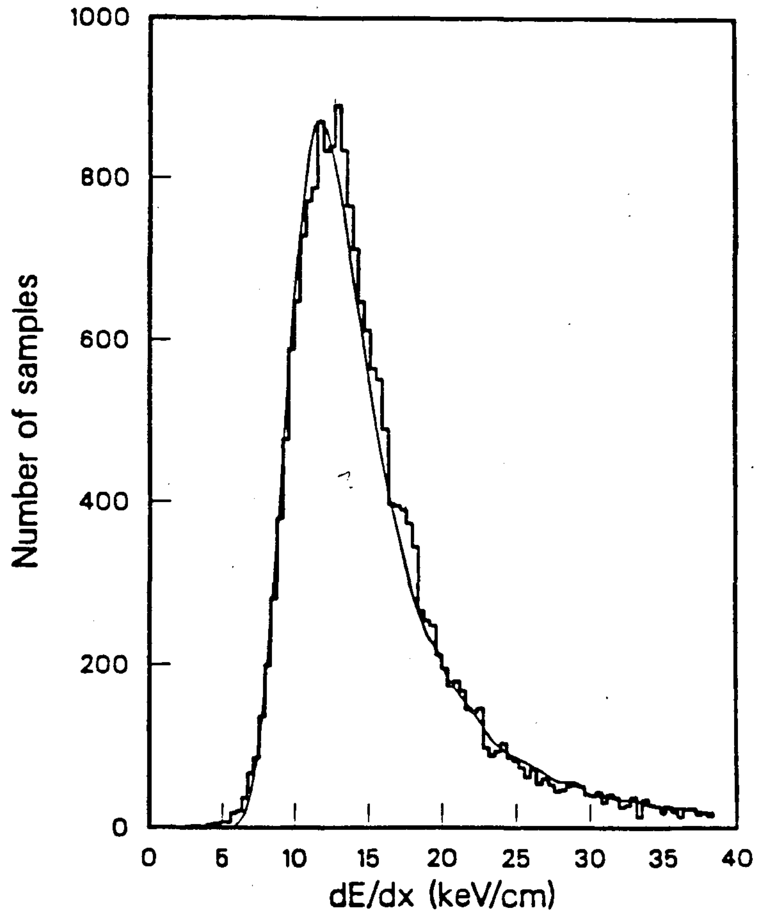

Figure 4.6: Distribution of measured dE/dx per 4 mm track sample. Solid curve is theoretical model.

of dE/dx for each sample on the track. These measurements must be corrected for several effects. The electronics calibration and ^{55}Fe source calibrations, which have already been described, are applied. In addition, the overall gain of the TPC varies by up to 10% from day to day, mostly because the fraction of Methane in the gas mixture varies. The gain is measured for each run by measuring the mean dE/dx of minimum ionizing pions. The dE/dx measurements must also be corrected for capture of electrons by electronegative contaminants in the TPC gas. The size of this correction is determined run by run.

For a typical track of 120 samples, the resolution of the dE/dx measurement is 3.5%. This is after additional corrections that depend on sector and dip angle of the track have been made to the dE/dx measurement for each track. These corrections were determined using minimum ionizing pions. If two tracks in the same sector are at about the same dip angle, many of the wire clusters associated with these tracks will be unusable, because the clusters from each will overlap. It is sometimes better to use the dE/dx measurements from the pads instead of from the wires. This is done if the number of usable pads is greater than 0.4 times the number of usable wires. The resolution for a typical track with 13 pad clusters is 8.%.

4.3.2 Particle Identification

In order to use dE/dx to identify particles, we form a χ^2 for each possible particle hypothesis. This χ^2 can then be used to determine the most likely identity of a particle, and thus can be used to select particles that are mostly of the desired type. In order to define this χ^2, we require a measurement of, and an error estimate of both the $dE/dx$and the momentum. We also need to know the relationship between dE/dx and p for each particle type. We can then define the χ^2 for the particle type i:

$$\chi_i^2 = \frac{\left((dE/dx)_i - (dE/dx)_{meas}\right)^2}{\sigma_{dE/dx}^2} + \frac{\left(p_i - p_{meas}\right)^2}{\sigma_p^2}. \tag{4.1}$$

dE/dx_i and p_i represent a point along the theoretical dE/dx versus p curve. This point is chosen so as to minimize χ_i^2. The resolution in dE/dx is measured using minimum ionizing pions and is parameterized as a function of number of samples and dip angle of the track. The resolution in p is determined from the track momentum fit.

A detailed calculation was made of the expected distribution of dE/dx samples on a track and of the dependance of the most probable dE/dx measurement on velocity (hence on p for a given particle type) [Cow88]. This calculation was based on an atomic model for ionization energy loss and takes into account resonant terms from six energy levels of Argon and Methane and also the contribution from Rutherford scattering. The distribution of dE/dx measurements is well reproduced by the model as seen in Fig. 4.6. The shape of the theoretical curve for dE/dx versus $\beta\gamma$ (where $\beta c = v$ and $\gamma = 1/\sqrt{1+\beta^2}$) compares well

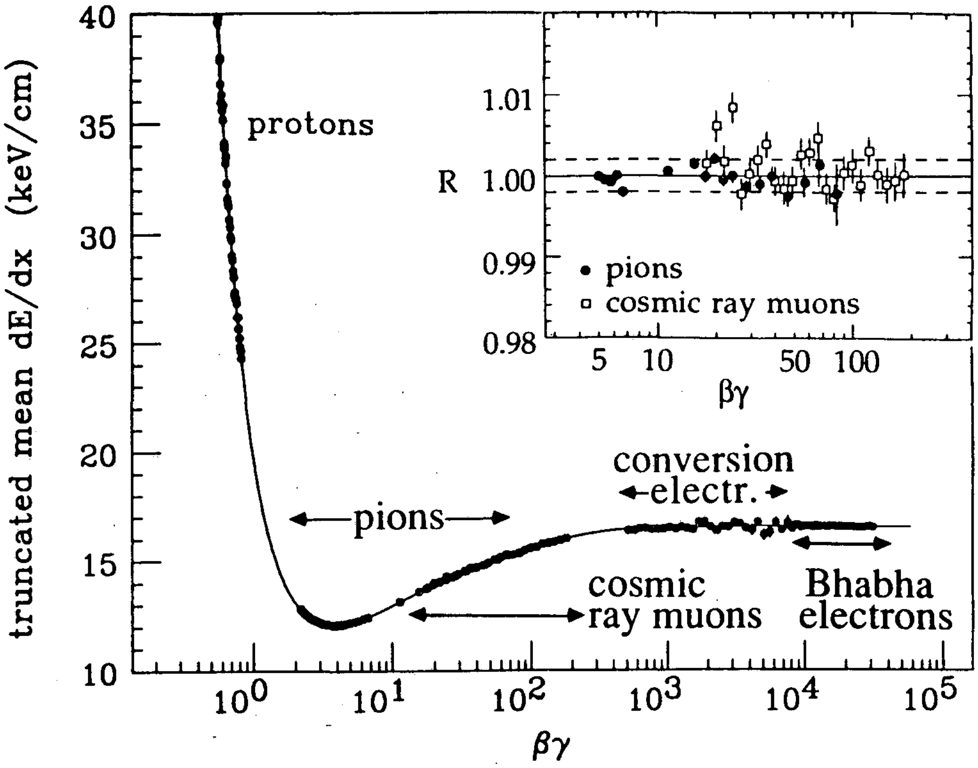

Figure 4.7: Average truncated mean dE/dx as a function of $\beta\gamma = p/m$ of a particle as determined from protons,pions, and conversion electrons in hadronic events, from cosmic ray muons and from Bhabha electrons. Curve is atomic model fit to data. Inset: Ratio R of data points and model in relativistic rise region.

with the measured shape, but it is found that in order for the agreement be good it is necessary to add some simple parameters to the theoretical curve. These are just a translation and a scaling factor in both dE/dx and in $\beta\gamma$. The theoretical curve is fit to measurements of dE/dx for particles whose identity is well known. The result of this fit is shown in Fig. 4.7 along with the residuals of the fit in a selected interval.

Although one can simply use the χ^2 as computed above to aid in identifying particles, for tracks in multihadron events it is also advantageous to use the measured particle fractions in determining the particle type. One uses the χ^2 along with a weight based on a simple parameterization of the particle fractions (as measured by the TPC) to compute a probability for each particle hypothesis. This probability is defined as:

$$P_i = \frac{f_i(p)\exp^{-\chi_i^2/2}}{\sum_{j=1}^{4} f_j(p)\exp^{-\chi_j^2/2}}. \tag{4.2}$$

$f_i(p)$ is a parameterization of the particle fraction for particle type i. The parameterization used is:

$$\begin{aligned} f_e &= (0.2/p)^2 \\ f_\pi &= max(0.8494 - 0.1350\ln(p), 0) \\ f_K &= max(0.1093 + 0.0916\ln(p), 0) \\ f_p &= max(0.0413 + 0.0434\ln(p), 0) \end{aligned}$$

One can then, for example, select a sample of pions only keeping tracks with $P_\pi > 0.7$.

4.4 Data Filtering

In addition to the reconstruction of each event, an equally important part of analysis is determining which events contain interesting physics, and finally which are to be used as a sample of multihadron e^+e^-annihilation events. The TPC analysis is performed in several passes, and involves several event filters. Event filtering insures that computer time is not wasted processing junk events, and that the number of data tapes produced at each stage is minimized. Detailed descriptions of these filters can be found in the Refs. [Kay87,Gar85].

The first pass is performed by our online computer (VAX 782) while data is being collected. All events are first run through the PREANALYSIS filter. The PREANALYSIS filter provides a high speed check of triggered events so that obvious background events eliminated and not written to tape. These are mostly cosmic rays, or events resulting from interaction of the beam with gas in the beam pipe. All events that pass PREANALYSIS (about 65%) are written to tape. As many as possible of these (about 75%) are analysed further online.

After cluster finding and track reconstruction, events are again filtered, this stage being called the TPC_SELECT filter. The goal is, again, to reduce the background from cosmic rays and beam-gas interaction events, while keeping all potential multihadronic events, 2γ events, $\mu^+\mu^-$events, and Bhabha events. Cuts can be tighter than during PREANALYSIS because of the improved TPC information available. Muon chambers are also used to reject some obvious cosmic rays that miss the TPC. Also at this stage, low angle Bhabha events are counted (as a monitor of luminosity), and 1 out of 10 are kept. These filters eliminate about 40% of the events that passed PREANALYSIS. Those that pass are analysed to the point of track fitting. Several of the constants that are required for this analysis are not yet known online since they must be determined from the data. A best guess is made for this initial analysis pass. Histograms are made at this time from which calibration constants that vary from run to run are computed. These are averaged over several runs, and offline reprocessing with the correct constants can be done within a day.

The raw data tapes are brought to Berkeley for the first offline analysis pass, also done on Vax computers. Cluster finding and pattern reconstruction is not repeated but is performed on those events that were not analysed online. Events are only processed and output at this stage if they pass the TPC_SELECT filter described above. The events are analysed with the correct calibration constants, but with only a preliminary set of distortion corrections, up to the point of creating a DST (Data Summary Tape). The DST is a concise summary of data that is likely to be needed for most analyses. For example, the momentum vector of each track is given in several useful forms but not the measured space points along each track. The fully analysed events are written to tape, including a DST block, but not the raw data block. These tapes are referred to as 'E' tapes.

Another selection is made at this point, referred to as the SELQQTAU filter. This selection of events keeps multihadronic hadronic events and most $\tau^+\tau^-$ events, and rejects most 2γ events. These are output to tapes (called 'F' tapes) and the DST blocks are also written to separate files containing just the DST's. The DST files are further analysed by routines that search for secondary vertices and that label conversion pair electrons. The final selection of multihadronic annihilation events is made by the routine LABEL_HADRON. The output events from this filter are kept in DST files on disk.

The 'F' tapes (SELQQTAU selection) are reprocessed once distortion and final dE/dx corrections have been studied (this was several months after data had been collected). The reprocessing begins with the distortion corrections and proceeds as above to the production of final DST's.

4.4.1 Multihadron Event Selection

The purpose of this event selection is to provide a relatively pure sample of multihadron events that result from the interaction $e^+e^- \to q\overline{q}$, (with possibly one or more gluon radiating from the final-state). The distinctive topology of these events makes it possible select a pure sample with good efficiency, based on the charged tracks in the event. Tracks that pass the following criteria are used for this event selection. These cuts are primarily to insure that the tracks used are likely to have originated from the event vertex, are well within the fiducial volume of the TPC, and are well described by the detector Monte Carlo.

1. Track must be associated with the vertex. The track's closest approach to the vertex must be within 6 cm in radius, and within 10 cm in z of the nominal vertex.

2. The angle between the track and the beam axis must be greater than 30°.

3. The curvature of the track, $C = 1/p_{xy}$, must have an error dC that satisfies $dC/C < 0.30$ or $dC < 0.30$ (GeV/c)$^{-1}$.

4. The momentum of the track in the TPC must be > 100 MeV/c.

5. The momentum of the track extrapolated to the vertex must be > 120 MeV/c.

These tracks are used to determine the sphericity tensor of the event, which quantitatively specifies the shape of the event:

$$M_{\alpha\beta} = \sum_{i=1}^{n} p_{i\alpha} p_{i\beta}.$$

The eigenvector corresponding to the largest eigenvalue is the direction with respect to which the sum of the squares of the transverse momenta is minimized. This direction is called the sphericity axis. The sphericity is defined as,

$$S = 3/2(\lambda_2 + \lambda_3)$$

where $\lambda_1 \geq \lambda_2 \geq \lambda_3$ are the eigenvalues of M. The sphericity is an indication of how much the event is elongated, and can therefore be used to select 2-jet events (for which $S \sim 1$). The criteria for being accepted as a good hadronic annihilation events are the following:

1. There must be at least five good non-electron tracks, where electron identification is done either by dE/dx or by geometric reconstruction of photon conversions. This rejects Bhabha events where one of the particles showers on entering the TPC.

2. The total energy of the charged good tracks, E_{ch}, must be > 7.25 GeV. This rejects 2γ events that typically have lower visible energy.

3. The longitudinal momentum balance of good tracks must satisfy $|\Sigma p_z| < 0.4E_{ch}$. This rejects 2γ and radiative $q\bar{q}$ events.

4. At least half the tracks of the event must be good tracks, according to the above criteria.

5. The reconstructed vertex of the event must be within 2 cm of the nominal vertex in the x–y plane and within 3.5 cm in z. This rejects beam-gas interaction events.

6. At least one event hemisphere (defined by the sphericity axis of the event) must contain either at least four charged non-electron good tracks or an invariant mass of at least 2 GeV. This is to reject $\tau^+\tau^-$ events.

With these cuts, the contamination of background events as computed by Monte Carlo is $(0.4 \pm 0.1)\%$ from $\tau^+\tau^-$ events, $(0.5 \pm 0.1)\%$ from two-photon events, and $< 0.1\%$ from beam-gas and Bhabha events. About 78% of generated Monte Carlo hadronic annihilation events (generated without initial state radiation) satisfy the hadronic event selection. (The simulation of hadronic events using the Lund Monte Carlo and our detector simulation Monte Carlo is described in Ref. [Aih88].)

Chapter 5

Analysis of Two-Pion Correlations

Particle correlations can be measured by comparing the distribution of particles pairs with a similar distribution in which the correlations of interest are absent. For the purposes of this analysis, the Bose-Einstein correlation function will be defined as:

$$R(p_1, p_2) = P(p_1, p_2)/P_0(p_1, p_2)$$

where $P(p_1, p_2)$ is the probability distribution of like-sign pion pairs and $P_0(p_1, p_2)$ is what that distribution would be in the absence of Bose-Einstein correlations. Of course, this definition is incomplete until we specify how to obtain $P_0(p_1, p_2)$, which is not directly available for measurement. This is ultimately what makes the measurement of Bose-Einstein correlations difficult.

Since Bose-Einstein correlations are expected to be largest for pairs of particles of the same momentum, we measure the correlations as a function of the four-momentum difference, $q = (q_0, \mathbf{q}) = p_1 - p_2$. In principle, the correlation function would be a function of four independent variables. Lack of sufficient data requires some further reduction in the number variables used. The invariant quantity, $Q \equiv \sqrt{-q^2}$, has been widely used in Bose-Einstein correlation work. Measurements by several groups indicate that Bose-Einstein correlations are well described by a function that depends only on Q. Data in e^+e^- experiments [Ave85,Aih85b,Alt86,Jur87] are found to be consistent with the form

$$R(Q) = 1 + \alpha \exp\left[-(rQ)^2\right]. \tag{5.1}$$

If such a description is correct, it implies that Bose-Einstein correlations depend on how the pion source appears in the rest frame of the pion pair. This would be consistent with the assumption that the pion boost is due to the relativistic motion of the pion sources. As discussed in chapter 2, a model in which the particle source density was static would predict that the correlations additionally depend on the lab frame variable $q_0 = E_1 - E_2$. In particular, the enhancement would disappear for pairs that are highly boosted, such that $q_0 > r$. We therefore will measure the correlation function as a function of both Q and q_0 to check that correlations do not fall to zero for $q_0 > r$.

5.1 Discussion of Reference Distribution

The most important problem in defining the correlation function as above is to choose an appropriate distribution to use as the reference distribution. Ideally, this distribution should have all of the properties of the real distribution except for the existence of Bose-Einstein correlations. In particular, it should reproduce all correlations that originate from the jet structure of the event and also all correlations that are due to dynamics. There are two methods that we discuss, the use of unlike-signed pairs, and the use of tracks mixed from different events.

Unlike-sign Pairs

Since Bose-Einstein correlations only occur between identical particles, we can use pions of opposite sign to form pairs. Clearly, these pion pairs will have the same correlations due to jet structure and energy conservation as like-sign pairs have. Nevertheless, dynamical correlations such as the short range correlation due to local charge compensation, and correlations caused by the pions being decay products of resonances, will not be the same as for like-sign pairs. It is also possible that the acceptance for like-sign pairs may be different then for unlike pairs because of pattern recognition failure for close tracks.

Some of these problems may be overcome if we repeat the analysis for Monte Carlo generated events and normalize the data correlation function by the Monte Carlo correlation function. This method has been used by a number of experiments. In order for this to help, however, it must be known that the Monte Carlo correctly reproduces the two particle correlations of the unlike-sign pairs, and all but the Bose-Einstein correlations of the like-sign pairs. The extent to which this is true can be studied and will be discussed later.

Event Mixing Method

Another method, which has been used in the past by us, and others, is the event mixing technique [Aih85b,Kop74a]. Tracks from two different events are combined to form a pair, and the kinematic variables are found using the momenta of the particles relative to the event axis in each event. It is important to insure that the mixed-event distribution reproduces most of those correlations that are in the real data. There are several reasons why this may not be the case.

1. In the real particle pair distribution, energy conservation correlations. If there is a large momentum particle in the event then there is unlikely to be enough energy for another to have a similar momentum; thus, few pairs having such a track would have a small Q. In order to avoid this effect, an upper cut on track momentum can be applied.

2. The acceptance for a real track pair will depend on the relative momenta of the two tracks, since tracks that are close to each other will be more likely

to not be reconstructed by pattern recognition. There is no corresponding inefficiency for track pairs formed by event mixing.

3. Since the momentum of each track is described relative to the sphericity axis of that event, the regions of low acceptance will not necessarily overlap for tracks from two different events. The acceptance for track pairs as a function of their relative momentum may therefore be different for mixed pairs then for pairs from the same event. This is partly avoided by only combining events whose sphericity axis makes almost the same angle with respect to the beam.

4. As was the case with using unlike-sign pairs as the reference distribution, the correlations of dynamical origin will not be reproduced by the event mixed distribution.

We can take measures to try to minimize the above problems; however, there is bound to be some systematic uncertainty arising from any method for forming the reference distribution. Therefore we will use both of the above methods and compare results.

A description of the analysis method follows. This is followed by a discussion of Monte Carlo studies of some of the above effects and their impact on the measured correlations. We then present the results of fits to the measured correlations, followed by a discussion of the systematic errors, and a discussion of the results.

5.2 Analysis Method

5.2.1 Measurement of Two-Pion Distributions

Event and Track Selection

First we select good hadronic events as described in Sect. 4.4.1. The data sample used consists of 26,063 events ($77pb^{-1}$) taken in 1982-1984 (with 3.89 kG magnetic field), and 25,782 events ($67pb^{-1}$) taken in 1985-1986 (with 13.25 kG magnetic field). In each good hadronic event, the sphericity algorithm is used to compute the sphericity and the sphericity eigenvectors of the event. Only tracks that pass the following criteria are used for this and for all of the following analysis. These cuts are similar to, but tighter than, those described in Sect. 4.4.1. Again, they primarily to insure that the tracks used are well within the fiducial volume of the TPC, and are well described by the detector Monte Carlo.

1. Track must be associated with the vertex. The track's closest approach to the vertex must be within 3 cm in radius, and within 5 cm in z of the nominal vertex.

2. The angle between the track and the beam axis must be greater than 30°.

3. The curvature, $C = 1/p_{xy}$, must have an error dC that satisfies $dC/C < 0.15$ or $dC < 0.15$ (GeV/c)$^{-1}$.

4. The momentum, $p > 0.15$ GeV/c.

After the sphericity and sphericity eigenvectors have been computed, the following event cuts are applied.

1. In order to select primarily two-jet events, we require sphericity less than 0.025. This avoids correlations that arise because tracks are mixed from events that have very different topology.

2. We require that the angle that the sphericity axis makes with the beam axis be greater than 40°. This insures that the event is well within the fiducial volume of the detector and that sphericity axis is therefore well measured.

3. We require at least 5 good tracks as described by the above criteria.

After these cuts there are 19,803 events from the low field data and 19,225 from the high field data. No significant differences in any of the following analysis was found between the two sets of data, and they have therefore been combined for all of the following measurements unless otherwise noted.

The events that pass the above cuts are then used for the pion correlation analysis. In order to select good pion candidates from these events, we use the measurement of dE/dx in the TPC and the momentum measurement of the particle, as discussed in Sect. 4.3.2. A χ_i^2 is computed for each particle identification hypothesis, $i = e, \pi, K, p$, and this χ_i^2 is used along with the knowledge of the measured particle fractions as a function of momentum to compute a probability, P_i, for each hypothesis. We select a pion sample with these cuts:

1. We require that the dE/dx of the track is well measured. If the track uses wires for its dE/dx measurement there must be at least 30 wires useable for dE/dx. If the track uses pads for its dE/dx measurement there must be at least 8 pads useable for dE/dx. These cuts are quite loose for reasons that we discuss in the next section.

2. Pions are selected by requiring $P_\pi > 70\%$, and ${\chi^2}_\pi < 10$.

3. In order to eliminate electrons, particularly pairs from photon conversions that could contaminate the unlike-sign distribution if not eliminated, we apply these cuts:

   (a) $P_e < 15\%$

   (b) Reject if ${\chi^2}_e < 3$ and ${\chi^2}_{had} > 2$ and ${\chi^2}_e < {\chi^2}_{had}$

   (c) Reject if identified as part of a conversion pair by pair finding program.

4. We reject tracks with momentum greater than 10% of the beam energy (1.45 GeV) in order to avoid correlations that originate from the constraint of energy conservation within the event.

5. A tight cut is made on the track's closest approach to the vertex in order to eliminate tracks that originate from a K^0 or Λ. Since the impact parameter resolution depends on the momentum of the track, this cut is momentum dependent:
$$\Delta r \ , \ \Delta z < \sqrt{0.2(1 + 1/p^2)} \text{ cm}$$
where is Δr (Δz) the distance to the point of closest approach to the nominal interaction point in the r (z) direction.

6. In order to avoid the possibility of confusing a μ from π decay with a pion, the track is required to have a hit near the inner radius of the TPC. The beginning of the track is required to be at a radius of less than 40 cm.

Discussion of Pair Acceptance

As stated previously, it is important that the acceptance for pion pairs be the same for the real distribution as for the reference distribution. The two most important sources of inefficiency for track pairs are the the loss of good dE/dx measurements for nearby tracks and failure to reconstruct overlapping tracks.

A typical TPC analysis using dE/dx information, will only use those tracks that use dE/dx as measured by wires. This is because the dE/dx resolution is worse for tracks that use pads to measure dE/dx (both because of a smaller number of samples and a shorter portion of the track length being sampled). A track uses pads instead of wires for dE/dx if there are fewer than 2.5 times as many good wires as good pads on the track. This can happen when two tracks are within the same sector and at about the same dip angle so that the wire signals interfere and are thus unusable for dE/dx measurement, while the pad signals are well separated azimuthally. The effect of the loss of wire information is seen clearly if we observe the percentage of tracks that use wires for dE/dx as a function of the difference in dip angle of the closest track within the same sector, Fig. 5.1. If we include those tracks that use pads for dE/dx measurement, this inefficiency for close track pairs is greatly reduced.

The second acceptance problem for track pairs is that even if there is no minimum cut on the number of pads or wires, there is inefficiency for tracks that are close to each other within the TPC because of track overlap. This inefficiency is seen in the distribution of track pairs as a function of the opening angles between them. The opening angles were defined as the difference in dip ($\Delta\lambda$) and in azimuth ($\Delta\phi$) of a point on each track near the center of the TPC (at a radius of 60 cm). There is an inefficiency for track pairs where $\Delta\lambda < 25$ mrad and $\Delta\phi < 40$ mrad of about 40% for like-sign pairs and about 10-20% for opposite sign pairs. We estimated this inefficiency by comparing a band with $\Delta\lambda < 25$ mrad with a side band where there is no inefficiency due to track overlap

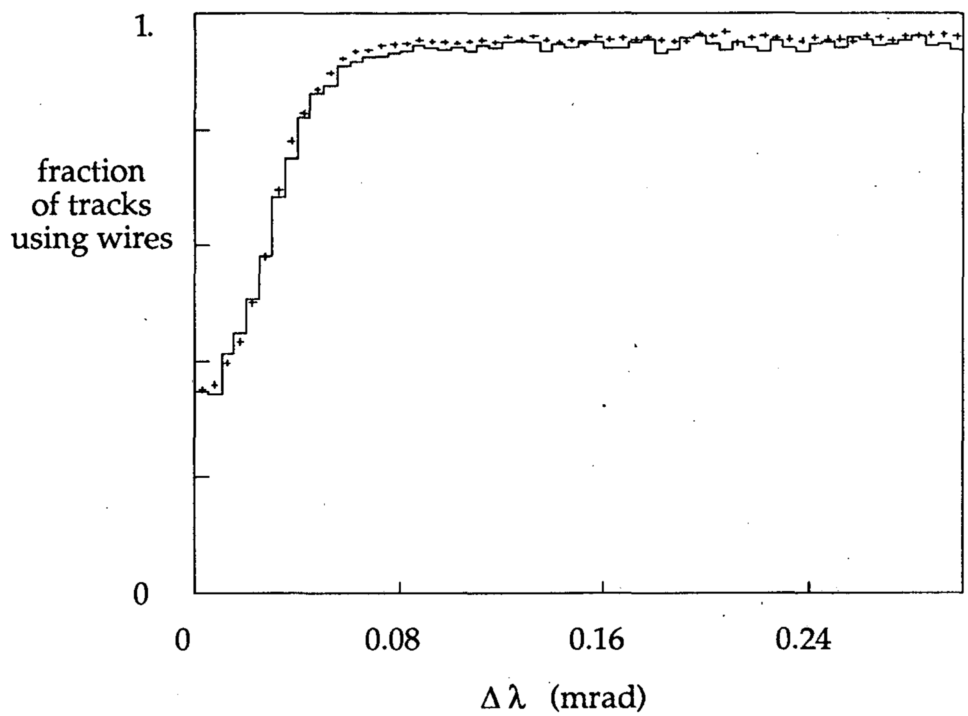

Figure 5.1: The fraction of tracks that use > 40 wires for dE/dx as a function of the difference in dip angle of the closest track within the same sector. The solid histogram is the prediction of a Monte Carlo detector simulation.

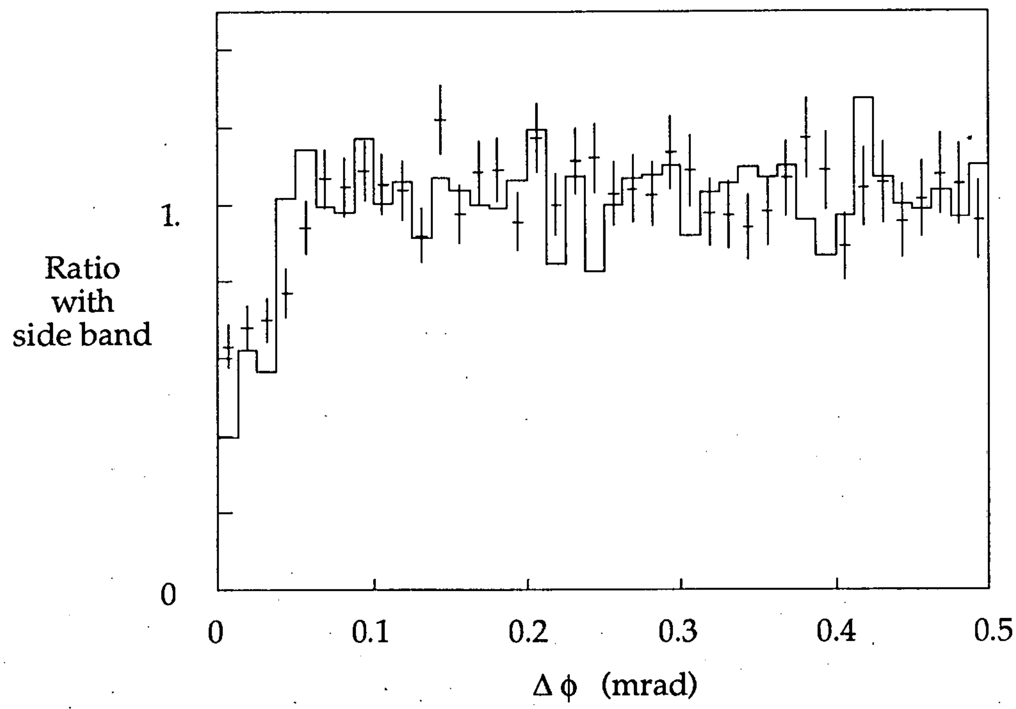

Figure 5.2: The ratio of track pairs for which the difference in dip angle (as defined in Sect. 5.2.1) is $<$ 25mrad to those in a side band ($75 < \Delta\lambda < 100$ mrad), plotted as a function of the azimuthal opening angle. The solid histogram is the prediction of a Monte Carlo detector simulation.

(Fig. 5.2). To reduce the effect of this inefficiency on our measurement, we cut on the opening angle of the track pair as measured at the vertex. This eliminates those tracks that are in the region of decreased efficiency. Since the cut is applied to both the real data distribution and the reference distribution, the ratio will be unaffected by the loss of events.

Track pairs that non-zero opening angle have at the vertex may nonetheless overlap in the TPC, due to track curvature in the magnetic field; therefore, a simple cut on the track opening angle at the vertex may not necessarily remove all tracks which overlap in the TPC. In order to remove those tracks that overlap but have different curvatures, the cut is increased by a term proportional to the difference in curvature. The difference in opening angle at the event vertex and central portion of the tracks in the TPC is given by

$$\Delta\theta_{vertex} = r\Delta C = (100\text{mrad GeV/c})\Delta C \text{ , for a 13.25 kg magnetic field}$$

where $r = 50$ cm is midpoint of the TPC and ΔC is the curvature difference of the two tracks. The cut applied to the track opening angle is then

$$\theta_{vertex} < A + B|1/p_1 - 1/p_2| \tag{5.2}$$

where,

$$A = 50\text{mrad, region over which pair tracking is inefficient}$$

$$B = 100\text{mrad GeV/c}, = \Delta\theta_{vertex}/\Delta C$$

The effect of track pair acceptance losses on our measurement after these measures are taken is small enough that there is no need for an acceptance correction to our measured correlation function. Our detector simulation Monte Carlo will be used to check that this is true (see Sect. 5.3.1). The comparison of Data and Monte Carlo in Figs. 5.1 and 5.2 indicate that the detector Monte Carlo simulates well the two important acceptance effects that we have considered. (The detector simulation Monte Carlo for the TPC is described in Ref. [Aih88].)

5.2.2 Measurement of the Reference Distribution

A list of good pions is saved from each good event for use in forming the mixed event reference distribution. Caution must be taken that false correlations don't result from combining events having different characteristics. Events are binned according to the dip angle of the sphericity axis, so that we combine two tracks only if the sphericity axis dip angles agree to within 5°. This insures that the acceptance for tracks within the two events is about the same. If the events are described in terms of the three sphericity eigenvectors, the acceptance holes surrounding the beam pipe do not necessarily overlap between the two events. Since we have selected primarily two-jet events, rotating about the major sphericity axis should have no effect, so that we can always rotate the event so that the acceptance holes are always in the same azimuthal direction. The reference distribution formed in this way is not significantly different from that obtained by aligning all three sphericity eigenvectors or by aligning the major sphericity axis and arbitrarily rotating the events azimuthally.

In forming the mixed-event reference distribution, pions from each event are combined with pions from several events in order to minimize the fluctuations in a particular bin. Fluctuations in the overall shape of the distribution will not be decreased, since the same set of events is being used. Thus one may expect the shape of the distribution to have larger fluctuations than would be predicted based on the assumption that the occupation of each bin obeys simple Poisson statistics (this effect is discussed in Ref. [Zaj82]). Since the real distribution is derived from the same events, these fluctuations in distribution shape should be highly correlated and cancel when the ratio of the real and the reference distribution is taken. To test if this was true, 10 independent sets of Monte Carlo data were generated, and the scatter of points within each bin was compared the scatter expected based on the assumption of Poisson statistics within each bin. This was done for the reference distribution, which did in fact show larger fluctuations than Poisson statistics would predict, and also was done for the ratio of the real distributions to the reference distribution, which showed fluctuations consistent with those based on Poisson statistics. This study indicates that we can safely use Poisson statistics as long as we only look at correlation functions (ratios of distributions) rather than at the reference distribution itself.

5.2.3 Corrections to the Correlation Function

To insure that the correlation function as closely as possible reflects the size of Bose-Einstein correlations, several corrections are necessary.

Since the final-state coulomb interactions between the charged pions are well understood and are important for low Q pairs, it is possible to remove their contribution to the correlation function. The effect of these interactions is to weight the real distribution by the Gamow factor for the pair[Gyu79],

$$G(\eta) = \frac{2\pi|\eta|}{e^{2\pi\eta} - 1} \text{ where } \eta = \pm\frac{m_\pi \alpha}{Q} \tag{5.3}$$

The sign of η is $+$ for like-sign pairs,$-$ for unlike. The real distribution is divided by $G(\eta)$ to correct for this effect. At low Q this correction is about 3%.

Since the particle identification ability of the TPC is imperfect, particularly for particles whose momenta are close to a crossover region in dE/dx vs momentum space, it is necessary to correct our distributions for non-pion contamination. The problem is that the measured distribution of pion pairs is actually the sum of the real two-pion distribution and the distribution for one pion and another track misidentified as a pion,

$$P(\pi\pi)^{meas} = P(\pi\pi)^{real} + P(\pi X)$$

where X is anything misidentified as a pion (it is assumed that $P(XX)$ is negligible). Given a reasonable estimate for $P(\pi X)$, it can be subtracted from the measured distribution (similarly one needs to estimate the contribution of contamination to the reference distribution, $P_0(\pi X)$). Several reasonable choices can be made, all based on the the detector simulation Monte Carlo, using events generated by the Lund event generator.

$$\begin{aligned} P(\pi X) &= P(\pi X)^{MC} && (5.4) \\ P(\pi X) &= P_0(\pi\pi)^{meas}\frac{P(\pi X)^{MC}}{P(\pi\pi)^{MC}} && (5.5) \\ P(\pi X) &= P(\pi X)^{MC}\frac{P_0(\pi\pi)^{meas}}{P_0(\pi\pi)^{MC}} && (5.6) \end{aligned}$$

(For the reference distribution, P_0 is substituted for P in the above). The first choice, (5.4), suffers somewhat from heavy dependence on the Monte Carlo for the distribution shape. With the other two methods we try to remove this dependence by normalizing to a reasonable estimation of the ratio of the Data to the Monte Carlo distributions. In fact, the correlation function is not very sensitive to which method is used, and the differences can be used to estimate the systematic errors due to this correction (see Sect 5.5). The last method, eqn:background 3, is the one actually used.

As first observed by Zajc [Zaj82], if Bose-Einstein correlations distort the inclusive single particle distributions, then the reference distribution that we measure will also be distorted by the Bose-Einstein correlations. The true Bose-Einstein correlations are given by

$$R(p_1, p_2) = P(p_1, p_2)/P_0(p_1, p_2)$$

with $P_0(p_1, p_2)$ the two-particle distribution in the absence of Bose-Einstein correlations. But rather than measuring $P_0(p_1, p_2)$, we are in effect measuring the product of single particle densities, $P(p_1)P(p_2)$, which are distorted by Bose-Einstein correlations. We correct for this effect by weighting $P(p_1)$ by $1/W(p_1)$, where

$$P(p_1) = W(p_1)P_0(p_1)$$

$$W(p_1) = \int R(p_1, p_2)P_0(p_2)dp_2$$

We estimate $W(p_1)$ for each track by using our initial measurement of $R(Q)$ using the functional form of Eqn. 5.1, and summing over the like-sign pions of the current event to estimate the integral,

$$W(\pi_i) = 1/N_\pi \sum_{\pi_j \neq \pi_i} R(Q_{ij}).$$

If necessary, this process can be iterated with the newly found $R(Q)$. This correction results in a 5% change (increase) in the measured strength of the correlation. Iteration is therefore not necessary.

5.3 Studies of Other Sources of Correlations

It is clearly important to this analysis that all sources of correlations between the like-sign pions that might become apparent be well understood. Monte Carlo studies provide a useful test of how effective this analysis technique is in eliminating such correlations. Several types of Monte Carlo generators have been used to check possible problems of the analysis.

5.3.1 Correlations Caused by Event Mixing Method

A Monte Carlo generator based on an Uncorrelated Jet Model [vHo64] was used to test if the analysis technique that is used has introduced any false correlations. This generator produces events with similar momentum, rapidity and transverse momentum distributions as the real data, and produces events that satisfy energy conservation but whose tracks were otherwise uncorrelated. Except as noted below, no detector simulation was performed for these events, and tracks were only required to be pions with momentum < 1.5 GeV/c. The analysis was done on events with the following different configurations:

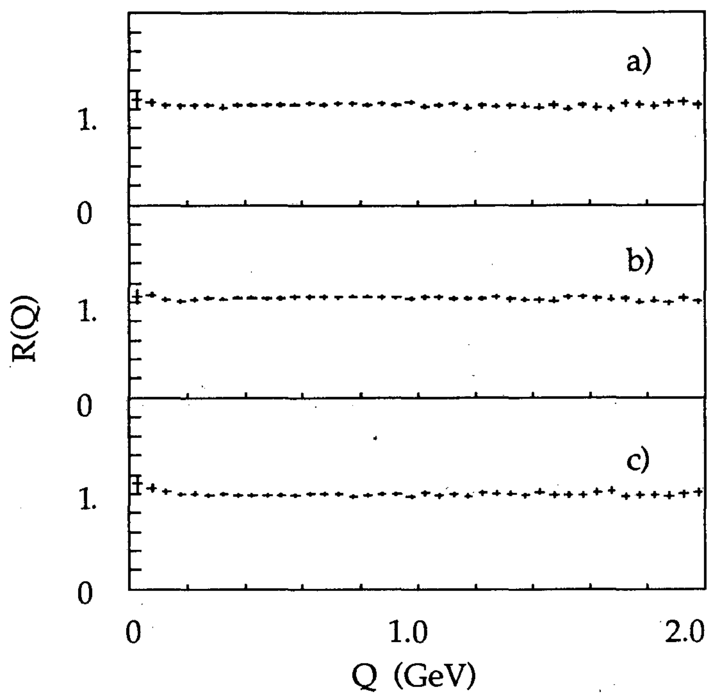

Figure 5.3: Correlation function using UJM Monte Carlo events. a-c) correspond to configurations 1-3), as described in the text.

1. Events all generated along the same axis and event mixing done with respect to that axis.

2. Events generated with the usual $1 + \cos^2\theta$ distribution, and mixing done with respect to the computed sphericity axis.

3. Same as above, but detector acceptance holes crudely simulated. Tracks with dip angle $> 60°$ or tracks closer than $3°$ to sector boundaries were not used.

The correlation function is formed using the distribution of all pion pairs as the real distribution, and the distribution of mixed-event pairs as the reference sample. (Since the particles are produced independently in this model, there is no difference between like-sign and unlike-sign pairs.) In all of these cases the correlation function is found to be flat, as can be seen in Fig. 5.3. If the momentum cut is not made, a positive correlation at low Q is seen. If energy conservation within the event is turned off in the event generator, this positive correlation disappears, confirming that the correlation is due to energy conservation.

As discussed above (Sect. 5.2.1), a possible source of false correlations is that the acceptance for particle pairs is different for the like-sign pairs is different than for the pairs that make up the reference distribution (whether the reference is unlike-sign pairs or mixed events). The extent to which those measures to avoid

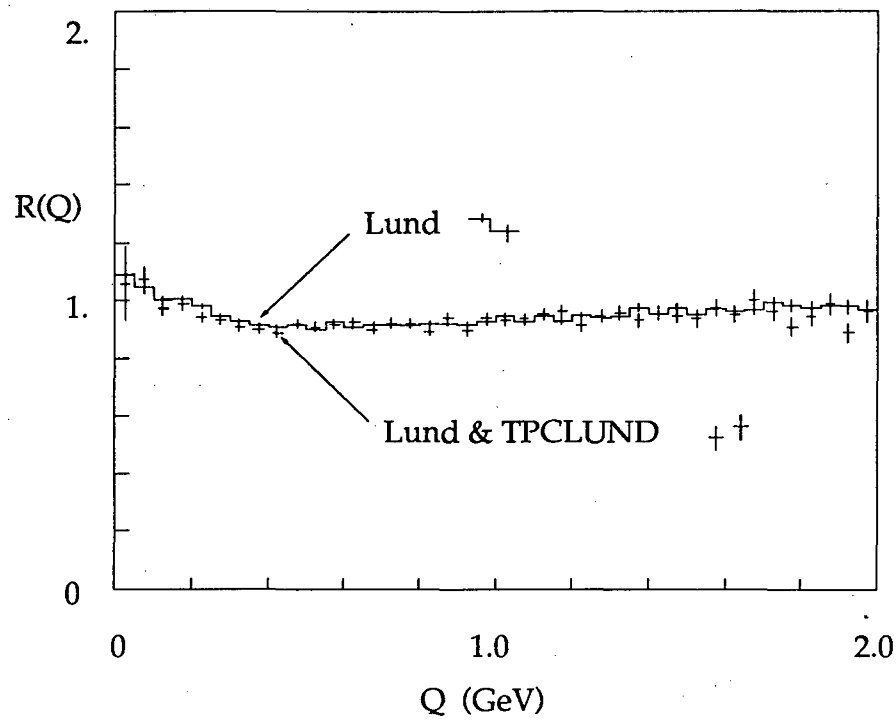

Figure 5.4: Comparison of like-sign correlation function using Lund Monte Carlo events with and without detector simulation (TPCLUND)

these problems described in Sect. 5.2.1 were effective can be tested by use of the detector simulation Monte Carlo. This is done by comparing the correlation function found when using events generated by the Lund Monte Carlo generator with that found using events generated by the same generator but which have been passed through our detector simulation Monte Carlo (TPCLUND). In analysing the events without a detector simulation, the events were selected by the same criteria as in the data analysis and it was required that the tracks used were real pions not originating from K^0 or Λ decays, and within the momentum cuts of the standard analysis ($0.15 < p < 1.45$ GeV/c). The events that were passed through the detector simulation were analysed in the same way as the real data except that the Coulomb interaction correction and the correction of the distortion of the reference distribution described at the end of Sect. 5.2.3 were not done (since these correlations are not simulated in the Lund Monte Carlo). The results are shown in Fig. 5.4

What one first notices is that the correlation function is not flat, as would be desired. The correlation function, however, is not changed after the events have passed through the detector simulation (within the statistical errors); thus, the correlations seen do not originate from detector acceptance effects. The correlations seem to be real physics correlations in the Lund generated events. The origin of these correlations is discussed next.

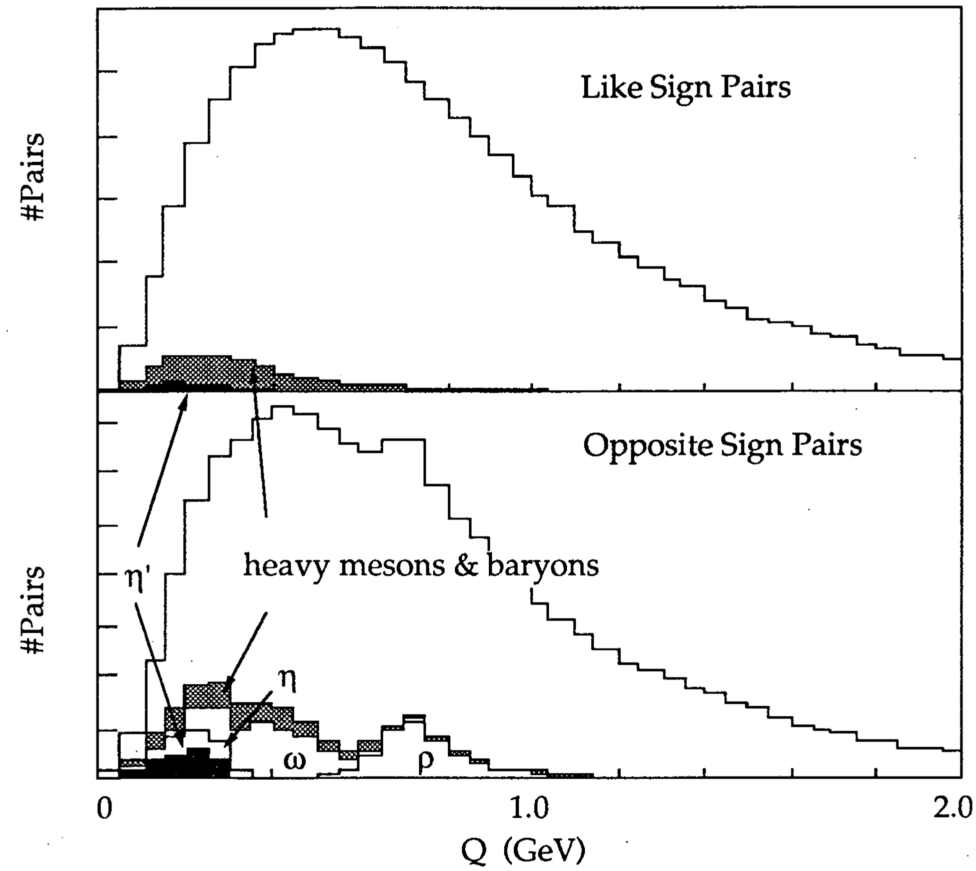

Figure 5.5: Distribution as a function of Q of pairs in which both pions come from the specified common ancestor. (Pions originating from K^0 decay were explicitly excluded from this plot)

5.3.2 Physics Correlations

If both pions that make up a pair are decay products of a resonance, then the limited mass of the resonance will force these pairs to be in regions of low Q (or to be at a fixed Q if the decay is just due to the two pions). There are many resonances that have pions of opposite sign in their decay chains. Fortunately there are fewer decays to like-sign pairs. These come primarily from two sources, pions from the decay chain $\eta' \to \eta\pi^+\pi^-$ with $\eta \to \pi^+\pi^-\pi^0$ or $\pi^+\pi^-\gamma$, and pions from heavy quark mesons. The distribution of these pairs in Q as predicted by the Lund Monte Carlo is shown in Fig. 5.5. The production of η' is not yet well known experimentally and is probably strongly overestimated in the standard version of Lund; therefore, a correction to the data for effects of these resonances is problematic.

An additional source of correlations that the Lund model predicts are the short range correlations. Within the Lund model this effect can be understood by noting that in the Lund string model, it is impossible for two like-signed mesons to be produced adjacent to each other along the string, resulting in an anti-correlation of like-sign pions. This effect manifests itself as a slow rise with

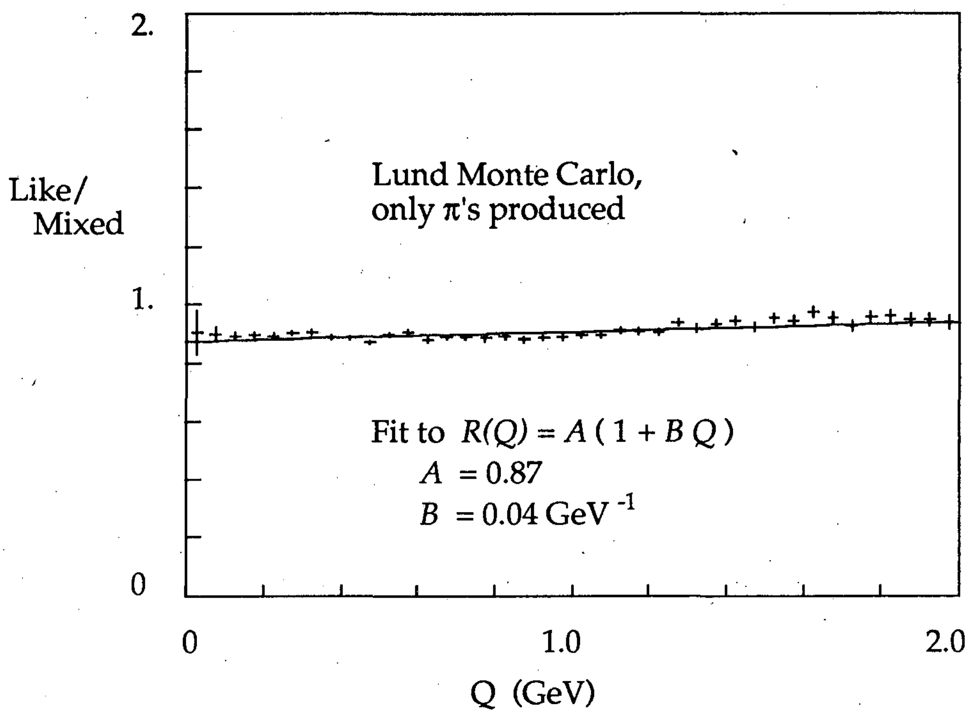

Figure 5.6: Correlation function (like-sign pion distribution divided by mixed-event reference distribution) formed using events from the Lund Monte Carlo, modified so as to only produce pions. Straight line fit is shown.

Q in the correlation function (also seen in the Data). If the effects of resonances are removed from the correlation function (either by looking at unrelated pions or running a modified Lund that only produces primary pions), one finds that this rise is close to linear over the range that we will measure and fit the correlation function, and therefore easily separated from Bose-Einstein correlations. Figure 5.6 shows the correlation function formed using the Lund Monte Carlo modified so as to only produce pions. A straight line fit to the correlation function has a slope of 0.04 GeV^{-1}.

How Well Monte Carlos Reproduce Correlations

The event mixing method provides a useful test of how well a Monte Carlo reproduces correlations from sources other than Bose-Einstein; in addition to measuring the correlations of like-sign pairs, one can measure the correlations of unlike-sign pairs, which should not exhibit Bose-Einstein correlations in either the real data or the Monte Carlo data. Figure 5.7 shows that there is a discrepancy between the two, particularly for Q in the region around 0.3 to 0.7. (The K^0 is seen at $Q = 0.4$ GeV, although most K^0's are removed by the vertex cut on the tracks.) To make things worse, it appears that this discrepancy is dependent on q_0. As seen in Fig. 5.8, the discrepancy seems to be largest for $q_0 < 0.5$

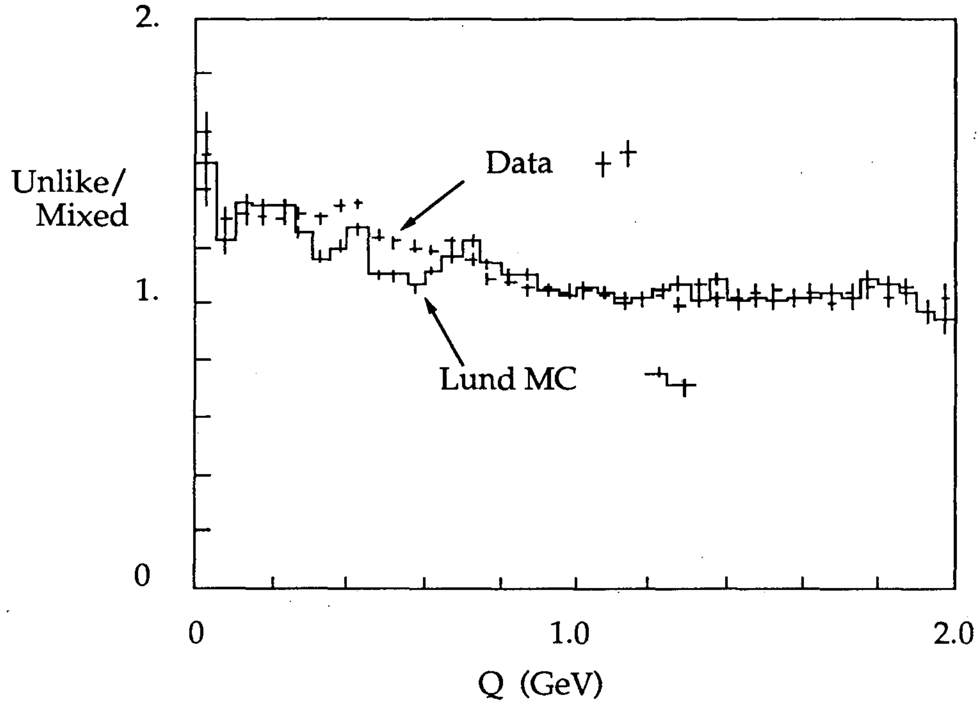

Figure 5.7: Comparison of unlike-sign correlations between Monte Carlo and Data. (The the K^0 is the peak at $Q = 0.4$ GeV, and the ρ is at $Q = 0.72$ GeV.)

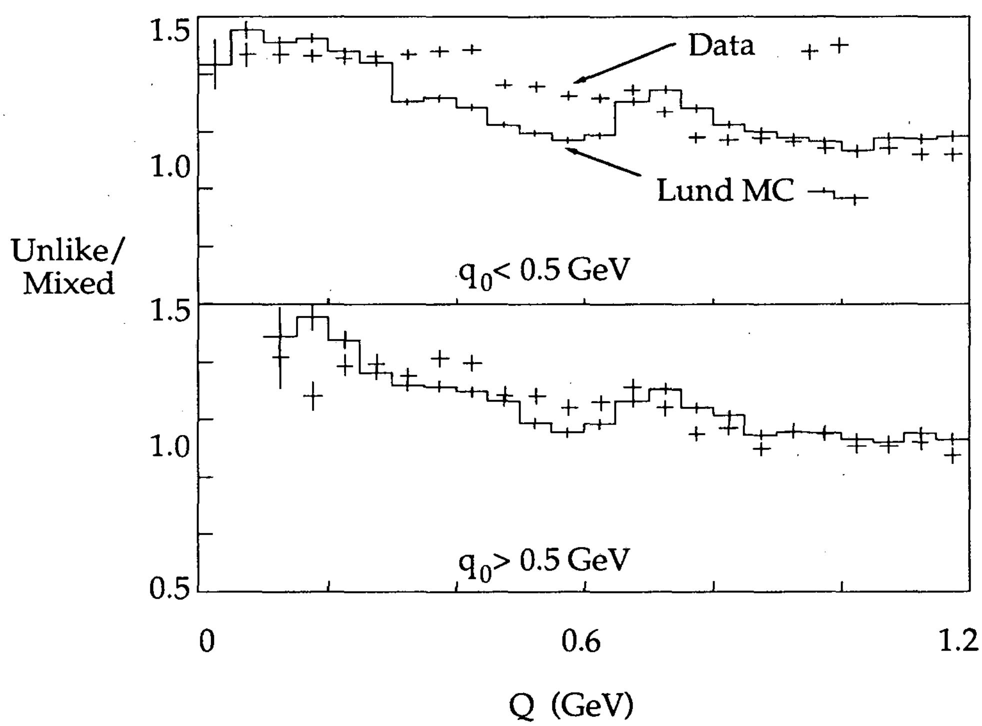

Figure 5.8: Comparison of unlike-sign correlations between Monte Carlo and Data for a) $q_0 < 0.5$ GeV, and b) $q_0 > 0.5$ GeV.

GeV, and is less evident for larger q_0. (The K^0 is explicitly removed from the Monte Carlo histogram, since the detector simulation was not done in this case.) The discrepancy is relatively small compared to the correlations predicted by the Lund Monte Carlo for unlike-sign pairs, but comparable to the correlations predicted for the like-sign pairs.

It is unclear whether it is worthwhile to attempt to use the Monte Carlo to correct the like-signed correlation function, since the uncertainty in the reliability of the Monte Carlo is of the same order of magnitude as the correlations being corrected for. Therefore we will compute the correlation function using the following three methods and use the variation as an estimate of the systematic uncertainty in the non-Bose-Einstein correlations that exist in the data. The three methods used are,

1. Form the correlation function using the mixed-event distribution as the reference sample, without using the Monte Carlo to correct the correlation function.

2. Form the correlation function using the mixed-event distribution as the reference sample, normalize the correlation function with the correlation function obtained with Monte Carlo data.

3. Form the correlation function using the unlike-sign distribution as the reference sample, normalize the correlation function with the correlation function obtained with Monte Carlo data.

In methods (2) and (3) the events generated by the Lund Monte Carlo generator are used form a correlation function just as was done for the real data (using the Mixed-event reference sample for (2) and the unlike-sign reference sample for (3)). The normalized correlation function is the ratio of the real-data correlation function and the Monte Carlo correlation function.

Since the unlike-sign correlation function displays significant structure that is approximately simulated by the Monte Carlo, the unnormalized unlike-sign correlation function will not be considered reliable (although it can be compared with the other correlation functions). Also, since the amount of η' produced is not well known, and probably overestimated by Lund, a modified version of Lund in which η' is not directly produced will be used as normalization and uncertainty due to the contribution of η' will be included in the systematic errors.

The discrepancy between the unlike data and Monte Carlo bears further discussion. The discrepancy is found to be insensitive to changes in the Lund parameters that change the general shape of the events. Using the Webber Monte Carlo produced similar disagreement, as did use of newer versions of Lund containing parton showers (version 6.3). A possible explanation of why the existing Monte Carlo event generators do a poor job of reproducing two-particle distributions is that these event generators do not include the effects of final-state interactions due to the strong interaction. Bowler computed (in [Bow88]) the effect of final-state interactions on the correlations of like-sign pions produced in e^+e^- annihilation. These interactions are found to be of significance if the source size is comparable to the range of strong interactions (roughly 0.2 fermi). He shows that Bose-Einstein enhancement is suppressed by final-state interactions and that the amount of suppression may be consistent with measurements of Bose-Einstein correlations in e^+e^- annihilation data. He is not able to make reliable predictions of unlike-sign pion correlations, but indicates that final-state interactions would be attractive, possibly leading to an enhancement in unlike pion correlations. However, final-state correlations would not be expected to depend on q_0; instead one would expect that they would only depend on Q, the momentum difference between the pions in their own rest frame.

5.4 Results of Fits to Correlation Functions

5.4.1 Single Variable Distribution

The measured correlation function is fit to the following function with 4 parameters,

$$\begin{aligned} R(Q) &= A(1+BQ)(1+\alpha \exp\left[-(rQ)^2\right]), \\ Q &\equiv \sqrt{-q^2}. \end{aligned} \tag{5.7}$$

α is interpreted as the amount of enhancement at $Q=0$ relative to the number of pairs that would exist in the absence of Bose-Einstein correlations, and r is interpreted as the effective size of the source of pions. Since the reference distribution does not perfectly reproduce the Bose-Einstein correlations outside of the region of strong correlation, it is necessary to introduce a linear background term and an overall normalization.

All bins of the pair distributions in Q are well populated so that the errors on the correlation function can be assumed to be gaussian, and a least squares fit can be made using Eqn. 5.7. For the correlation function that uses unlike-sign pairs as the reference distribution, the regions $Q = 0.35 - 0.45$ and $0.6 - 0.8$ are excluded from the fit because of large contributions from ρ and K^0 decays. The results of the fits to the correlation function, $R(Q)$, are shown in Fig. 5.9 and in Table 5.1.

One can see that the variation among the different methods is significant, so that systematic error due to uncertainty in the non-Bose-Einstein correlations will be a major limitation to our understanding the measured parameters. In particular, we cannot reliably distinguish between subtle differences in the functional shape at low Q. The correlation measured using the mixed-event method is somewhat more sharply peaked than a gaussian, but this feature is not obvious when the unlike-sign reference distribution is used.

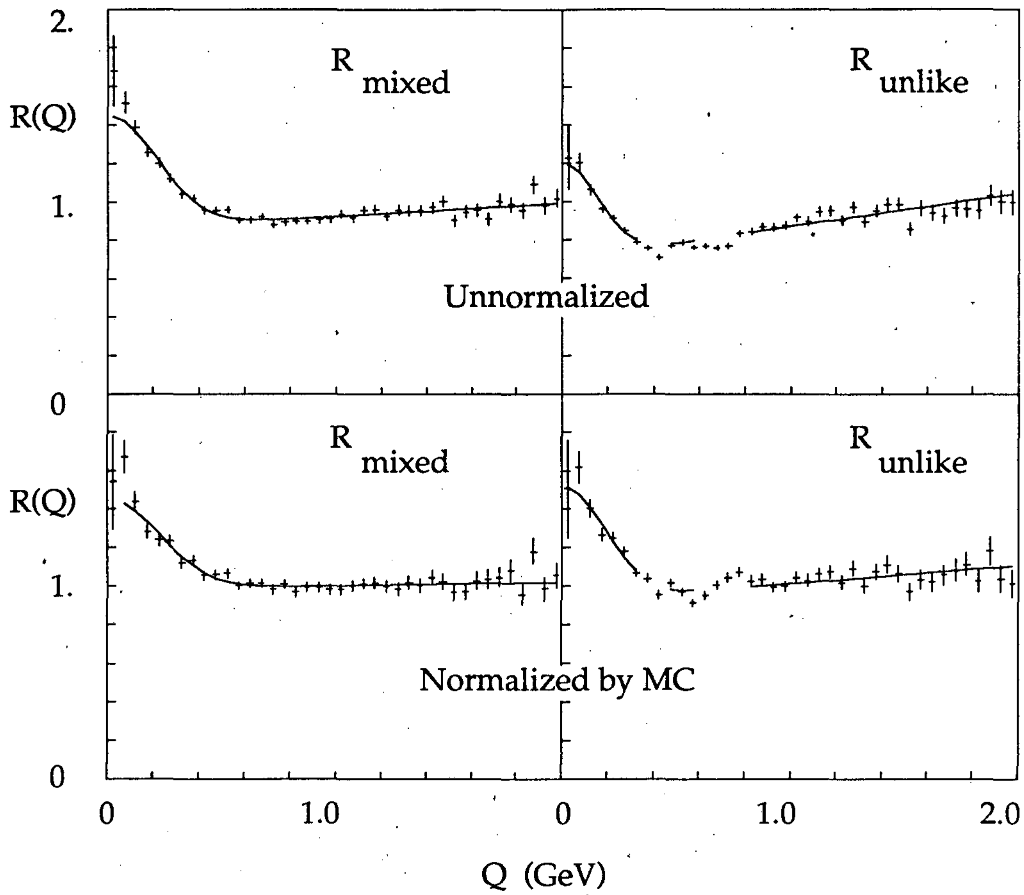

Figure 5.9: Correlation function vs Q with fit. Mixed-event distribution used as the reference distribution on left. Unlike-sign distribution used as reference distribution on right. Plots on bottom are normalized by correlation function obtained from Lund MC Data.

Reference Distribution	α (strength)	Radius (fermi)	Background A	B GeV^{-1}	χ^2/d.o.f.
Mixed	0.69 ± 0.03	0.66 ± 0.02	0.86 ± 0.01	0.09 ± 0.01	57.3/36
Unlike	0.71 ± 0.05	0.94 ± 0.04	0.69 ± 0.01	0.25 ± 0.02	55.8/30
Mixed;norm.	0.51 ± 0.03	0.63 ± 0.03	0.98 ± 0.01	0.03 ± 0.01	53.2/36
Unlike;norm.	0.65 ± 0.05	0.75 ± 0.04	0.92 ± 0.02	0.10 ± 0.02	50.8/30
Average (Syst. Err.)	$0.62 \pm .03$ $\pm .13$	$0.66 \pm .03$ $\pm .11$			

Table 5.1: Fit Parameters to $R(Q)$. (Average excludes unlike unnormalized measurement). The source of systematic error are listed in Table 5.2 and discussed in Sect. 5.5.

5.4.2 Two-Variable Distributions

We now form $R(Q)$ in bands of q_0 to determine how well Bose-Einstein correlations can be described as depending only on Q. $R(Q)$ is shown for each method in Figs. 5.10 – 5.11. The size of the q_0 bins are finer at low q_0 where the statistics are larger, but are still large compared to the momentum resolution. The fits are done just as above, however the background parameters, A and B, have been fixed at the values obtained in the fit to the data averaged over q_0. The resulting parameters are plotted as a function of q_0 in Figs. 5.12. In Fig. 5.13 is plotted the average (weighted by statistical errors) of the three different methods, including an estimation of the systematic errors.

5.5 Systematic Errors

The different sources that contribute to the systematic error in the measured value of the strength parameter, α, and the radius parameter, are listed in Table 5.2. We have found no evidence that any of these errors has any dependence on q_0, so the same errors are assumed for each bin in q_0. It should be clear from the data that the largest contribution is the uncertainty in how well the reference distributions correctly reproduce the non-Bose-Einstein correlations of the real distribution. This is estimated, by observing the spread in the parameter values obtained using the different methods, to be 0.1 for α and 0.1 fm for the radius. In addition we must consider the uncertainty in contribution of pions decaying from the η' which can distort the shape of the correlation function. This error is estimated by normalizing the correlation function to the Lund Monte Carlo with and without any η' being generated. This results in a 0.07 error on α and a 0.04 fm error on the radius.

The error introduced into the correlation function because of unequal acceptance for each distribution (as discussed in Sect. 5.2.1) can be estimated by varying the cuts on the number of wires and pads, and by varying the cut on the opening angle. For both of these cuts, the correlation function was not strongly dependent on the value of the cut, and the assigned error reflects the variation that was seen. The size of additional errors caused by unequal acceptances can be estimated by comparing the correlation function obtained after normalizing with the Monte Carlo with and without the detector simulation being used.

The error due to fake pion contamination is not large, since the correction itself is only about 7%. The error is estimated based on variation in the parameters when using the different prescriptions for this correction discussed in Sect. 5.2.3.

5.6 Discussion of Results

The measurement of the radius parameter is consistent with what we expect for hadronization processes and with what has been previously measured. The

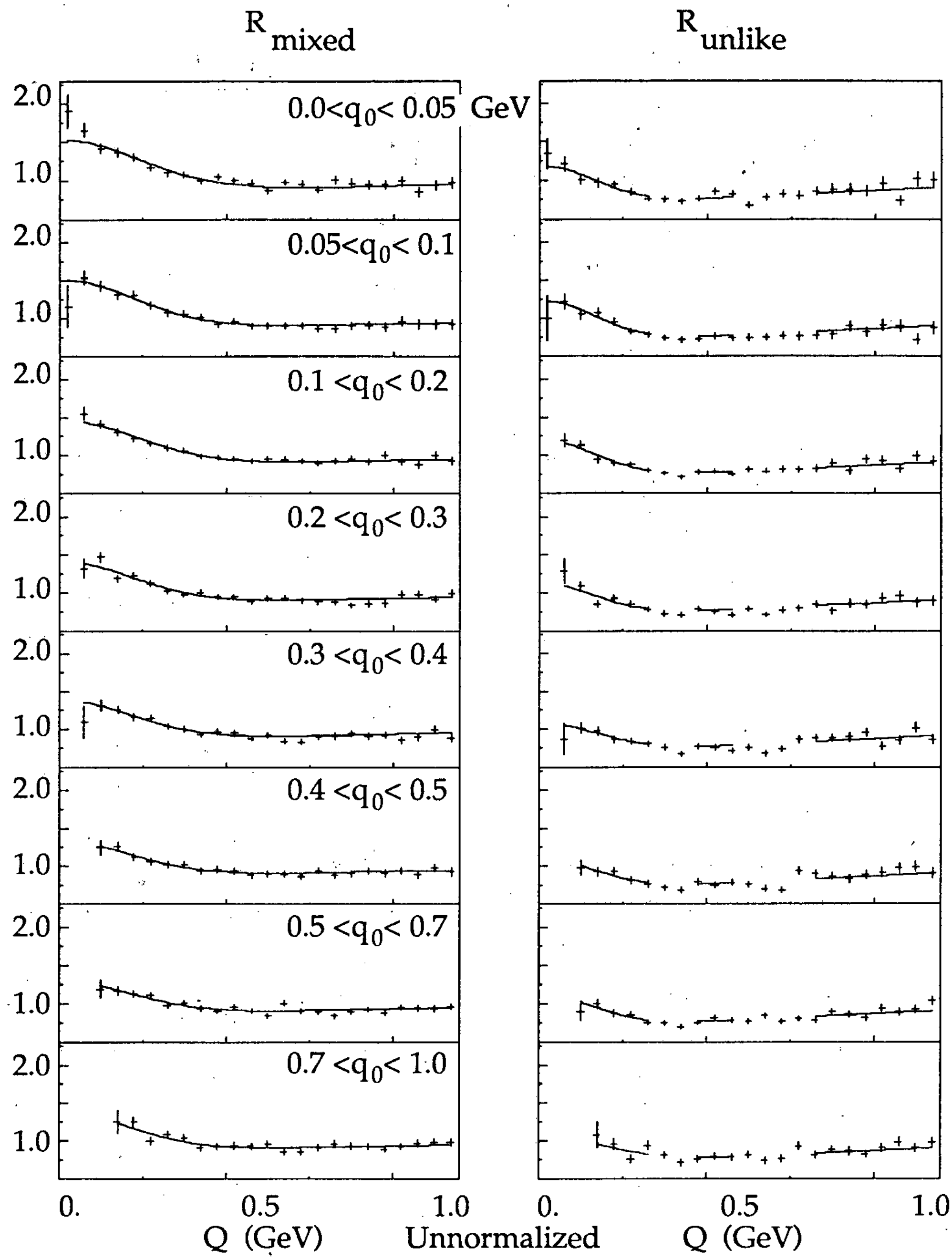

Figure 5.10: Correlation function vs Q with fit in bands of q_0. Mixed-event distribution used as reference distribution on left. Unlike-sign distribution used as reference distribution on right.

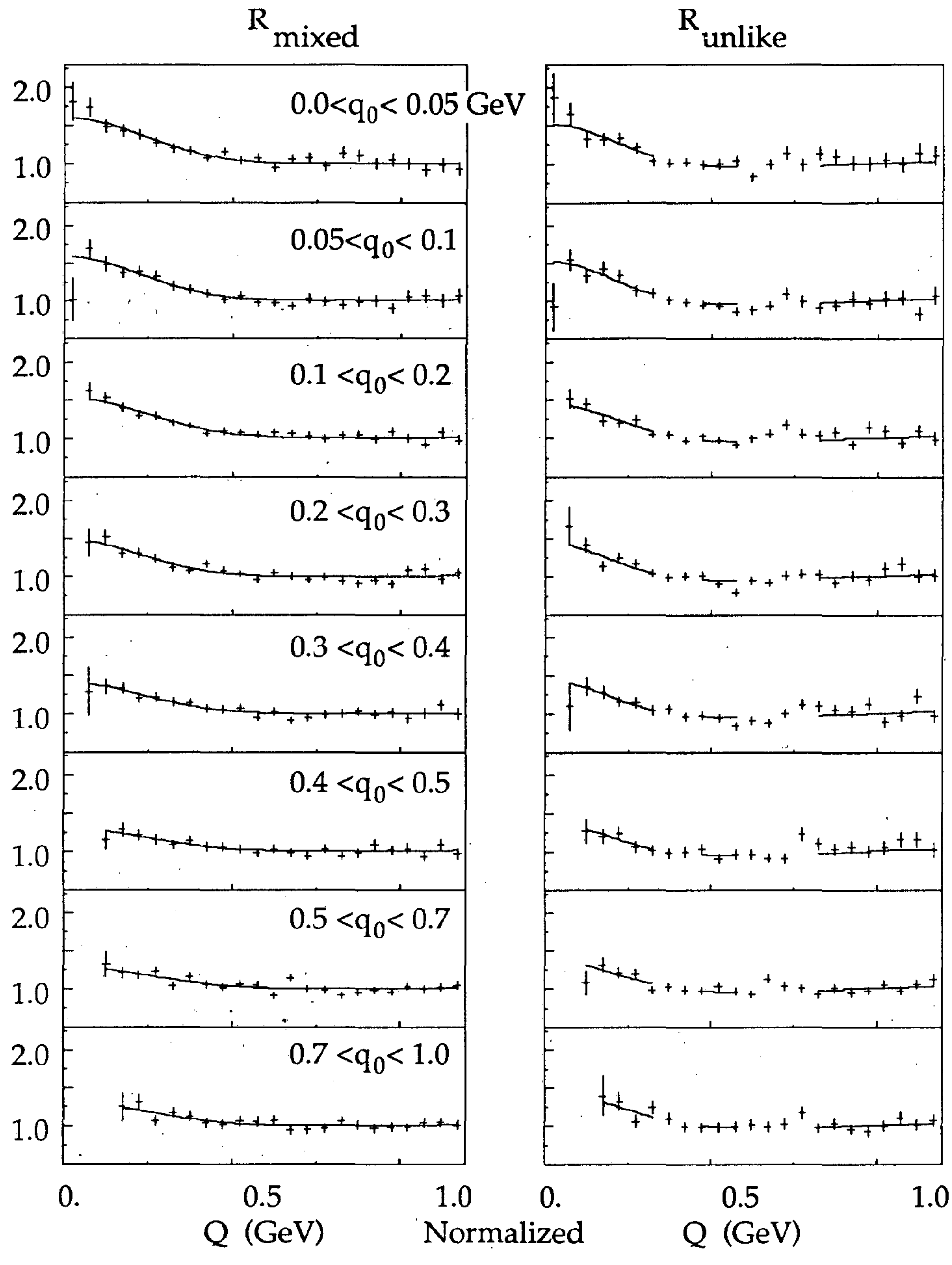

Figure 5.11: Correlation function vs Q with fit in bands of q_0. Mixed-event distribution used as reference distribution on left. Unlike-sign distribution used as reference distribution on right. Plots are normalized by correlation function obtained from Lund MC Data.

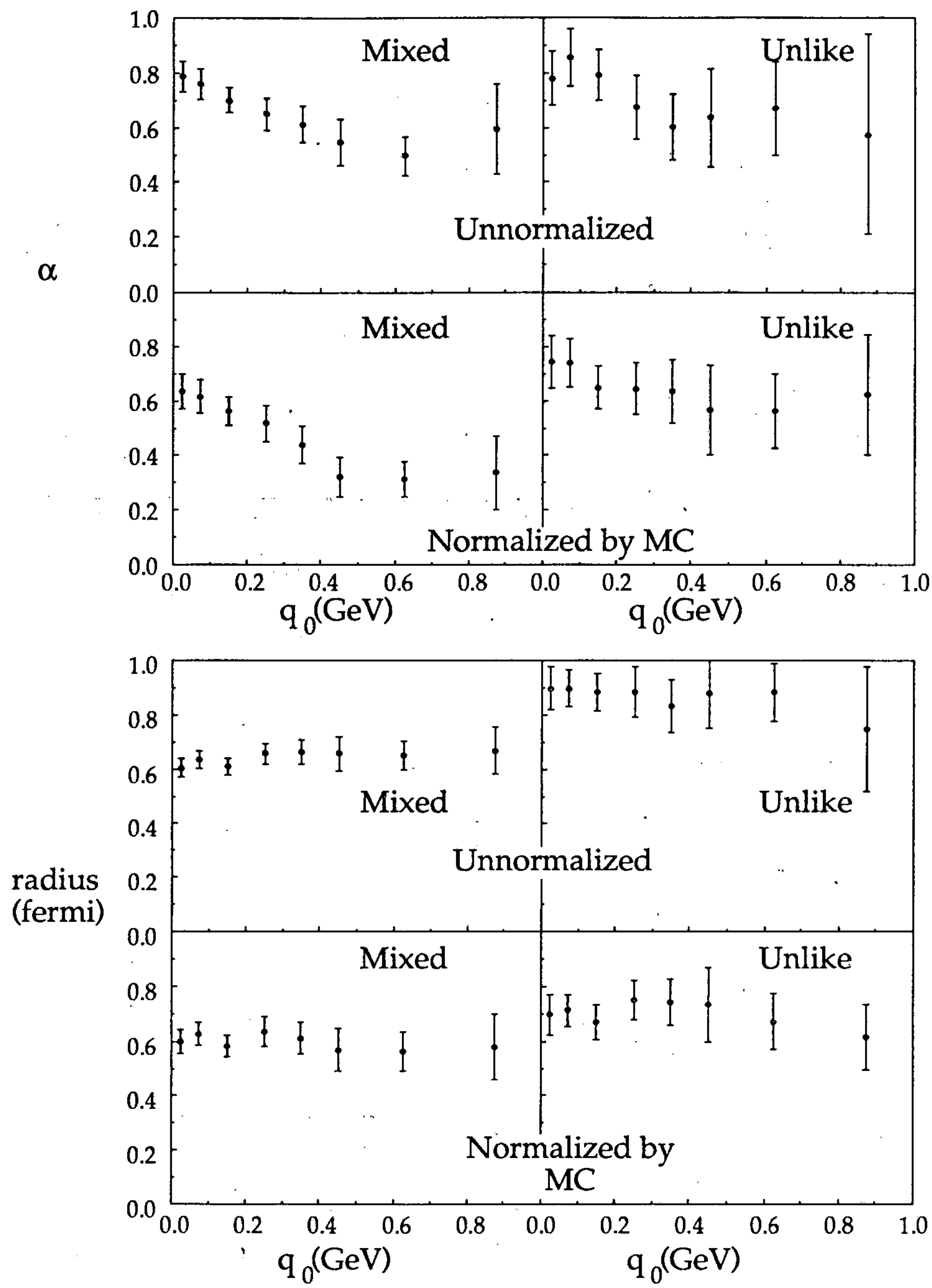

Figure 5.12: Parameters from fits vs q_0 for each method. Mixed-event distribution used as reference distribution on left. Unlike-sign distribution used as reference distribution on right. Plots on bottom are normalized by correlation function obtained from Lund MC Data.

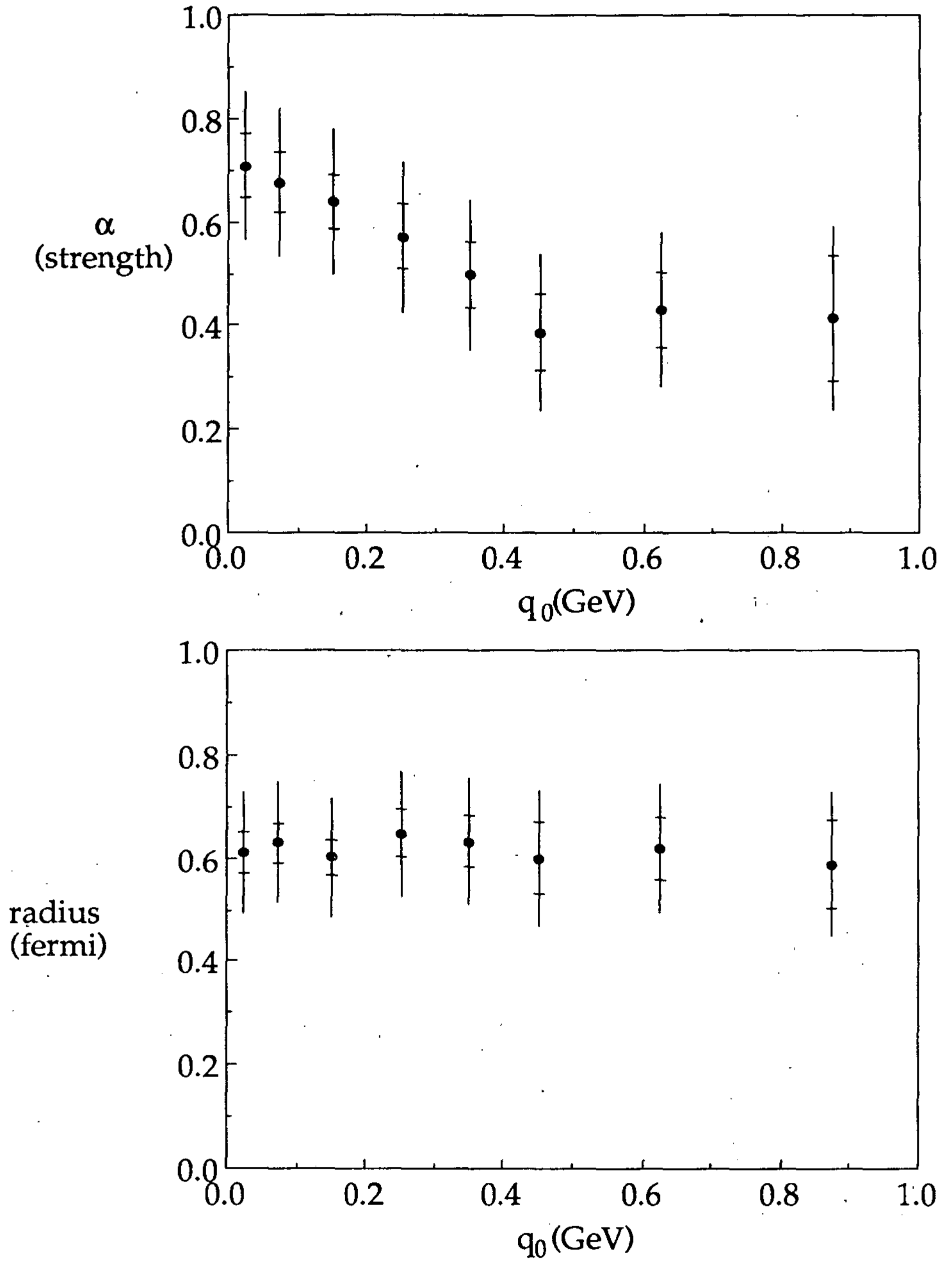

Figure 5.13: Weighted average of parameters from fits vs q_0 for each method (unnormalized unlike-sign method not included in average). Ticks indicate statistical errors. Full error bars indicate statistical and systematic errors added in quadrature.

Error Source	Error	
	α	Radius (fm)
Background Correlations	0.10	0.10
π's from η'	0.07	0.04
Acceptance:		
a) Wire & Pad Cuts	0.01	< 0.01
b) Opening angle Cut	0.02	0.01
c) Other	0.02	0.02
Fake π correction	< 0.01	< 0.01
Total (in quadrature)	0.13	0.11

Table 5.2: Systematic Errors

radius parameter is consistent with being constant with q_0, which is what we expect if Bose-Einstein correlations are not dependent on the lab frame variables but only on variables describing the pion pair in its own rest frame.

The strength parameter, α, is clearly non-zero up to $q_0 = 1$GeV. The correlations are measured to be less than their maximal possible value, as has been previously seen in this and other experiments. The strength parameter, α, decreases with q_0; however, it is not clear that this decrease is significant. This effect is much more prominent when the event mixed reference distribution is used than when the unlike-sign reference distribution is used. In fact, if the the unlike sign distribution is used, the q_0 dependence is essentially flat (although the first few bins are somewhat higher). We consider the several reasons that that α is not the maximum value of 1 and determine if any of these effects may have a q_0 dependence.

The most likely explanation for the lack of maximal Bose-Einstein correlation (evidenced by $\alpha < 1$) is the effect due to pions that originate from long lived resonances[Gra77]. Pions that originate from a resonance should be subject to Bose-Einstein correlations, just as primary pions are; however, the effective size as measured by Bose-Einstein correlations will reflect the production point of the pion when the resonance decays. Thus, for a large fraction of pion pairs where one of the pions is the decay product of a long lived resonance, the effective size of the pion emitting source will be much larger than the size of the hadronization region. For resonances with widths smaller than ~ 10 MeV this will result in a Bose-Einstein enhancement only for Q that is small compared to the momentum resolution of our detector; therefore, the correlated pairs are likely to be washed out. This is more strongly true since the phase space for pair production is very small in this region.

We use the Lund Monte Carlo to estimate how much resonances may cause Bose-Einstein correlations to be suppressed. We generate the usual distribution

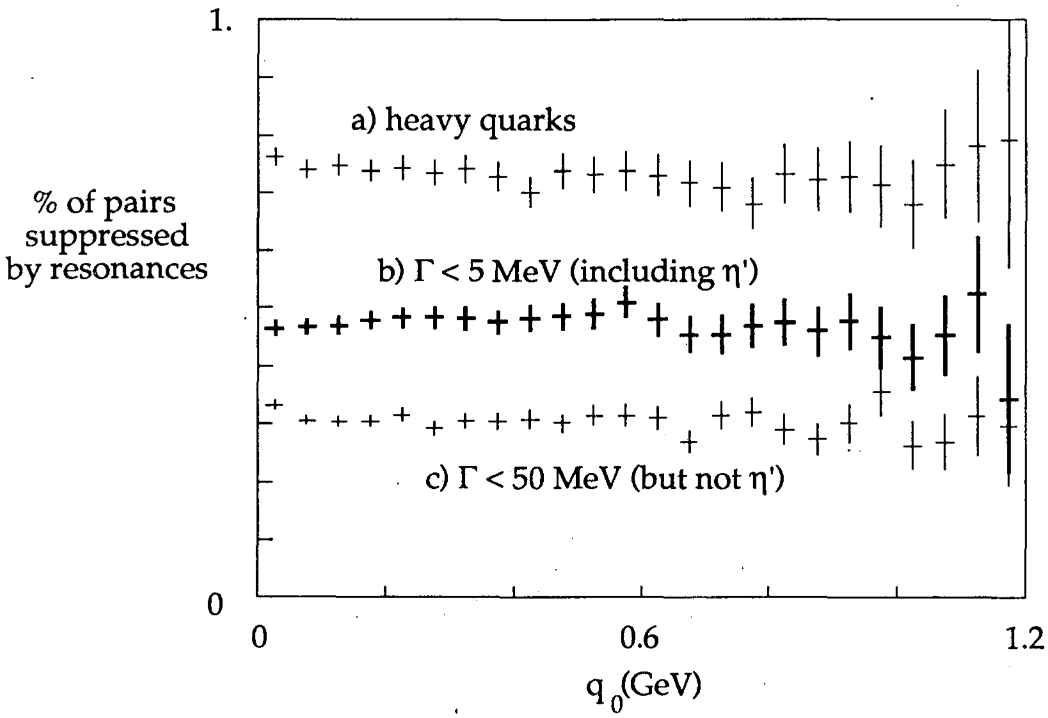

Figure 5.14: Fraction of pairs for which Bose-Einstein correlation is suppressed. a) Only charm and other weakly decaying hadrons contribute to suppression. b) All resonances of width less than 5 Mev contribute to suppression. c) All resonances of width less than 50 Mev contribute to suppression, but ignoring the suppression due to η'.

of pairs using the Lund Monte Carlo as described in Sect. 5.3. We also generate a distribution where we exclude pairs in which one of the pions is descended from what is considered to be a long lived resonance. The amount of suppression that we measure in this way depends strongly on what we consider to be long lived, which is not generally agreed upon. It is generally believed that resonances of width similar to the ρ will decay on roughly the same time scale at which hadronization occurs and thus may not contribute to suppression of correlations[Bow86]. Recent evidence from MarkII shows that all of the suppression may be attributable to charm decays [Jur87]. We show here that although the amount of suppression varies greatly depending on the assumptions made, that there is in no case any substantial q_0 dependence. Using pairs of limited Q ($Q < 0.4$GeV), we plot, Fig. 5.14, the ratio of the non-resonance distribution to the total distribution, assuming:

1. Only charm and other weakly decaying hadrons contribute to suppression.

2. All resonances of width less than 5 Mev contribute to suppression.

3. All resonances of width less than 50 Mev contribute to suppression, but

ignoring the suppression due to η' (as suggested by Bowler[Bow86]).

Although there is a wide range of suppression, in each case the suppression is not strongly dependent on q_0.

If we are incorrect in our assumption that the correlations are gaussian in shape, then it is possible that our measured value of α does not correctly reflect the suppression of correlations. The AFS collaboration at the ISR have found that the sum of two gaussians provides a better fit to their data than a single gaussian [Ake87]. A more sharply peaked shape would lead to a strength parameter closer to the maximal value. Using an exponential instead of a gaussian, for example, results in fits that are close to or exceed the maximal value of $\alpha = 1$. Depending on whether we use the event mixed reference distribution or the unlike-sign reference distribution, our fit to an exponential is better than or worse than the fits obtained with a gaussian shape. It is plausible that use of the wrong shape could result in a different dependence on q_0, since the distribution of pairs in Q varies with q_0; however, when we perform exponential fits to the data binned in q_0, we find that the resulting strength parameter has the same q_0 dependence as when the gaussian shape is used.

The dependence of α on q_0 appears less strong when the unlike-sign reference distribution is used. This may indicate that there is some non-Bose-Einstein correlation common to both the like and unlike distribution that is responsible for this apparent q_0 dependence. The errors obtained when using unlike-sign reference distribution are large, however, so that the unlike-sign α dependence is consistent with that obtained using the mixed-event reference distribution with the present statistics. It has already been noted (see Sect. 5.3) that the discrepancy in the ratio of unlike-sign pairs to mixed pairs between Lund Monte Carlo and data indicates a q_0 dependent correlation that is not well described by the Monte Carlo. It is therefore not possible to conclude from the data that there is a real dependence of the Bose-Einstein correlation strength on q_0.

That Bose-Einstein correlations are seen even where q_0 is large (compared with the range in Q of the Bose-Einstein correlations) is the most significant result of this analysis. The shape of the correlation in Q does not depend on q_0. This is consistent with predictions of current models of how Bose-Einstein correlations are produced in e^+e^- fragmentation. Our observed dependence of α on q_0 is difficult to explain with these models; however, this dependence is probably due to some other physics correlation not yet modeled by fragmentation models, and not due to Bose-Einstein correlations.

Chapter 6

Analysis of Three-Pion Correlations

This chapter discusses the study of three-pion correlations. In the previous chapter, clear evidence for Bose-Einstein enhancement was presented, including evidence that these correlations are affected by the dynamics of hadron production in e^+e^- annihilation physics. Because of the large systematic uncertainty in our knowledge of background correlations, we would like to find independent ways to observe the consequences of Bose-Einstein enhancement. Three-pion correlations are another tool with which we can extend our understanding of Bose-Einstein enhancement [Gol81,Alt86,Liu85]. Although it is clear that the correlations seen in pion triplet momenta are partly just the result of correlation between the pairs within a triplet, Bose-Einstein interference predicts that there will be an additional amount of correlation for multiplets. As shown in Sect. 2.1.1, for a multiplet of n particles, it is expected that interference will increase the probability for small relative momentum n-tuplets by a factor of $n!$. If we can observe this extra enhancement for pion triplets, we will have additional confidence that the correlations we observe are truly a result of Bose-Einstein interference. This chapter will discuss the measurement of three-pion correlations and in particular a method by which we can separate the part of the three-pion correlations that is not simply due to correlations between pairs.

Three-pion correlations are observed using a simple generalization of the method used for two pions. The correlation function is defined as the ratio of the multiplet distribution divided by a reference distribution. As shown in Sect. 2.1.1, the correlation function for triplets of identical particles is:

$$\begin{aligned} R_3(p_1,p_2,p_3) &= 1+|\tilde{\rho}(q_{12})|^2+|\tilde{\rho}(q_{23})|^2+|\tilde{\rho}(q_{31})|^2 \\ &\quad +2Re[\tilde{\rho}(q_{12})\tilde{\rho}(q_{23})\tilde{\rho}(q_{31})], \qquad (6.1) \\ q_{ij} &= p_i-p_j. \end{aligned}$$

The first three enhancement terms are just the correlations that must occur between pairs of pions in the triplet, and are really the same correlations that we have already measured. The last term is unique to triplets, and becomes small if any one particle in the triplet has a large momentum difference from the others. It derives from interference terms resulting from the permutations that are not just between one pair within the triplet.

Although the form of Eqn. 6.1 suggests that best variables to use in our study of correlations between triplets would be q_{ij} for each pair, this is not practical. Instead we use the single variable,

$$Q_3^2 = Q_{12}^2 + Q_{23}^2 + Q_{31}^2.$$

This is a generalization of the variable Q^2 used in two-pion correlation studies and is a relativistic invariant. The maximal correlation will occur in the region near $Q_3 \sim 0$. Three-pion correlations in this variable have been measured by several groups studying e^+e^- annihilation events [Alt86,Jur87].

The possible methods for constructing a suitable reference sample for three-particle correlations are more limited than those for two-particle correlations. The method used in this analysis will be the event mixing technique. This is a straightforward generalization of the two-particle method. Tracks are mixed from three separate events'to form the triplet reference density. The reference density produced in this way is equivalent to the product of three inclusive single particle densities. The correlation function defined in this way will exhibit the full three-pion Bose-Einstein correlations. The unlike-sign method used for pion pairs in the last chapter does not generalize in an obvious way to three pions, since there are only two distinct types of charged pions available to combine. One can use the distribution of triplets with total charge ± 1; however, the like-signed pair within this triplet will still be correlated. This unlike-sign distribution also suffers from the effect of resonances on its shape. In order to avoid these difficulties, we will not use this method here.

It is clearly interesting to try to separate the last term of Eqn. 6.1 from the enhancement between the pairs within the triplet, especially if in doing so some of the uncertainties originating from background pair correlations can be eliminated. One approach used by Liu [Liu85] is to subtract the measured pair correlations from the triplet distribution. The distribution obtained by mixing a pair of tracks from one event with a track from another event can be used to measure the correlation between pairs of pions within a triplet. We define three distributions as follows, establishing a notation where brackets indicate tracks combined from one event, and absence of brackets implies that tracks are mixed from different events:

1. $P^{[+++]}(p_1, p_2, p_3)$ = Like-signed triplet distribution, all tracks from one event.

2. $P^{[++]+}(p_1, p_2, p_3)$ = Like-signed pair from one event mixed with one track from different event.

3. $P^{+++}(p_1, p_2, p_3)$ = Triplets formed with each track from a different event.

The distributions are normalized (as described in the next section) such that that the total number of triplets per event is expected to be the same for each distribution. The standard three-pion correlation function is given by,

$$R_3(Q_3^2) = \frac{P^{[+++]}(Q_3^2)}{P^{+++}(Q_3^2)}.$$

The enhancement from $P^{[+++]}$ due to one pair within the triplet is given by the measured distribution, $(P^{[++]+} - P^{+++})$. The correlations due to the three pairs within $P^{[+++]}$ can be subtracted, forming a triplet distribution that now only exhibits the "pure" triplet enhancement plus an uncorrelated background,

$$\begin{aligned} P^{pure}(p_1, p_2, p_3) &= P^{[+++]}(p_1, p_2, p_3) \\ &- \sum_{pairs_{(ij)}} [P^{[++]+}(p_i, p_j, p_k) - P^{+++}(p_i, p_j, p_k)]. \end{aligned}$$

If we express the above distribution in the variable Q_3^2, the expression is simplified. The variable Q_3^2 is symmetric under permutations of the three particles, so that functions of Q_3^2 do not depend on the order of the particles. Expressing the distributions in the variable Q_3^2 effectively integrates over the other degrees of freedom. The sum over the three pairs is replaced by three times the distributions in the variable Q_3^2:

$$P^{pure}(Q_3^2) = P^{[+++]}(Q_3^2) - 3[P^{[++]+}(Q_3^2) - P^{+++}(Q_3^2)]. \tag{6.2}$$

We can define the "pure" three-pion correlation function as,

$$R_3^{pure}(Q_3^2) = \frac{P^{pure}(Q_3^2)}{P^{+++}(Q_3^2)}. \tag{6.3}$$

Clearly it is important that the distributions are correctly normalized if this method is to be reliable.

We begin by describing the measurement of three-particle distributions and corrections that are made to them. These three-particle distributions are used for both the standard three-pion correlation function and for the pure-three-pion correlation function. In Sect. 6.2 we describe the more straightforward measurement of the full three-pion correlation function, R_3. In Sect. 6.3 we describe the measurement of the pure-triplet correlation function, R_3^{pure}.

6.1 The Measurement of Three-Pion Distributions

The pions are selected according to the same criteria as used in the two-pion study. A triplet is rejected if any pair within the triplet is inside of the opening angle cut used for the two-pion analysis, Eqn. 5.2. This results in the following numbers of triplets in each distribution:

Distribution	# of triplets	Normalization
$P^{[+++]}$	126,000	
$P^{[++]+}$	1,619,000	$N^{[++]+} = 12$
P^{+++}	3,367,000	$N^{+++} = 24$

The third column shows normalization factors used for the mixed event distributions when forming correlation functions. These are necessary because the average number of triplets per event obtained by event mixing is larger than the number of real triplets, since there are more non-redundant combinations available, and because all sign combinations may be used for event mixed triplets. N is the number of mixed triplets expected per real triplet based on the assumption that the pion multiplicities obey Poisson statistics. Deviation from this assumption is an indication of correlations.

The coulomb final-state interaction correction for three pions is discussed in Y. Liu's thesis [Liu85]; for three like sign particles the coulomb repulsion affects the correlation function by this factor:

$$G_3(\eta_{12}, \eta_{23}, \eta_{31}) = G(\eta_{12})G(\eta_{23})G(\eta_{31})$$

$G(\eta_{ij})$ is the gamow factor for the pair ij, and was defined defined in Eqn. 5.3. We remove the affect of the coulomb interaction, dividing the real distribution by $G_3(\eta)$.

The correction for non-pion contamination is similar to that done in the two-pion case. Similar to the two-pion case, the measured distribution is the sum of the distribution of real pion triplets and of triplets containing misidentified non-pions,

$$P^{[\pi\pi\pi]}_{meas} = P^{[\pi\pi\pi]}_{real} + P^{[\pi\pi X]},$$

where it is assumed that the contribution from two or more misidentified non-pions may be neglected. The two correctly identified pions exhibit Bose-Einstein correlations, and the estimate for $P^{[\pi\pi X]}$ must reflect this. This can be done making use of the distribution $P^{[\pi\pi]\pi}$ (the distribution of pairs mixed with a third pion). We correct the measured distribution using,

$$P^{[\pi\pi X]} = P^{[\pi\pi X]}_{MC} \frac{P^{[\pi\pi]\pi}_{meas}}{P^{[\pi\pi]\pi}_{MC}}.$$

The pair-plus-mixed distribution is also contaminated by misidentified particles,

$$P^{[\pi\pi]\pi}_{meas} = P^{[\pi\pi]\pi}_{real} + P^{[\pi\pi]X} + P^{[\pi X]\pi},$$

and is corrected using,

$$P^{[\pi\pi]X} = P^{[\pi\pi]X}_{MC} \frac{P^{[\pi\pi]\pi}_{meas}}{P^{[\pi\pi]\pi}_{MC}},$$

$$P^{[\pi X]\pi} = P^{[\pi X]\pi}_{MC} \frac{P^{\pi\pi\pi}_{meas}}{P^{\pi\pi\pi}_{MC}}.$$

And finally, we also correct the reference distribution,

$$P^{\pi\pi\pi}_{meas} = P^{\pi\pi\pi}_{real} + P^{\pi\pi X},$$

$$P^{\pi\pi X} = P^{\pi\pi X}_{MC} \frac{P^{\pi\pi\pi}_{meas}}{P^{\pi\pi\pi}_{MC}}.$$

6.2 The Three-Pion Correlation Function

Checks on our method for measuring two-particle correlations are repeated for our three-particle study. We again can use Monte Carlo generated events to examine whether the the event mixed reference distribution reproduces the real distribution. The events generated according to the Uncorrelated Jet Model were used to generate the three-particle correlation function that was found to be flat to within 5%, confirming the observation before that the event mixing technique does not in itself introduce false correlations. The Lund Monte Carlo, modified so as to not produce η' directly, was used to generate events, the resulting correlation function being shown in Fig. 6.1(b). There is an enhancement in the correlation function at small Q_3^2. This enhancement does not occur if we only generate events using u,d or s quarks initially. If we only allow pions to be produced, then the correlation function is essentially flat, as seen in Fig. 6.1(c). The enhancement in Fig. 6.1(b) is interpreted as being due to π's from heavy hadron decays. Our uncertainty about this structure, stemming from our lack of knowledge about the number of pions coming from resonances in e^+e^- annihilation events, will clearly be a major limitation in our measurement. It is partially for this reason that we wish to make a measurement that is not so sensitive to pair correlations between pions. That measurement will be described in Sect. 6.3. However, we will present here the measurement of the more conventional correlation function despite the large systematic uncertainties of the measurement.

6.2.1 Fitting

Eqn. 6.1 shows that the three-pion correlation function is not simply a function of Q_3^2, but also depends on Q_{ij} for each pair. If we assume that $\tilde{\rho}(Q_{ij}) = \sqrt{\alpha_2}\exp\left[-1/2(r_2 Q_{ij})^2\right]$ in Eqn. 6.1 and neglect any possible effects of phase, then we would expect,

$$R_3(p_1,p_2,p_3) = 1 + \sum \alpha_2 \exp\left[-(r_2 Q_{ij})^2\right] + 2\alpha_2^{3/2} \exp\left[-1/2(r_2 Q_3)^2\right] \qquad (6.4)$$

With the assumption that on the average $Q_{ij}^2 \approx 1/3 Q_3^2$ this becomes the sum of two gaussians. Since this is at best an approximation to the real shape of the distribution, it has become usual practice to measure the size of three-pion correlations using a single gaussian, as is done in the two-pion case,

$$R_3(Q_3^2) = A(1 + BQ_3^2)(1 + \alpha_3 \exp\left[-(r_3 Q_3)^2\right]). \qquad (6.5)$$

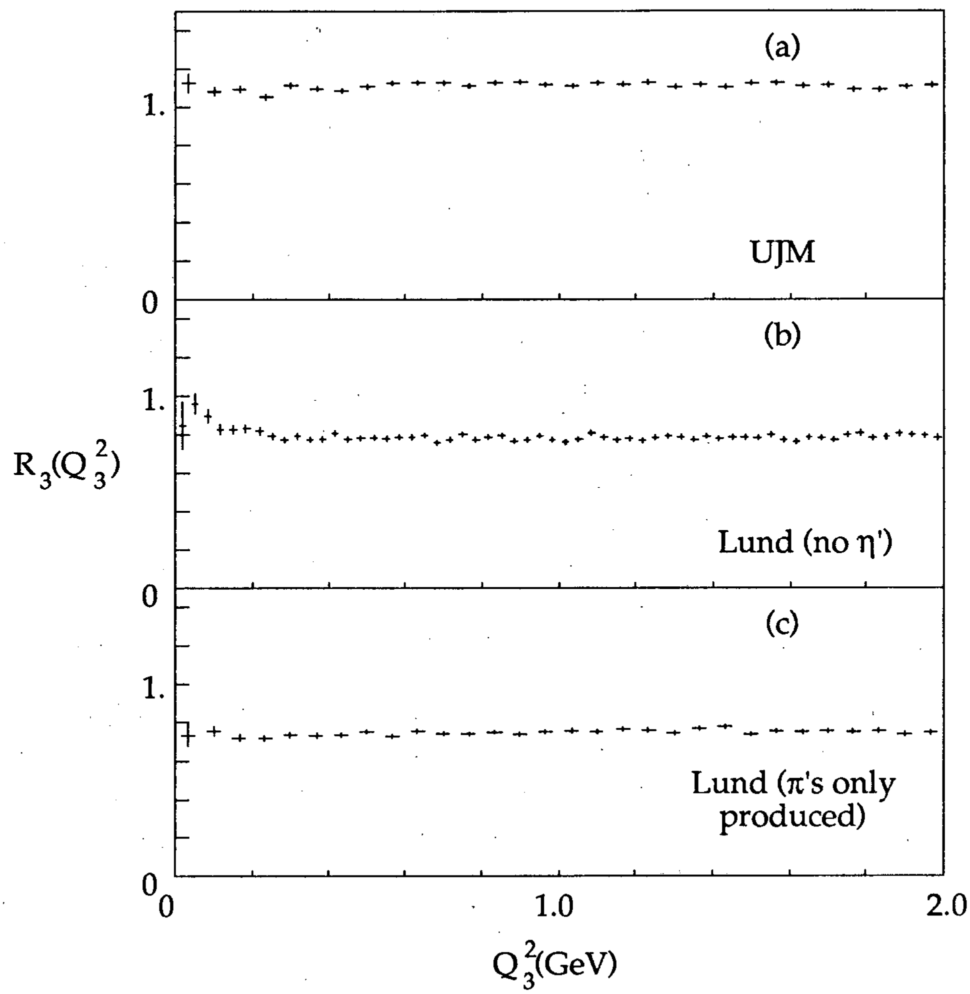

Figure 6.1: Three-pion correlation function formed using Monte Carlo events. a) Uncorrelated Jet Model (UJM). b) Lund Monte Carlo (with no direct η' produced). c) Lund Monte Carlo (modified to only produce pions in the final state)

Reference Distribution	α_3 (strength)	r_3 (fermi)	Background A	B GeV^{-2}	χ^2/d.o.f.
Unnorm.	1.49 ± 0.10	0.41 ± 0.02	0.86 ± 0.01	0.09 ± 0.01	66.5/56
Normalized	1.13 ± 0.12	0.35 ± 0.09	0.98 ± 0.01	0.03 ± 0.01	54.7/56

Table 6.1: Fit Parameters to $R_3(Q_3^2)$.

We then try to relate the measured parameters to what one expects based on the two-pion correlation parameters. We then expect the radius, r_3, to be in the range delimited by the two exponential terms of Eqn. 6.4:

$$r_3^2 = (1/2 - 1/3)r_2^2$$

$$r_3 = 0.38 - 0.47 \quad \text{fermi}$$

and α_3 to be *at most* the sum of the maximum of the enhancement terms in Eqn. 6.4:

$$\alpha_3 < 3\alpha_2 + 2\alpha_2^{3/2} = 1.86 + 0.98 = 2.84$$

where the measured value of α_2 and r_2 from the last chapter have been inserted.

Figure 6.2 and Table 6.1 show the results of the fit to Eqn. 6.5, using the unnormalized data and the data normalized with events generated using the Lund MC. The result of the fit is seen to be quite sensitive to whether the correlation is normalized to the Monte Carlo correlation function. The systematic error is entirely dominated by uncertainty in the background correlations, the effect of which is seen in the spread in fit values depending on whether the MC correlation function is used to normalize the Data. We take our measurement as the weighted average of parameters extracted from the normalized and unnormalized correlation functions. We then estimate the systematic error from the variation in the parameters when the correlation function is or is not normalized by the Monte Carlo. The result is,

α_3	$1.31 \pm 0.11 \pm 0.10$
r_3	$0.40 \pm 0.03 \pm 0.04$

The radius parameter is within the range expected, being closer to the term corresponding to the correlations between pairs. The strength parameter α_3 is smaller than the maximal amount given above, and in fact is smaller than the term from just the correlations between pairs. Although the three-pion correlations seem inconsistent even with what one might expect if the pure-three-pion correlation term were zero, it is dangerous to conclude anything from this, both because of the large uncertainties of the measurement, and because of the broad assumptions made in the interpretation of the fitted parameters of the three-pion correlation function. In particular, it is not obvious that the correlations between

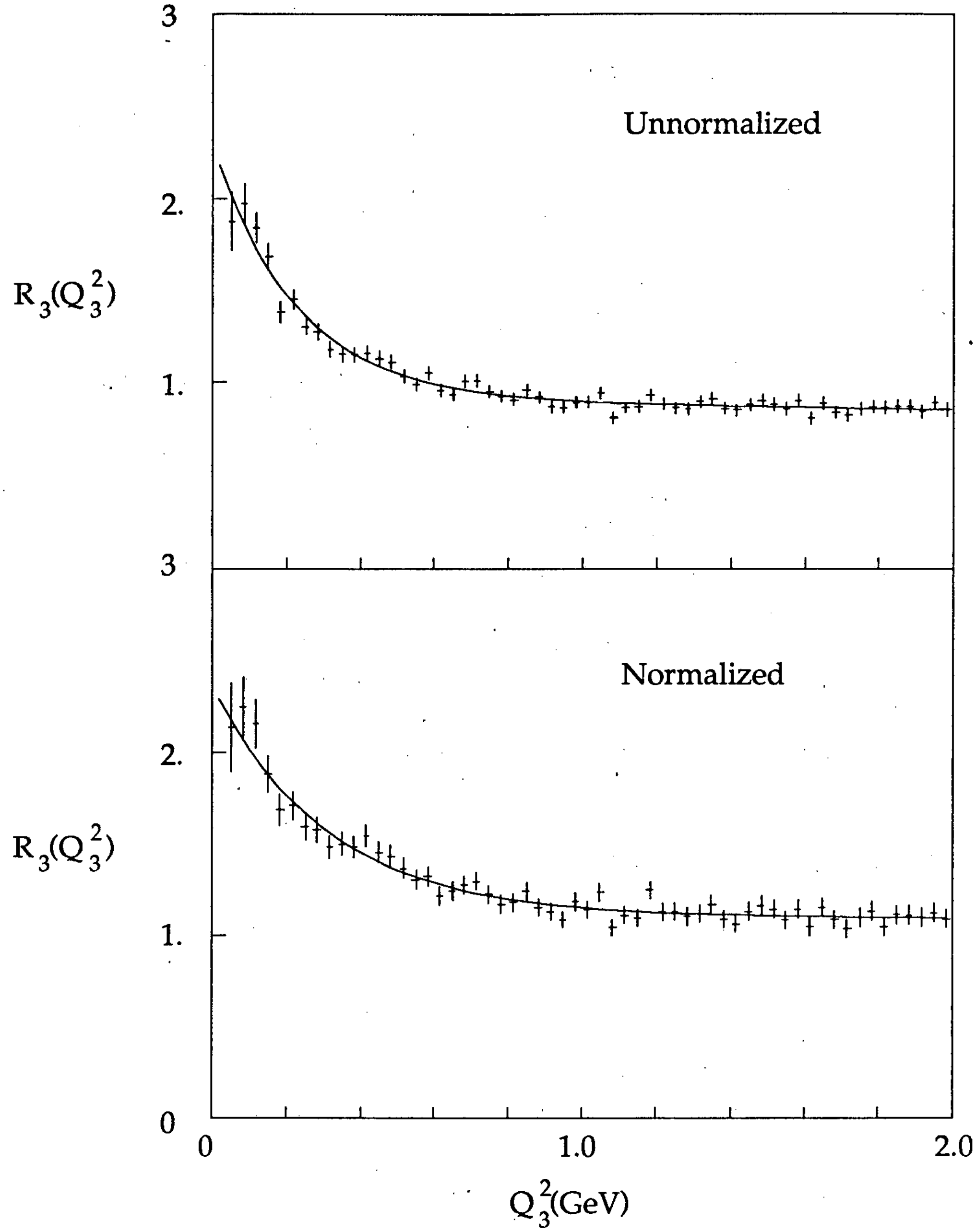

Figure 6.2: 3 pion correlation function formed using Data. a) Not normalized with Monte Carlo, b) Normalized with Lund Monte Carlo correlation function.

pairs of the triplet should really behave as a gaussian in Q_3. A better way to test if the pure-three-pion enhancement exists is to measure the pure-three-pion correlation function, which was described in the introduction of this chapter.

6.3 The Pure-Three-Pion Correlation Function

The pure-three-pion correlation function is defined as

$$R_3^{pure}(Q_3^2) = \frac{P^{[+++]}(Q_3^2) - 3[P^{[++]+}(Q_3^2) - P^{+++}(Q_3^2)]}{P^{+++}(Q_3^2)}.$$

The measurement of the distributions $P^{[+++]}(Q_3^2)$, $P^{[++]+}(Q_3^2)$, and $P^{+++}(Q_3^2)$ has been described in section 6.1. Correlations that depend only on the relative momenta of a *pair* of pions do not contribute to the function. Only correlations which depend on the relative momenta of all three pions will cause an enhancement in R_3^{pure}. The background to a measurement of three-pion Bose-Einstein correlations can have contributions from the various physics correlations described in Section 5.3.2. If these correlations are pair correlations, that is, if they depend only on the relative momenta of a pair of pions, then they will not cause an enhancement in R_3^{pure}. We expect that correlations within like-sign pion multiplets, other than those arising from Bose-Einstein interference, are mostly correlations between pairs of pions. There is no structure to be expected from resonances that would involve three like-sign pions. The Lund Monte Carlo is used to confirm this expectation. Figure 6.3(a) shows R_3^{pure} for Lund Monte Carlo events (including pions from η'decays). The correlation function, R_3^{pure} is flat and approximately equal to 1.0. There is no structure due to resonances or other sources, as there had been in the standard three-pion correlation function (Fig. 6.1). We conclude that the sources of background correlations which are included in the Lund Monte Carlo are all due to correlations between pairs. There may be correlations in the data which are not described by the Lund Monte Carlo, other than the Bose-Einstein correlations. If these are correlations between pairs, they will not cause an enhancement in R_3^{pure}; however, if there are correlations that depend on relative momenta of three (or more) pions then it will be impossible to separate these from the pure-triplet correlations due to Bose-Einstein interference.

We have shown that pair correlations that exist in the Lund Monte Carlo do not cause an enhancement in R_3^{pure}. We must also show that the pure-three-pion correlations due to Bose-Einstein interference will be correctly measured. Unfortunately, although the correlations that exist between pairs do not in themselves cause an enhancement in R_3^{pure}, the existence of such correlations can affect the measured value of pure-triplet correlations. This effect, discussed in detail in Appendix A, is similar and related to the effect of improper relative normalization of the triplet distributions that are used to derive the pure-triplet distribution. We attempt to correct for this affect by properly normalizing the distributions

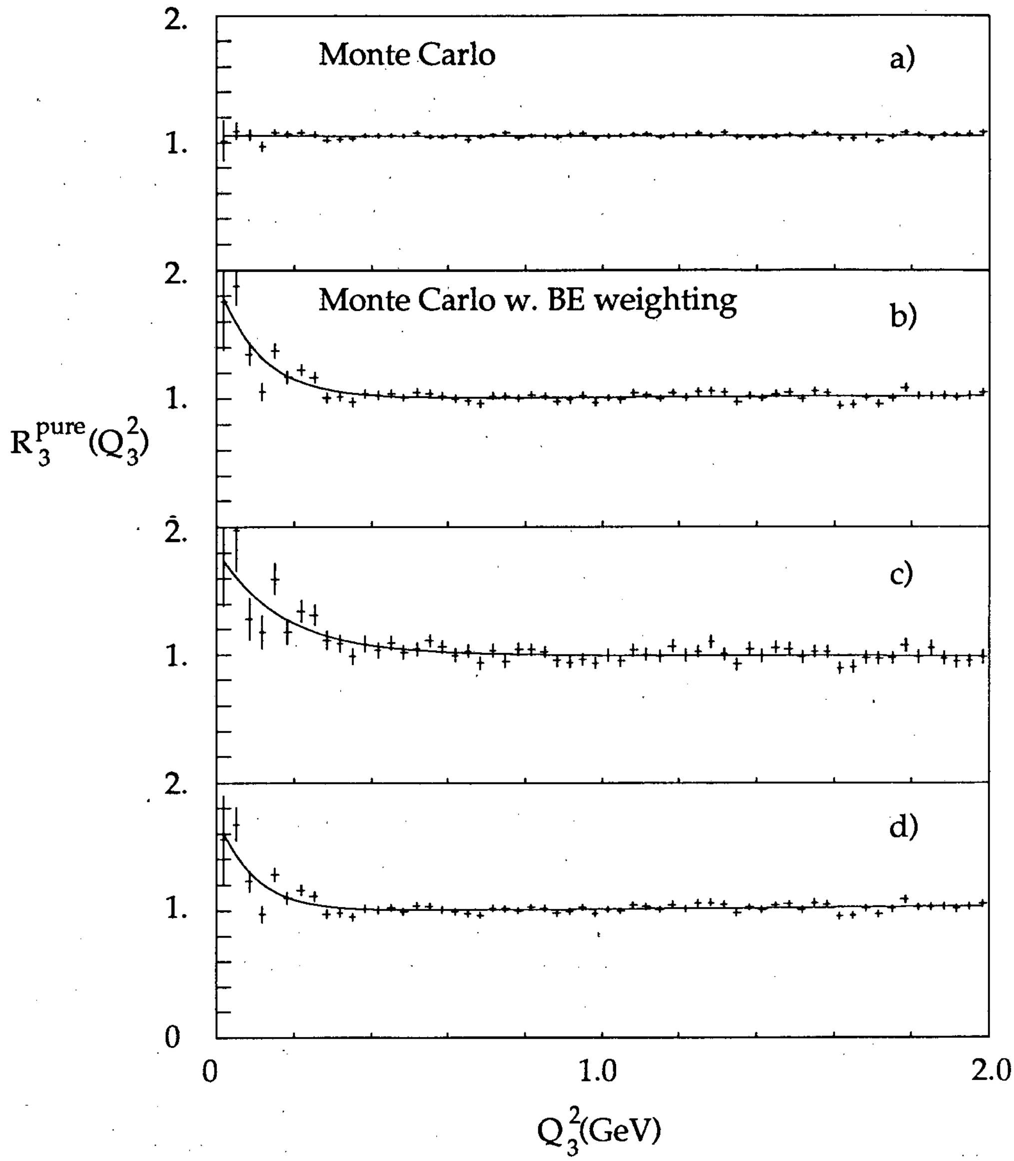

Figure 6.3: Pure-three-pion correlation function (R_3^{pure}) formed using Monte Carlo events. a) Lund Monte Carlo (with no direct η' produced). b-d) Lund Monte Carlo events weighted by model for Bose-Einstein interference using $\alpha_2 = 0.6$ and $r_2 = 0.7$. The correlation function is computed using each of the normalization methods described in Sect. 6.3.

$P^{[+++]}(Q_3^2)$, $P^{[++]+}(Q_3^2)$, and $P^{+++}(Q_3^2)$, which are used to compute the pure-three-pion distribution, $P^{pure}(Q_3^2)$.

6.3.1 Normalization

We will estimate the error introduced in our measurement of the correlations due to improper normalization of the distributions by using several different normalization techniques. As already discussed in Sect. 6.1, the distributions involving pions from mixed events ($P^{[++]+}(Q_3^2)$ and $P^{+++}(Q_3^2)$) are normalized so that the number of triplets per event would be the same as the number of real triplets (those making up $P^{[+++]}(Q_3^2)$) if the pion multiplicities obeyed Poisson statistics. We then attempt to correct for influence of pair correlations on the distributions $P^{[+++]}(Q_3^2)$ and $P^{[++]+}(Q_3^2)$ using one of the following normalization techniques:

None: We compute $P^{pure}(Q_3^2)$ as in Eqn. 6.2 without any normalization, ignoring the effect of pair correlations.

MC: We normalize each distribution by the appropriate correlation function determined from Lund Monte Carlo events:

$$
\begin{aligned}
P_N^{[+++]}(Q_3^2) &= P^{[+++]}(Q_3^2)/R_{MC}^{[+++]}(Q_3^2) \\
P_N^{[++]+}(Q_3^2) &= P^{[++]+}(Q_3^2)/R_{MC}^{[++]+}(Q_3^2)
\end{aligned}
$$

where,

$$
\begin{aligned}
R_{MC}^{[+++]}(Q_3^2) &= P_{MC}^{[+++]}(Q_3^2)/P_{MC}^{+++}(Q_3^2) \\
R_{MC}^{[++]+}(Q_3^2) &= P_{MC}^{[++]+}(Q_3^2)/P_{MC}^{+++}(Q_3^2)
\end{aligned}
$$

This method corrects $P^{[+++]}(Q_3^2)$ and $P^{[++]+}(Q_3^2)$ for all correlations included in the Lund Monte Carlo. This may be wrong since correlations between particles from a resonance are corrected for, even though Bose-Einstein enhancement does not occur in between such particles.

Constant: We assume that the pair correlations can be corrected for by normalizing the distributions to agree at large Q_3^2. It is found (both in data and in Monte Carlo) that the following normalization results in good agreement between $P^{[+++]}(Q_3^2)$, $P^{[++]+}(Q_3^2)$, and $P^{+++}(Q_3^2)$ at large Q_3^2:

$$
\begin{aligned}
P_N^{[+++]}(Q_3^2) &= P^{[+++]}(Q_3^2)/(1-3\epsilon), \\
P_N^{[++]+}(Q_3^2) &= P^{[++]+}(Q_3^2)/(1-\epsilon),
\end{aligned}
$$

with $\epsilon = 0.06$.

The measurement of pure-three-pion correlations is particularly sensitive to the relative normalizations of the three distributions at low Q_3^2, where the Bose-Einstein correlations are non-zero.

6.3.2 Fitting

We could fit the correlations using the functional form that we used for the standard three-pion correlations:

$$R_3^{pure}(Q_3^2) = A(1 + BQ_3^2)(1 + \alpha_3 \exp[-(r_3 Q_3)^2]). \tag{6.6}$$

However, we wish to express the parameters in such a way that they can be more easily compared with what we expect based on the two-pion correlation parameters. We expect that the measured correlations will be given by the pure-triplet correlations, *i.e.* to be given by Eqn. 6.4 but with the second term removed. We therefore fit to the modified form:

$$R_3^{pure}(Q_3^2) = A(1 + BQ_3^2)(1 + 2\alpha_2^{3/2} \exp[-1/2(r_2 Q_3)^2]). \tag{6.7}$$

r_2 and α_2 are simple related to r_3 and α_3 by comparison of the above two forms:

$$\alpha_2 = 1/2\alpha_3^{2/3}$$

$$r_2 = \sqrt{2} r_3.$$

The results of fits will be expressed using r_2 and α_2.

6.3.3 Monte Carlo Consistency Check

We check the consistency of our method by forming distributions using Monte Carlo events, and weighting these according to the simple three-pion correlation model presented in Sect. 6.2.1. Using these weighted Monte Carlo distributions to form the pure-three-pion correlation function, and fitting this function to Eqn. 6.7, we can confirm that the fitted parameter values, α_2 and r_2, are the same as those that we put in when weighting the events.

We form the distribution $P_{BE}^{[+++]}(Q_3^2)$ by measuring the number of real triplets, with each triplet weighted by the Bose-Einstein enhancement, (from Sect. 6.2.1),

$$R_3(p_1, p_2, p_3) = 1 + \sum \alpha_2 \exp[-(r_2 Q_{ij})^2] + 2\alpha_2^{3/2} \exp[-1/2(r_2 Q_3)^2] \tag{6.8}$$

The values of parameters α_2 and r_2 are chosen approximately to be those measured from two-pion correlations. We form the distribution $P_{BE}^{[++]+}(Q_3^2)$ from triplets consisting of a pair from a real event and a third particle from a mixed event, weighting the triplet by,

$$R_2(p_1, p_2, p_3) = 1 + \alpha_2 \exp -(r_2 Q_{12})^2 \tag{6.9}$$

(Q_{12} being for the real pair). We now form the pure-triplet correlation function, using these weighted Monte Carlo distributions as data:

$$R_3^{pure}(Q_3^2) = \frac{P_{BE}^{[+++]}(Q_3^2) - 3[P_{BE}^{[++]+}(Q_3^2) - P^{+++}(Q_3^2)]}{P^{+++}(Q_3^2)}.$$

Normalization	α_2 (strength)	r_2 (fermi)	Background A	B GeV^{-2}	χ^2/d.o.f.
None	0.64 ± 0.08	0.91 ± 0.06	1.02 ± 0.01	0.00 ± 0.01	109.5/116
MC	0.60 ± 0.10	0.73 ± 0.07	1.01 ± 0.01	0.00 ± 0.01	130.9/116
Constant	0.55 ± 0.09	1.01 ± 0.08	1.01 ± 0.01	0.01 ± 0.01	116.3/116
Input	0.60	0.70			

Table 6.2: Fit Parameters to $R_3^{pure}(Q_3^2)$. Monte Carlo events weighted with simple Bose-Einstein form.

The resulting pure-triplet correlations should then be consistent with the input parameters.

In Fig. 6.3 (b-d) we show the pure correlation function obtained using Monte Carlo events weighted using $\alpha_2 = 0.6$ and $r_2 = 0.7$, using each of the normalization methods. Table 6.2 shows the results of fits using the pure-three-pion correlation fitting function, Eqn. 6.7. The unweighted Monte Carlo is expected to reproduce the input parameters, which it does. The unnormalized and constant normalized methods do less well at reproducing the input parameters, but this is not surprising. These methods assume that two-pion correlations caused by resonances do not affect the shape of the pure-three-pion correlation function, which may be a reasonable assumption for the actual data. In this simple model, however, the Monte Carlo triplets were given a Bose-Einstein weight regardless of whether the pair was from a resonance, thus since pions from resonances are contributing to this Bose-Einstein weight, such assumptions do not work so well. The measured value of r is larger than the value put in when these other two methods were used. The differences will give us an indication of systematic uncertainties in our measurement that result from uncertainty in the appropriate normalization.

6.3.4 Results

The pure-triplet correlation function obtained from the data is shown in Fig. 6.4, using each normalization method. A clear signal is seen regardless of which normalization method is used, giving us confidence that the signal does not arise from incorrect normalization of the distributions. The results of the fits are in Table 6.3.

The primary systematic uncertainty in this measurement is in the correction for the effect that two-particle correlations have on the pure-three-pion correlations, as described in Appendix A, or equivalently, in the uncertainty in the relative normalization of the distributions at low Q_3. We expect the so called Constant method of normalization to be more reliable than the other methods, for reasons discussed in the appendix. Therefore, we will take our result to be

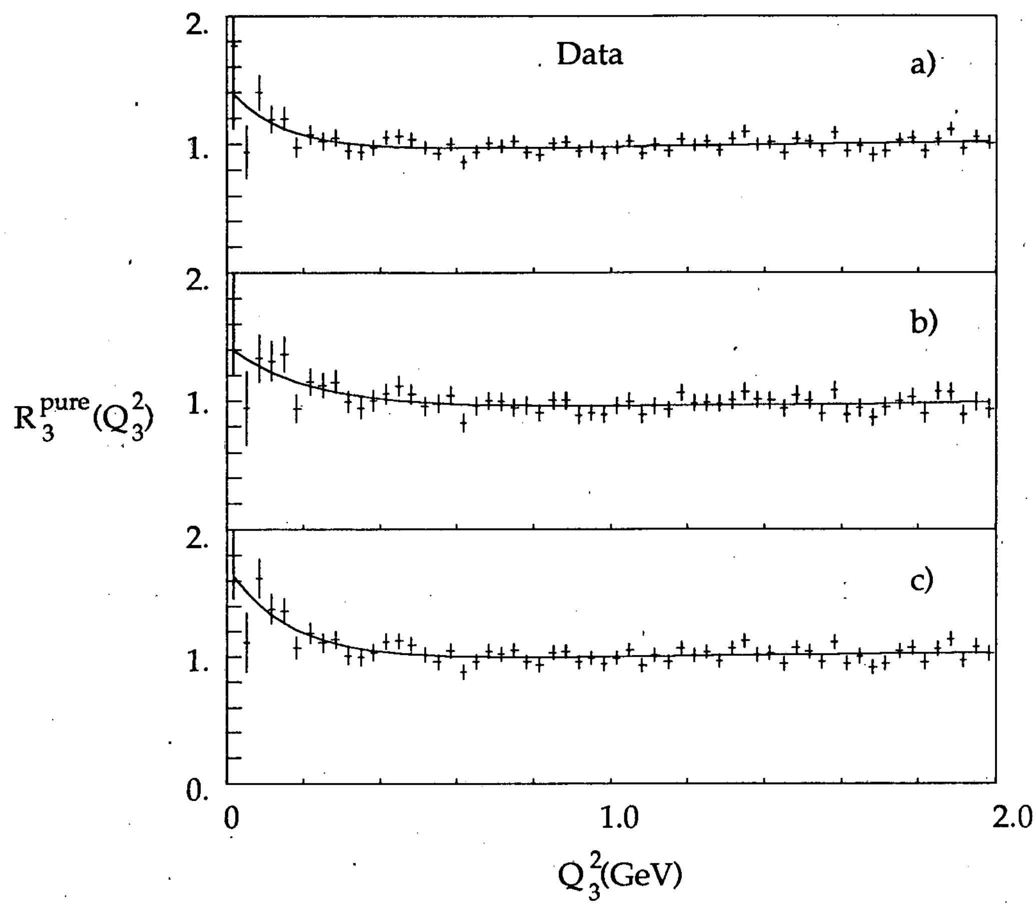

Figure 6.4: 3 pion correlation function formed using Data. a-c) Using each of the normalization methods described in Sect. 6.3.

Normalization	α_2 (strength)	r_2 (fermi)	Background A	B GeV^{-2}	χ^2/d.o.f.
None	0.44 ± 0.13	0.87 ± 0.13	0.97 ± 0.01	0.01 ± 0.01	126.5/116
MC	0.43 ± 0.10	0.66 ± 0.10	0.95 ± 0.02	0.02 ± 0.01	100.1/116
Constant	0.55 ± 0.10	0.77 ± 0.09	1.00 ± 0.01	0.01 ± 0.01	126.1/116

Table 6.3: Fit Parameters to $R_3^{pure}(Q_3^2)$. Data.

that of the Constant method; however, we will take our systematic error as the variation in the three methods, including the method of not normalizing at all. The systematic errors in the parameters are taken to be: $Error(\alpha_2) = 0.1$ and $Error(r_2) = 0.1$ fermi. The other sources of systematic error, such as the correction due to fake pions, and the inequality in acceptance for real pion multiplets and mixed multiplets, are small enough to be neglected in comparison.

The primary significance of this measurement is that the pure-three-pion correlation is seen to be be non-zero, as is expected in our simple model for three-pion Bose-Einstein interference. The measured values, $\alpha_2 = 0.55 \pm 0.10 \pm 0.10$ and $r_2 = 0.77 \pm .09 \pm 0.1$ fermi, agree (within the large errors) with the corresponding two-pion correlation parameters measured in the previous chapter ($\alpha_2 = 0.62 \pm 0.03 \pm 0.13$, and $r_2 = 0.66 \pm 0.03 \pm 0.11$ fermi). This measurement thus provides additional confidence that these correlations are really the result of Bose-Einstein interference. There is an indication of a larger radius and of a smaller strength than that measured using two-pion correlations, but this cannot be considered significant, given the size of the systematic uncertainty. A similar indication is also seen in the Monte Carlo test that was done (see Table 6.2). Although the systematic uncertainties prevent us from making more substantial comparisons with theory, the confirmation of the existence of a pure-three-pion correlation is in itself significant. The measurement of pure correlations for multiplets higher than two is difficult because the amount of phase space for these multiplets in which correlations appear is small (since the momenta of all the particles must be approximately the same). Given that the pure correlation function is found to be non-zero only for the lowest few bins of Q_3, it is perhaps not surprising that the standard three-pion correlation function did not reveal evidence for this extra correlation, and that the correlation is only observable after the pair correlations are subtracted.

Chapter 7

Summary and Conclusions

This thesis describes measurements of two and three particle correlations between like-sign pions produced in e^+e^- annihilation at 29 GeV center-of-mass. The analysis is based on approximately 144 pb^{-1} of data taken during the period 1982–1986 using the TPC/2γ detector at PEP. We measured the two particle correlation function as a function of the variables Q, the momentum difference as measured in the rest frame of the pion pair, and q_0, the energy differences as measured in the lab frame. We observe Bose-Einstein enhancement when Q is small, even when the energy difference, q_0, is large compared to c/r, r being the source size parameter that was measured. This measurement provides evidence that the Bose-Einstein correlations are best described by a model that correctly accounts for the relativistic motion of the particle sources, as opposed to a simple model that assumes that the distribution of particle sources is static. The strength of the correlation as measured by the fit parameter α depends somewhat on q_0; however, this dependence is within the range of our estimate of systematic errors, and probably results not from Bose-Einstein interference but from some other source of correlations.

We measure the three-pion correlations both by using a standard three-pion correlation function, and also by using a correlation function for which the correlations between the pairs of pions within the triplet have been subtracted. The standard three-pion correlation function provides a measure of sources size parameter that is consistent with that measured for two-pion correlations. The "subtracted" or "pure" three-pion correlation function reveals a non-zero correlation that is consistent with the two-pion correlation results. The observation of three-pion correlations after pair correlations have been subtracted supports the interpretation of correlations as being due to Bose-Einstein correlations.

The future of the study of Bose-Einstein correlations in high energy reactions seems to be hampered by large systematic uncertainties that will be difficult to ever overcome. Unless more is understood about other possible sources of correlations, it will be difficult to untangle the meaning of Bose-Einstein correlation measurements. Nonetheless, measurements in a different regime, such as those at higher energy, are bound to be of interest. Although there is reason to think that Bose-Einstein correlations should have the same form and essentially the same parameters at the higher energies provided by LEP and SLC, it would certainly be worthwhile to confirm that this is true.

Appendix A

The Effect of non-Bose-Einstein correlations on R_3^{pure}

The pure-three-pion correlation function, R_3^{pure}, has been defined so as to measure only those correlations which are not due to correlations between pairs. Pair correlations which are not due to the Bose-Einstein effect will affect the Bose-Einstein correlations, since they change the particle distributions which would exist in the absence of Bose-Einstein correlations. In this appendix we show how these correlations affect R_3^{pure}, and what may be done to eliminate or correct for their effect. Let $P_0^{[+++]}$, $P_0^{[++]+}$, P_0^{+++} represent the distributions (corresponding to $P^{[+++]}$, $P^{[++]+}$, P^{+++} defined in Chapter 6) which would be measured if there were no Bose-Einstein correlations. These will not all be equal if there are pair correlations from other sources. The distributions which we expect in the presence of Bose-Einstein correlations will then be of the form (from Eqn. 6.1) (it is assumed that the effect of Bose-Einstein correlations on the single particle distribution discussed in Sect. 5.2.3 is already taken into account):

$$\begin{aligned} P^{[+++]}(p_1,p_2,p_3) &= [1+\sum_{i=1,3}\Delta_2(q_{ij})+\Delta_3(p_1,p_2,p_3)]\,P_0^{[+++]}(p_1,p_2,p_3) \\ P^{[++]+}(p_1,p_2,p_3) &= [1+\Delta_2(q_{12})]\,P_0^{[++]+}(p_1,p_2,p_3) \\ P^{+++}(p_1,p_2,p_3) &= P_0^{+++}(p_1,p_2,p_3), \end{aligned} \tag{A.1}$$

where Δ_2 represents the pair and Δ_3 the pure triplet Bose-Einstein correlation enhancement. The pure triplet density which we measure will then be,

$$P^{pure}(p_1,p_2,p_3) = P^{[+++]}(p_1,p_2,p_3) - \sum_{i=1,3}[P^{[++]+}(p_i,p_j,p_k) - P^{+++}(p_i,p_j,p_k)]$$

Substituting our expressions for $P^{[+++]}$, $P^{[++]+}$, P^{+++},

$$\begin{aligned} P^{pure}(p_1,p_2,p_3) &= [1+\Delta_3(p_1,p_2,p_3)]P_0^{+++}(p_1,p_2,p_3) \\ &\quad +[P_0^{[+++]} - P_0^{+++}] - \sum_{i=1,3}[P_0^{[++]+}(p_i,p_j,p_k) - P_0^{+++}] \end{aligned}$$

$$+\sum_{i=1,3} \Delta_2(q_{ij})[P_0^{[+++]}(p_i,p_j,p_k) - P_0^{[++]+}(p_i,p_j,p_k)]$$
$$+\Delta_3(p_1,p_2,p_3)[P_0^{[+++]} - P_0^{+++}]. \quad \text{(A.2)}$$

The first line is the three-pion Bose-Einstein correlation which we are interested in. The second line is the contribution from non-Bose-Einstein pure-three-pion correlations, which we cannot expect to distinguish from actual Bose-Einstein correlations. This contribution is predicted to be zero by the Lund Monte Carlo program. The last two lines show that existence of non-Bose-Einstein correlations will affect the measured $P^{pure}(p_1,p_2,p_3)$. The origin of these terms is that the Bose-Einstein enhancement acts on the actual (possibly correlated) three-particle distributions, rather than to the uncorrelated reference distribution (P_0^{+++}).

The simplest way to eliminate this contribution would be to correct the distributions $P^{[+++]}$, $P^{[++]+}$ for non-Bose-Einstein correlations before forming the pure triplet correlation function, to the extent that we know what these correlations are. For example, if we trust the Lund Monte Carlo to reproduce the correlations correctly, we can normalize the measured distributions, $P^{[+++]}$, $P^{[++]+}$, by the correlation functions measured from Lund generated events:

$$\begin{aligned} P_N^{[+++]}(Q_3^2) &= P^{[+++]}(Q_3^2)/R_{MC}^{[+++]}(Q_3^2), \\ P_N^{[++]+}(Q_3^2) &= P^{[++]+}(Q_3^2)/R_{MC}^{[++]+}(Q_3^2), \end{aligned}$$

where,

$$\begin{aligned} R_{MC}^{[+++]}(Q_3^2) &= P_{MC}^{[+++]}(Q_3^2)/P_{MC}^{+++}(Q_3^2), \\ R_{MC}^{[++]+}(Q_3^2) &= P_{MC}^{[++]+}(Q_3^2)/P_{MC}^{+++}(Q_3^2). \end{aligned}$$

As discussed in Sect. 5.3.2, the correlations predicted by the Lund Monte Carlo are generally of two kinds. There is the so called short range correlation which is slowly varying with Q_3. In the triplet distribution this essentially amounts to a change in normalization. There is correlation between pairs originating from resonances, which results in structure at low Q_3. These pions do not contribute to Bose-Einstein enhancement except for at extremely low values of Q_3, therefore it may be argued that these correlations do not contribute to the effect described above. If this is the case, then it is better to only correct for the effect of short range correlations. This can be done approximately by changing the overall normalization of the distributions so that they agree at large Q_3^2.

Bibliography

[Ake87] T. Åkesson *et al.* (AFS Collaboration), Z. Phys. C **36**, 517 (1987).

[Aih83a] H. Aihara *et al.* (TPC/2γ Collaboration), Nucl. Instrum. Methods **217**, 259 (1983).

[Aih83b] H. Aihara *et al.* (TPC/2γ Collaboration), IEEE Trans. Nucl. Sci. **NS-30**, 153 (1983).

[Aih83c] H. Aihara *et al.* (TPC/2γ Collaboration), IEEE Trans. Nucl. Sci. **NS-30**, 67 (1983).

[Aih83d] H. Aihara *et al.* (TPC/2γ Collaboration), IEEE Trans. Nucl. Sci. **NS-30**, 63, 76, 162 (1983).

[Aih85a] H. Aihara *et al.* (TPC/2γ Collaboration), Phys. Rev. Lett. **54**, 270 (1985).

[Aih85b] H. Aihara *et al.* (TPC/2γ Collaboration), Phys. Rev. D **31**, 996 (1985).

[Aih88] H. Aihara *et al.* (TPC/2γ Collaboration), "Charged Hadron Production in e^+e^- Annihilation at $\sqrt{s} = 29$ GeV," LBL Report LBL-23737, Lawrence Berkeley Laboratory, March 1988.

[Alt86] M. Altoff *et al.* (Tasso Collaboration), Z. Phys. C **30**, 355 (1986).

[And83] B. Andersson *et al.*, Phys. Rep. **97**, 31 (1983).

[And86] B. Andersson and W. Hofmann, Phys. Lett. **169B**, 364 (1986).

[Art74] X. Artru and G. Mennessier, Nucl. Phys. B **70**, 93 (1974).

[Art88] X. Artru and M. G. Bowler, Z. Phys. C **37**, 293 (1988).

[Ave85] P. Avery *et al.* (CLEO Collaboration), Phys. Rev. D **32**, 2294 (1985).

[Bar83] W. Bartel *et al.* (Jade Collaboration), Z. Phys. C **21**, 37 (1983).

[Bow85] M. G. Bowler, Z. Phys. C **20**, 617 (1985).

[Bow86] M. G. Bowler, Phys. Lett. **180B**, 299 (1986).

[Bow88] M. G. Bowler, Z. Phys. C **39**, 81 (1988).

[Buc82] C. Buchanan *et al.*, in *Proceedings of the Gas Calorimeter Workshop* (Batavia, 1982), p. 284.

[Cai84] M. P. Cain *et al.*, Phys. Lett. **147B**, 232 (1984).

[Cas79] A. Casher, H. Neuberger, and S. Nussinov, Phys. Rev. D **20**, 179 (1979).

[Cow88] G. D. Cowan, *Inclusive $\pi^{\pm}$, $K^{\pm}$, and p, $\overline{p}$ Production in e^+e^- Annihilation at $\sqrt{s} = 29$ GeV*, PhD thesis, University of California, Berkeley, January 1988. LBL-24715.

[Edb87] T. Edberg, "A Neopyte's Guide to Track Fitting in the TPC," TPC Note TPC-LBL-87-16, Lawrence Berkeley Laboratory, 1987.

[Fer50] E. Fermi, Prog. Theor. Phys. **5**, 570 (1950).

[Fow77] G. N. Fowler and R. Weiner, Phys. Lett. **70B**, 201 (1977).

[Fuz84] R. Fuzesy, N. J. Hadley, and P. R. Robrish, Nucl. Instrum. Methods **223**, 40 (1984).

[Gar85] J. W. Gary, *Tests of Models for Parton Fragmentation in e^+e^- Annihilation*, PhD thesis, University of California, Berkeley, November 1985. LBL-20638.

[Glu63] R. L. Gluckstern, Nucl. Instr. Meth. **24**, 381 (1963).

[Gol59] G. Goldhaber *et al.*, Phys. Rev. Lett. **3**, 181 (1959).

[Gol60] G. Goldhaber *et al.*, Phys. Rev. **120**, 300 (1960).

[Gol81] G. Goldhaber, in *Proceedings of the International Conference on High Energy Physics.* (Lisbon, Portugal, 1981).

[Gol86] G. Goldhaber and I. Juričic, "New Results on the Bose-Einstein Effect in e^+e^- Interactions or the GGLP Effect Revisited.," in *Proceedings of the Second International Workshop on Local Equilibrium in Strong Interaction Physics.*, edited by P. Carruthers and D. Strottmann (World Scientific Publishing Co., 1986).

[Gra77] Grassberger, Nucl. Phys. B **120**, 231 (1977).

[Gyu79] M. Gyulassy *et al.*, Phys. Rev. C **20**, 2267 (1979).

[Had83] N. J. Hadley, *Charged Hadron Production in e^+e^- Collisions at Pep with the TPC*, PhD thesis, University of California, Berkeley, May 1983. LBL-16116.

[Han56] R. Hanbury-Brown and R. Q. Twiss, Nature (London) **178**, 1046 (1956).

[Hut84] J. Huth and R. E. Avery, "An Electrostatic Model for Sense Wire Pickup of Gated Grid Pulses," TPC Note TPC-LBL-84-49, Lawrence Berkeley Laboratory, 1984.

[Jar82a] R. C. Jared *et al.*, IEEE Trans. Nucl. Sci. **NS-29**, 282 (1982).

[Jar82b] R. C. Jared *et al.*, IEEE Trans. Nucl. Sci. **NS-29**, 57 (1982).

[Jur87] I. Juričic, *Bose-Einstein Correlations in* e^+e^- *Collisions*, PhD thesis, University of California, Berkeley, December 1987. LBL-24493.

[Kay87] H. S. Kaye, "PEP4 Offline Processing of Experiments 14–18," TPC Note TPC-LBL-87-1, Lawrence Berkeley Laboratory, Jan 1987.

[Kop74a] G. I. Kopylov, Phys. Lett. **50B**, 472 (1974).

[Kop74b] G. I. Kopylov and M. I. Podgoretskiĭ, Sov. J. Part. Nucl. **18**, 336 (1974).

[Kop74c] G. I. Kopylov and M. I. Podgoretskiĭ, Sov. J. Part. Nucl. **19**, 215 (1974).

[Lan82] D. A. Landis *et al.*, IEEE Trans. Nucl. Sci. **NS-29**, 573 (1982).

[Liu85] Y. Liu, *Three-Pion Correlations in Relativistic Heavy Ion Collisions*, PhD thesis, University of California, Riverside, June 1985. Unpublished. I would like to thank Ivanna Juričic for bringing this work to my attention.

[Mad84] R. Madaras and P. Oddone, Phys. Today **37**(8), 1 (1984). And references therein.

[Mar82] J. Marx, TPC Note TPC-LBL-82-84, Lawrence Berkeley Laboratory, 1982.

[Nem83] P. Nemethy, P. Oddone, N. Toge, and A. Ishibashi, Nucl. Instrum. Methods **212**, 273 (1983).

[Pra84] S. Pratt, Phys. Rev. Lett. **53**, 1219 (1984).

[Ron82] M. T. Ronan, IEEE Trans. Nucl. Sci. **NS-29**, 427 (1982).

[Ron87] M. T. Ronan, "The PEP-4 (TPC) Trigger System," TPC Note TPC-LBL-87-12, Lawrence Berkeley Laboratory, May 1987.

[vHo64] L. van Hove, Rev. Mod. Phys. **36**, 655 (1964).

[Wil74] K. G. Wilson, Phys. Rev. D **10**, 2445 (1974).

[Zaj82] W. A. Zajc, *Two-Pion Correlations in Heavy Ion Collisions*, PhD thesis, University of California, Berkeley, August 1982. LBL-14864.

[Zaj88] W. A. Zajc, "Bose-Einstein Correlations: from Statistics to Dynamics.," in *Hadronic Multiparticle Production*, edited by P. Carruthers (World Scientific Publishing Co., 1988).

LAWRENCE BERKELEY LABORATORY
TECHNICAL INFORMATION DEPARTMENT
1 CYCLOTRON ROAD
BERKELEY, CALIFORNIA 94720